Supporting Information for

NRF1/NFE2L1 orchestrates spatiotemporal regulation of protein degradation network in skeletal muscle

Zhendi Wang, Wei Shen, Rui Zhang, Xirui Yan, Jinzhi Wu, Shengnan Liu, Zhiyuan Liu, Lei Zhang, Lei Chang, Ping Xu, Xinyu Liu, Guowang Xu, Rui Zhao, Bei Yang, Yanyan Chen, Yi Wang, Huihui Wang, Hongbo Liu, Qiang Zhang, Masayuki Yamamoto, Yuanyuan Xu, Jingqi Fu, Jingbo Pi

Corresponding author: J.P., jbpi@cmu.edu.cn or jingbopi@163.com, Phone: +86 18900910300 and J.F., jqfu@cmu.edu.cn, Phone: +86 18040051018.

This PDF file includes:

Supporting text

SI References

Figures S1 to S33

Tables S1 to S11

Supporting text

Materials and Methods:

Publicly Available RNA-seq Data Mining. Four publicly available RNA-seq datasets were used in this study: GTEx_Analysis_2017-06-05_v8 obtained from the Genotype-Tissue Expression (GTEx) database(1), and three datasets (GSE167186(2), GSE175495(3), and GSE200398(4)) downloaded from the Gene Expression Omnibus (GEO) database. All omics data were analyzed using R software (v4.3.2). For data preprocessing, the tidyverse package (v2.0.0) was employed to clean and standardize the datasets. Specifically, for the GTEx dataset, groups containing fewer than three male or female samples were excluded to ensure statistical reliability.

Statistical analysis was then conducted using various packages. The clinfun package (v1.1.5) with the Jonckheere trend test was applied for multiple-group trend analysis, where a $P < 0.05$ was considered statistically significant. Pearson's correlation coefficient (R) and significance tests were calculated using the cor.test function, with $R > 0.5$ and $P < 0.05$ indicating a significant association with *NFE2L1*.

Protein-protein interaction (PPI) analysis was performed using the online tool STRING(5). Differential expression analysis (DEA) between two groups was conducted using DESeq2 (v1.42.0)(6). The clusterProfiler(7) package (v4.10.0) was used for enrichment analysis to identify the top ten most significant pathways, biological processes, or terms with P-adjust < 0.05. Gene set files for enrichment analysis included C2 (Kyoto encyclopedia of genes and genomes, namely KEGG, and Reactome), C3 (regulatory target gene sets), and C5 (Biological processes of gene ontology, BP of GO) for humans, as well as M2, M3, and M5 for mice. These were downloaded from the Molecular Signatures Database (MSigDB)(8) or via the KEGGREST (v1.42.0) package.

Unless otherwise specified, omics data visualization in this study was performed using the ggplot2 package (v3.5.0). Heat maps were visualized using ComplexHeatmap (v2.18.0) and pheatmap (v1.0.12).

Candidate Gene Association Study (CGAS). To evaluate the association of *NFE2L1* variants with muscle quantity and quality, we performed a CGAS of appendicular lean mass (ALM) and hand grip strength (HGS) within the UK biobank (UKB) cohort as described previously(9). Ethical approval for the UKB study was granted by the North West Centre for Research Ethics Committee (approval number: 11/NW/0382), and informed consent was obtained from all participants. Our study (project number: 41542) fell under the general ethical approval framework of the UKB initiative.

Only participants who self-identified as white (data field 21000) were included. Exclusion criteria comprised individuals with self-reported gender inconsistent with genetic gender, sex chromosome aneuploidy, incomplete genotype imputation, or those who withdrew consent. Genome-wide genotypes for all participants were available at 784,256 genotyped autosome markers and were imputed using the UK10K haplotype, 1000 Genomes project phase 3, and Haplotype Reference Consortium (HRC) reference panels. Participant relatedness was inferred from the total genotyped markers using KING software(10) and a subset of genetically unrelated participants was drawn from the analysis.

We extracted variants within *NFE2L1* (GRCH37 chr17:46,125,686 - 46,138,907) and its 10 kb flanking regions on either side (GRCH37 chr17:46,115,686 - 46,148,907) from the imputed genotypes, yielding a total of 220 variants for testing. Lean body mass was measured via bioelectrical impedance analysis (BIA). Appendicular lean mass (ALM) was calculated as the sum of fat-free mass at the arms (data fields 23121 and 23125) and legs (data fields 23113 and 23117), while hand grip strength (HGS) was quantified as the aggregate of left and right HGS measurements (data fields 46 and 47).

Separate analyses were performed for each gender. In both groups, phenotypic outliers for each trait were identified using the Tukey method and excluded. Subsequently, each phenotype was adjusted for common covariates, including age, age squared, height, height squared, assessment center, genotyping batch, and the top 10 principal components (PCs) derived from genome-wide genotype data. Additionally, appendicular fat mass (AFM) was included as a covariate for ALM to mitigate potential confounding effects. The adjusted residuals were normalized to the inverse quantiles of the standard normal distribution, forming the basis for subsequent association analysis.

The association between each phenotype and *NFE2L1* variants was evaluated using a linear regression model implemented with the *lm* function in R. Following sex-specific analyses, summary statistics from both genders were meta-analyzed using an inverse-variance weighted fixed-effects model with METAL(11). To account for multiple testing, statistical significance was determined at the 0.05 level after applying the Bonferroni correction, calculated as 0.05 / (2 × *M*eff). Here, 2 represented the number of tested phenotypes, and *M*eff (the effective number of variants accounting for linkage disequilibrium [LD]) was estimated via a principal components-based approach(12), and determined to be 120. Thus, the significance threshold was set at 2.08×10^{-4}. Only variants significant in both gender groups (i.e., $P < 0.05$) were deemed credible and reported.

Animal Model Establishment. A line of striated muscle-specific *Nfe2l1*-knockout (*Nfe2l1*(SM)-KO) mice was generated by crossing mice carrying a LoxP-flanked *Nfe2l1* allele (13) with transgenic mice expressing the Cre recombinase gene driven by the muscle creatine

kinase promoter (*Ckm*-Cre$^{+/-}$) (J006475, Model Animal Research Center, MARC, Nanjing), as previously described(14, 15). In this study, KO mice with the genotype *Nfe2l1*$^{LoxP/LoxP}$;*Ckm*-Cre$^{+/-}$ and their littermate controls with the genotype *Nfe2l1*$^{LoxP/LoxP}$;*Ckm*-Cre$^{-/-}$ (*Nfe2l1*-Floxed, Flox) were used. Additionally, a group of mice with the genotype *Ckm*-Cre$^{+/-}$ (Cre) was included as an additional control group to validate the phenotype of the KO mice. Genotyping was performed using genomic DNA isolated from tail snips. The sequences of the genotyping PCR primers are listed in SI Appendix, Table S7.

Analysis of Body Composition and Tissue Collection. Body composition analysis of the mice was performed using a Minispec LF-50 nuclear magnetic resonance (NMR) spectrometer with Minispec NF software (Bruker Biospin GmbH, Rheinstetten, Germany), following the manufacturer's protocols as detailed previously(16).

For tissue collection, mice were euthanized by CO_2 exposure. Various relevant tissues were collected after appropriate treatments and immediately weighed. Selected skeletal muscle (SkM) tissue samples, including quadriceps, calf, and triceps brachii muscles, were stored at −80 °C until subsequent analysis. Isolated SkM (e.g., quadriceps and calf muscles) were fixed with 4% paraformaldehyde, followed by paraffin embedding, sectioning, and staining for subsequent histopathological examination.

Athletic Performance Evaluation:

Treadmill Test: Mice were individually placed in a vertical closed-loop treadmill equipped with an electric shock grid at the base (Model YLS-10B, Yiyankeji Co., Jinan, China). The exhaustion criteria used to determine the fatigue point were as follows: 1) Continuous exposure to the electric grid for >10 seconds without attempt to escape, and/or 2) mouse spends >50% of the time spent receiving shocks, for any rolling time interval, and/or 3) Cessation of movement with no response to gentle manual stimulation. After the weakened group mice reaching the exhaustion criteria, we recorded the fatigue point (the exhaustion time and frequency of electric shocks).

Grip Strength Test: Maximal limb grip strength was measured using a digital force gauge (Grip-Strength Meter, Model 47200, Ugo Basile, Comerio, Italy). Mice were gently grasped by the base of the tail and positioned horizontally above the apparatus until their forelimbs securely gripped the metal bar. A smooth and steady pulling force was then applied in the axial direction until both forelimbs released the bar, with the peak force (recorded in grams-force, gf) automatically captured by the device. Each mouse underwent 10 consecutive trials, and the highest value obtained was used for statistical analysis.

Rota-rod Test: The time for which an animal could remain on the rotating cylinder was measured using an accelerating Rotarod apparatus (Rota-Rod 7650, Ugo Basile). Each mouse

was given three attempts and the time was recorded that the mice stayed on the rod until falling off and were calibrated by body weight. One week prior to the test, mice were trained twice to remain on the Rota-rod apparatus to exclude differences in motivation and motor learning.

RNA Extraction and RT-qPCR analysis. The RNA extraction and RT-qPCR analysis were performed as previously detailed(17). Briefly, total RNA was extracted using RNAiso Plus (Cat. #9109, TaKaRa, Dalian, China) following the manufacturer's protocol. Genomic DNA contamination was removed using an RNase-free Recombinant DNase I kit (RR047A, TaKaRa). The purified RNA was dissolved in RNase-free water, quantified using a NanoDrop 2000 spectrophotometer (Thermo Fisher Scientific, Wilmington, DE, USA) at 260 nm, and stored at −80 ℃ until use.

The reverse transcription was conducted with iScript cDNA Supermix (RR047A, TaKaRa). Real-time PCR was performed with SYBR mix (RK02001, Biomaker, Wuhan, China) using a Q6 instrument (QuantStudio 6 Flex, Applied Biosystems, Foster City, CA, USA). The PCR results were analyzed using a delta CT method, where *18s* was employed as loading control for normalization. Primers were designed using Primer Express software (Applied Biosystems) and synthesized by Life Technologies (Shanghai, China). Sequences of all primers are provided in SI Appendix, Table S8.

Bulk RNA-seq and Data Analysis.

Bulk RNA-seq. RNA extraction, library preparation, and sequencing were conducted by Seqhealth Technology Co., Ltd. (Wuhan, China) and Personalbio Technology Co., Ltd. (Shanghai, China). Total RNA was extracted from skeletal muscles using TRIzol Reagent (Invitrogen, cat. no. 15596026), including the calf muscles (consisting of the soleus, and gastrocnemius muscles) in 20-week-old mice and the quadriceps muscles of mice in rescue study.

Data Analysis. Gene expression and RPKM matrices were analyzed using R software.. DESeq2 performed DEA, identifying significant changes with an absolute fold change above 2 and a *P*-value below 0.05. Gene set enrichment analysis (GSEA) was conducted with the clusterProfiler package, utilizing gene sets from the KEGG database, $P < 0.05$ was considered significant. The ggstatsplot (v0.12.2) package was used to draw the pie chart of DEG distribution, and the enrichplot package (v1.22.0) was used to draw the GSEA plot.

Protein Extraction and Western blot analysis. The quadriceps muscle tissues were prepared and lysed according to standard protocols as previously described(14). In brief, Protein concentrations of tissue lysates were determined using the BCA Protein Assay Kit

(TaKaRa). Protein quamsamples were separated by SDS-PAGE and transferred to PVDF membranes. The molecular weight (MW) of each protein shown on immunoblots was estimated based on the ColorMixed Protein Marker (PR1920, Solarbio Life Sciences, Beijing, China). The images of immunoblots were quantified with Image J software 1.50i, NIH). Antibodies for DRP1 (#8570S; 1:1000; CST), NFE2L1 (#1236; 1:1000; proteintech), p-RIP3 (#91702, 1:1000, CST), RIP3 (#15828, 1:1000, CST), p-RIP1 (#53286, 1:1000, CST), RIP1 (#3493, 1:1000, CST), p-MLKL (#37333, 1:1000, CST), MLKL (#37705, 1:1000, CST), DRP1, Mitofusin (#221661, 1:1000, Abcam), PGC1α (#54481, 1:1000,Abcam), NDUFS4 (O43181, 1:1000, Thermo Fisher), COXIV (#4844; 1:1000; CST) and α-TUBULIN (#7291; 1:1000, Abcam) were used.

Histological, Immunohistochemical, and Immunofluorescence Analyses. Isolated SkMs were fixed in 4% paraformaldehyde, followed by paraffin embedding, sectioning, and staining with H&E, IHC or immunohistochemistry as described previously(14). Briefly, quadriceps and calf muscles were fixed in 4% neutral-buffered formalin for 48 h, transferred to 70% ethanol, embedded in paraffin, and sectioned at 5 μm. Sections were stained with hematoxylin (H9627, Sigma-Aldrich) for 1 min and eosin (63184, Sigma-Aldrich) for 30 s, then mounted on slides and stored at room temperature. For immunohistochemistry, slides were deparaffinized with three 10-min xylene washes, rehydrated through ethanol grades, and antigen-retrieved using Target Retrieval Solution (S169984-2, Dako) in citrate buffer for 20 min. Endogenous peroxidases were blocked with 3% H_2O_2 for 20 min, followed by overnight 4°C incubation with primary antibodies (F4/80 [sc-377009, Santa Cruz, 1:200] and ASC/TMS1 [67824T, Cell Signaling]) in 1.5% BSA/PBS. After washing, biotinylated secondary antibodies and streptavidin-HRP (Zymed) were applied, with DAB chromogen (Zymed) for 1 min, hematoxylin counterstaining (Vector), and Crystal Mount coverslipping (EMS). For immunofluorescence, 10-μm transverse calf muscle cryosections were prepared via cryostat (CM1950, Leica) at −20°C and stored at −80°C. Sections were immunostained with MHC I (BA-D5, DSHB, 1:50), MHC IIA (SC-71, DSHB, 1:50), MHC IIB (BF-F3, DSHB, 1:50), and LAMININ (ab11575, Abcam, 1:50), followed by fluorophore-conjugated secondary antibodies, DAPI counterstaining for 2 min, and imaging via Nikon Eclipse 80i fluorescence microscope (Nikon Corporation, Japan).

Proteomics Experimental Protocol and Data Analysis. Protein samples were collected from calf muscles of Flox and Nfe2l1(KM)-KO mice, and analyzed for differentially expressed proteins by mass spectrometry at Beijing Proteome Research Center using the methods described previously(58, 59). In brief, calf SkM protein sample quality was first assessed. Equal quantities of samples from each group were subjected to protein alkylation and trypsin digestion to generate peptides. The peptides were then labeled with 8-channel Tandem Mass Tag (#90406, Thermo Fisher Scientific, Wilmington, DE, USA) reagents, followed by equilibration, desalting, and cleanup steps to prepare for Liquid Chromatograph-Mass Spectrometry/Mass Spectrometry (LC-MS/MS) analysis and quantitative profiling. In the experiment, Orbitrap Fusion ™ Lumos ™ was used for analysis with a gradient set as a 78-minute multi-segment linear gradient and a flow rate of 600 nL/min. The MaxQuant (v1.5.5.1) search engine was used for database searching. The database search employed the uniprot-mouse protein sequence database downloaded from UniProt. A target-decoy strategy was adopted for the search, and the decoy database was constructed using the protein-level reversal method, with its size matching that of the target database. After data normalization, the protein abundance of each sample was log10 transformed, and an unpaired Student's *t*-test was used to calculate significance. A *P*-value of less than 0.05 was considered statistically significant. The GSEA method was applied as described above, highlighting the most significant and interesting pathways, biological processes, or terms ($P < 0.05$).

Untargeted Lipidomics and Metabolomics. Approximately 10 mg of -80 °C frozen calf muscles (consisting of the soleus and gastrocnemius muscles in mice) samples were subjected to pretreatment and subsequent analyses for untargeted lipidomics and untargeted metabolomics. The calf SkM samples were weighed into pre-cooled (on ice) 2 mL centrifuge tubes, followed by the addition of zirconia grinding beads and 300 μL of methanol solution containing isotopic internal standards (SI Appendix, Table S11). Samples were homogenized using a bead mill at 30 Hz for 2 min. Subsequently, 1 mL of ice-cold MTBE was added, and the mixture was vortexed for 30 s at 4°C. To induce phase separation, 250 μL of ultrapure water was added, followed by another 30 s of vortexing at 4°C. After a 1-min ice bath, samples were centrifuged at 20,000 × g for 10 min at 4°C. The upper organic phase (450 μL) was transferred to cryotubes. Additionally, 20 μL of the remaining supernatant from each sample was collected, pooled, and 450 μL of the mixture was aliquoted into cryotubes as quality control (QC) samples. Both sample and QC aliquots were vacuum-dried at 4°C for 5 h, and the resulting lipid extracts were stored at −80°C for subsequent LC-MS analysis.

Prior to LC-MS analysis, 20 μL of chloroform/methanol (2:1, *v/v*) was added to the lyophilized lipid extracts and vortexed for 30 s at 4°C for reconstitution. Then, 40 μL of

acetonitrile/isopropanol/MilliQ water (65:30:5, *v/v/v*, containing 5 mM ammonium acetate) was added to dilute the reconstituted solution, followed by another 30 s of vortexing at 4°C. After centrifugation at 20,000 × g for 10 min at 4°C, 55 μL of the upper supernatant was transferred to a vial for analysis. An ultra-high-performance liquid chromatography (UHPLC) system (Thermo Scientific Vanquish) coupled with a Q Exactive quadrupole-orbitrap mass spectrometer (Thermo Fisher Scientific, Waltham, MA, USA) was employed.

Standard compounds used in the measurement, including lysophosphatidylcholine C19:0 (LPC 19:0), phosphatidylcholine C38:0 (PC 38:0), phosphatidylethanolamine C30:0 (PE 30:0), sphingomyelin C12:0 (SM 12:0), ceramide C17:0 (Cer 17:0), fatty acid C16:0-d3 (FA 16:0-d3), fatty acid C18:0-d3 (FA 18:0-d3), and triglyceride 45:0 (TG 45:0), were sourced from Avanti Polar Lipids (Alabaster, AL, USA). Ammonium acetate and tert-butyl methyl ether (MTBE) were obtained from Sigma-Aldrich (St. Louis, MO, USA), while acetonitrile, methanol, and isopropanol were purchased from Merck (Darmstadt, Germany). Ultrapure water was generated using a Milli-Q system (Millipore, Burlington, MA, USA).

Chromatographic separation was performed on an ACQUITY UPLC C8 column (100 × 2.1 mm, 1.7 μm) at 60°C. Mobile phases consisted of Phase A (60% acetonitrile/MilliQ water, 10 mM ammonium acetate) and Phase B (10% acetonitrile/isopropanol, 10 mM ammonium acetate) at a flow rate of 0.3 mL/min. The injection volume was 2 μL, and the autosampler temperature was maintained at 10°C. The gradient elution program was as follows: 50% B for 1.5 min, linearly increasing to 85% B over 7.5 min, rising to 100% B in 0.1 min and held for 1.9 min, then returning to 50% B in 0.1 min and equilibrating for 2.9 min (total run time: 14 min). Mass spectrometry parameters included full-scan acquisitions in positive (ESI+) and negative (ESI−) ion modes. Ion source settings were: sheath gas flow rate 45 arb, auxiliary gas flow rate 10 arb, spray voltage +3.5 kV (ESI+) and −3.0 kV (ESI−), capillary temperature 320°C, auxiliary gas temperature 350°C. Scan ranges were 300-1100 m/z (ESI+) and 160-1600 m/z (ESI−). For MS/MS analysis (performed separately in ESI+ and ESI− modes), parameters were: AGC target 1×10^5, maximum ion injection time 50 ms, loop count 10, normalized collision energy (NCE) 15 and 25 eV, with the same scan ranges as MS full scans.

A pooled QC sample was prepared by mixing supernatants from all samples to monitor sample pretreatment and instrumental stability. QC samples and blank (reconstitution solvent) were inserted every 10 samples, and the relative standard deviation (RSD) of components in QC samples served as the stability indicator. Lipidomics analysis was considered valid when lipids with RSD < 30% in QC samples were subjected to the following statistical analysis.

GC-MS based Untargeted Metabolomics. Fresh calf tissues were maintained on ice, and approximately 10 mg (with precise mass recorded) were weighed into a 2 mL microcentrifuge tube. Following the addition of grinding beads, 600 μL of ice-cold 80% methanol/water (4:1,

v/v) containing 2 μg/mL tridecanoic acid as an internal standard was added. The tube was vortexed or briefly shaked to submerge the tissue in the extraction solution, then homogenized in a grinding device at an oscillation frequency of 30 Hz for 1 min (two cycles). Post-homogenization, the mixture was centrifuged at 14,000 rpm (calculated using a rotor radius of 10 cm) for 10 min at 4°C. A 480 μL aliquot of the supernatant was transferred to a new tube, and remaining supernatants from all samples were pooled equally (equal volumes from each) to generate quality control (QC) samples. Take several 480ul quality control (QC) samples as QC aliquots. Both sample and QC aliquots were lyophilized under vacuum.

For derivatization, 50 μL of methoxyamine pyridine solution was added to the lyophilized samples, which were incubated at 37°C for 1.5 h to facilitate oximation. Subsequently, 40 μL of N-methyl-N-(trimethylsilyl)trifluoroacetamide (MSTFA) was added, and silylation was performed at 37°C for 1 h. Following derivatization, the solutions were centrifuged at 14,000 rpm for 10 min at 4°C, and supernatants were transferred to injection vials with insert for GC-MS analysis. Analysis was conducted using a Shimadzu GC-MS QP2010 Plus (Shimadzu Corporation, Kyoto, Japan) equipped with a DB-5MS column (30 m × 0.25 mm, 0.25 μm film thickness).

Metabolomics Data Analysis. After data normalization, the data were loaded into R software and subjected to orthogonal projections to latent structures discriminant analysis (OPLS-DA) dimensionality reduction using the ropls package (v1.22.0). The variable importance in the projection (VIP) values from the first principal component of the OPLS-DA model and *P*-values from two-tailed unpaired Student's *t*-tests were used to identify differentially expressed metabolites, where VIP values > 1 and $P < 0.05$ were considered statistically significant. Metabolite set enrichment analysis (MSEA) was performed using the MetaboAnalyst 5.0(20) online tool (https://www.metaboanalyst.ca/MetaboAnalyst/faces/home.xhtml), with $P < 0.05$ considered statistically significant.

snRNA-seq Protocol. Calf muscle samples from six 4-week-old male mice of each genotype were pooled, rinsed with pre-cooled RNase-free saline, minced on ice, and stored at -80 °C. Single-nucleus suspension preparation, separation, library construction, and sequencing were performed by Gene Denovo Biotechnology Co. (Guangzhou, China) following established protocols(14). Nuclear suspensions were processed on a 10X Genomics GemCode Single-cell instrument to create Gel Bead-In-Emulsion (GEMs). Libraries were prepared and sequenced from cDNAs using Chromium Next GEM Single Cell 3'Reagent Kits v3.1. Post GEM reaction mixture cleanup utilized silane magnetic beads to eliminate residual biochemical reagents and primers. Full-length, barcoded cDNAs were PCR-amplified for library construction. The R1 primer sequence was incorporated during GEM incubation, and P5, P7

sample indexes, and R2 primer sequence were added during library construction through end repair, A-tailing, adaptor ligation, and PCR. The final libraries, ready for Illumina sequencing, included P5 and P7 primers for bridge amplification. The Single Cell 3'Protocol yielded libraries with standard Illumina paired-end constructs, initiating and concluding with P5 and P7. The 16 bp 10x Barcode and 10 bp UMI were encoded in Read 1, with Read 2 sequencing the cDNA fragment. Sample index sequences were included as the i7 index read, with Read 1 and Read 2 serving as standard Illumina® sequencing primer sites for paired-end sequencing.

snRNA-seq Data Analysis

Upstream analysis:The 10x Genomics Cell Ranger analysis pipeline (v3.0.0) facilitated demultiplexing and generating FeatureBarcode Matrices. Initially, `cellranger mkfastq` converted snRNA-seq's raw base call (BCL) files into FASTQ files. Subsequently, `cellranger count` aligned these files with the reference genome mm10, performed filtering, and processed barcode data, thereby creating feature-barcode matrices for each sample.

Quality control, dimensionality reduction, clustering, and DEA: Following the acquisition of the expression matrix, subsequent analyses were conducted using R software with the Seurat package (v4.1.1)(21), adhering to quality control criteria including features (nFeature RNA) ranging from 200 to 3000, counts (nCount RNA) below 10,000, and mitochondrial gene percentages under 2%. The DoubletFinder package (v2.0.3) was utilized to eliminate potential doublets. After quality control measures, 11,634 high-quality nuclei from the Flox group and 20,478 from the KO group were retained for further analysis. Post-filtering, sample groups were merged for comprehensive analysis, which included normalization (via NormalizeData function, normalization.method = "LogNormalize", scale.factor = 10,000), identification of variable genes (FindVariableFeatures function, selection.method = "vst", nfeatures = 2,000), and data scaling (ScaleData function, vars.to.regress = "percent.mt").

Linear dimensional reduction was performed using PCA with the top 2,000 variable genes (RunPCA function), and an elbow plot (ElbowPlot function) informed the selection of 20 principal components (PCs) for calculating the shared nearest neighbor graph (FindNeighbors function) using Euclidean distance. Data clustering was achieved using the Louvain algorithm at a resolution of 1.0 (FindClusters function). Clusters were visualized via UMAP (RunUMAP function), and marker genes for each cluster were identified using the top ten genes (FindAllMarkers function) for nucleus type determination.

The FindMarkers function was used for between-group DEA for each nucleus type, with parameters set to `test.use = 'MAST'`, `min.pct = 0.1`, and others at default. A *P*-adjusted value of less than 0.05 and |log2(fold change)| > 0.25 was considered significant. The up-regulated and down-regulated genes were subjected to BP, KEGG, and Reactome enrichment analyses as previously described. The most significant pathways or pathways of interest (*P* <

0.05) were visualized. The eulerr package (v7.0.0) was used to draw the Venn diagram. Other visualizations were created using Seurat or ggplot2.

Single-cell regulatory network inference and clustering (SCENIC):TF regulons were identified using the docker-based pySCENIC analysis pipeline (v0.12.0)(22), a computational method to predict critical regulators and identify cell states from scRNA-seq data. First, we used a sampling method to obtain 1000 nuclei of each nucleus type, and then applied the pipeline for analysis. The gene co-expression network was generated using the gradient boosting machine via the grn function. Cis-regulatory motif analysis was performed using precomputed databases from cisTargetDB via the ctx function. The AUCell algorithm scored the activity of different regulons via the aucell function. The regulon specificity score was calculated using the calcRSS function of the SCENIC package (v1.3.1). Between-group differences were analyzed using the limma package (v3.58.1), with regulons having $P < 0.05$ and $|\log2(\text{fold change})| > 0.5$ considered significant. The ggraph package (v2.1.0) was used to plot the regulon regulatory network.

Cell-cell communication inference: Cell-cell communication inference was conducted using the CellChat package (v1.6.1)(23) to assess ligand-receptor interactions across various cell types. CellChat uses gene expression data and a comprehensive database of known ligand-receptor interactions. Normalized count data for each condition were used to construct CellChat objects, applying default preprocessing functions. The CellChatDB.mouse database was the reference for all ligand-receptor interactions. Interactions involving fewer than 10 cells were excluded. Finally, CellChat objects from different groups were consolidated and analyzed to compare inter-group differences in cell communication.

Trajectory inference analysis: RNA velocity analysis was conducted using the scVelo package (v0.2.3)(24). To count spliced and unspliced reads for each sample, the 10x velocyto pipeline was run on the filtered Cell Ranger-generated BAM files. For single-nucleus RNA velocity inference, the dynamical model of scVelo was applied. Pseudo-time trajectory analysis was performed using the monocle3 package (v1.0.0)(25). Monocle3 aims to understand how cells transition through a biological program of gene expression changes during an experiment. According to the Monocle3 analysis pipeline, the learn_graph function constructs the principal graph from the reduced dimension space using reversed graph embedding. The order_cells function arranges cells according to pseudotime. The plot_cells function visualizes cells along their trajectories. The graph_test function identifies genes with differential expression based on the low-dimensional embedding and the principal graph. The plot_genes_in_pseudotime function plots gene expression as a function of pseudotime.

Characteristic gene calculation, enrichment analysis, and gene set scoring analysis for different subpopulations of type IIb myonuclei:

The FindAllMarkers function was used to calculate characteristic genes for each subpopulation of type IIb myonuclei with default parameters. Enrichment analysis of characteristic genes was performed as described above. Gene set scoring analysis for pathways or biological processes of interest was conducted using the AddModuleScore function from the Seurat package.

Analysis of Publicly Available Human snRNA-seq Data. The processed aging human skeletal muscle single-nucleus transcriptomic cell atlas from Lai et al.(26) was obtained from a publicly available website (https://db.cngb.org/cdcp/hlma/download), including cell nucleus UMAP embedding and annotation information. The FindAllMarkers function from the Seurat package was used to calculate characteristic genes for each subpopulation of human type II myonuclei, with parameters logfc.threshold = 0.10 and min.pct = 0.10. Mouse gene symbols were converted to homologous human genes using the homologene package (v1.4.68). Subpopulation characteristic scoring was performed using the AddModuleScore function from the Seurat package, with the characteristic gene sets used for scoring described in detail in the results.

Analysis of Publicly Available ChIP-seq Datasets. Four ChIP-seq datasets (GSE227357(27), GSE170564(28), GSE230890(28), and GSE91934(28)) were downloaded from the GEO database as raw fastq files. Quality control of raw sequencing data was first performed using FastQC (v0.11.9). Trim Galore (v0.6.7) was used to remove low-quality reads and adapter sequences. Clean reads after quality control were aligned to the human reference genome (GRCh38/hg38) using Bowtie2 (v2.4.5) with default parameters. Alignment results were converted to BAM format, sorted, and indexed using SAMtools (v1.15). Peak calling was performed using MACS2 (v2.2.7) with parameters --format BAM --gsize hs --qvalue 0.05, using input as control. Downstream analyses were conducted in the R environment, with peak annotation and distribution visualization performed using the ChIPseeker package (v1.42.1), and genomic browser tracks visualized using the Gviz package (v1.50.0). Functional enrichment analysis of annotated genes was performed as described above.

Bulk RNA-seq Experimental Protocol and Data Analysis for Rescue Experiments. RNA extraction, library preparation, and sequencing were conducted by Shanghai Personal Biotechnology Cp. Ltd. Total RNA was isolated using Trizol Reagent (Invitrogen Life Technologies), and the concentration, quality, and integrity were assessed using a NanoDrop spectrophotometer (Thermo Scientific). Three micrograms of RNA were used as input material for the RNA sample preparations. Sequencing libraries were generated according to the following steps. Firstly, mRNA was purified from total RNA using poly-T oligo-attached magnetic beads. Fragmentation was carried out using divalent cations under elevated

temperature in an Illumina proprietary fragmentation buffer. First-strand cDNA was synthesized using random oligonucleotides and SuperScript II. Second-strand cDNA synthesis was subsequently performed using DNA Polymerase I and RNase H. Remaining overhangs were converted into blunt ends via exonuclease/polymerase activities, and the enzymes were removed. After adenylation of the 3′ ends of the DNA fragments, Illumina PE adapter oligonucleotides were ligated to prepare for hybridization. To select cDNA fragments of the preferred 400-500 bp length, the library fragments were purified using the AMPure XP system (Beckman Coulter, Beverly, CA, USA). DNA fragments with ligated adaptor molecules on both ends were selectively enriched using the Illumina PCR Primer Cocktail in a 15-cycle PCR reaction. Products were purified (AMPure XP system) and quantified using the Agilent High Sensitivity DNA Assay on a Bioanalyzer 2100 system (Agilent). The sequencing library was then sequenced on the NovaSeq 6000 platform (Illumina).

Samples were sequenced on the platform to generate image files, which were processed by the sequencing platform's software to produce original data in FASTQ format (Raw Data). The sequencing data contained a few adaptors and low-quality reads, so we used fastp (v0.22.0) software to filter the sequencing data and obtain high-quality sequences (Clean Data) for further analysis. The reference genome and gene annotation files were downloaded from the genome website. The filtered reads were mapped to the reference genome using HISAT2 (v2.1.0). HTSeq (v0.9.1) was used to calculate the read count values for each gene, representing the original gene expression, and fragment per kilobase of transcript, per million mapped reads (FPKM) was used to normalize the expression levels. The DEA and GSEA methods were the same as described above. The GSVA package (v1.50.0) was used for gene set variation analysis (GSVA).

Data Availability. The methods for obtaining publicly available omics datasets used in this study are described in the respective methodology sections. The newly generated omics data can be accessed at Zenodo (DOI: 10.5281/zenodo.16916832).

References:

1. Consortium GT, Human genomics. The Genotype-Tissue Expression (GTEx) pilot analysis: multitissue gene regulation in humans. *Science (New York, N.Y.).* **348**(6235):648-660 (2015).
2. Perez K, *et al.*, Single nuclei profiling identifies cell specific markers of skeletal muscle aging, frailty, and senescence. *Aging (Albany NY).* **14**(23):9393-9422 (2022).
3. Trim WV, *et al.*, Divergent immunometabolic changes in adipose tissue and skeletal muscle with ageing in healthy humans. *J Physiol.* **600**(4):921-947 (2022).
4. Semenova EA, *et al.*, Genome-Wide Association Study Identifies CDKN1A as a Novel Locus Associated with Muscle Fiber Composition. *Cells.* **11**(23):3910 (2022).
5. Szklarczyk D, *et al.*, The STRING database in 2023: protein-protein association networks and functional enrichment analyses for any sequenced genome of interest. *Nucleic acids research.* **51**(D1):D638-D646 (2023).
6. Love MI, Huber W, & Anders S, Moderated estimation of fold change and dispersion for RNA-seq data with DESeq2. *Genome Biol.* **15**(12):550 (2014).
7. Xu S, *et al.*, Using clusterProfiler to characterize multiomics data. *Nat Protoc.* **19**(11):3292-3320 (2024).
8. Castanza AS, *et al.*, Extending support for mouse data in the Molecular Signatures Database (MSigDB). *Nature methods.* **20**(11):1619-1620 (2023).
9. Wei XT, *et al.*, Pleiotropic genomic variants at 17q21.31 associated with bone mineral density and body fat mass: a bivariate genome-wide association analysis. *European journal of human genetics : EJHG.* **29**(4):553-563 (2021).
10. Manichaikul A, *et al.*, Robust relationship inference in genome-wide association studies. *Bioinformatics (Oxford, England).* **26**(22):2867-2873 (2010).
11. Willer CJ, Li Y, & Abecasis GR, METAL: fast and efficient meta-analysis of genomewide association scans. *Bioinformatics (Oxford, England).* **26**(17):2190-2191 (2010).
12. Li J & Ji L, Adjusting multiple testing in multilocus analyses using the eigenvalues of a correlation matrix. *Heredity.* **95**(3):221-227 (2005).
13. Ohtsuji M, *et al.*, Nrf1 and Nrf2 play distinct roles in activation of antioxidant response element-dependent genes. *The Journal of biological chemistry.* **283**(48):33554-33562 (2008).
14. Li L, *et al.*, Hepatocyte-specific Nrf2 deficiency mitigates high-fat diet-induced hepatic steatosis: Involvement of reduced PPARγ expression. *Redox biology.* **30**:101412 (2020).
15. Shen W, *et al.*, Single-nucleus RNA-sequencing reveals NRF1/NFE2L1 as a key factor determining the thermogenesis and cellular heterogeneity and dynamics of brown adipose tissues in mice. *Redox biology.* **67**:102879 (2023).
16. Hou Y, *et al.*, Adipocyte-specific deficiency of Nfe2l1 disrupts plasticity of white adipose tissues and metabolic homeostasis in mice. *Biochemical and biophysical research communications.* **503**(1):264-270 (2018).
17. Xue P, *et al.*, Long isoforms of NRF1 negatively regulate adipogenesis via suppression of PPARγ expression. *Redox biology.* **30**:101414 (2020).

18. Shevchenko A, *et al.*, In-gel digestion for mass spectrometric characterization of proteins and proteomes. *Nature protocols.* **1**(6):2856-2860 (2006).
19. Wiśniewski JR, Zougman A, Nagaraj N, & Mann M, Universal sample preparation method for proteome analysis. *Nature methods.* **6**(5):359-362 (2009).
20. Pang Z, *et al.*, Using MetaboAnalyst 5.0 for LC-HRMS spectra processing, multi-omics integration and covariate adjustment of global metabolomics data. *Nat Protoc.* **17**(8):1735-1761 (2022).
21. Butler A, *et al.*, Integrating single-cell transcriptomic data across different conditions, technologies, and species. *Nat Biotechnol.* **36**(5):411-420 (2018).
22. Van de Sande B, *et al.*, A scalable SCENIC workflow for single-cell gene regulatory network analysis. *Nat Protoc.* **15**(7):2247-2276 (2020).
23. Jin S, *et al.*, Inference and analysis of cell-cell communication using CellChat. *Nature Communications.* **12**(1):1088 (2021).
24. Bergen V, *et al.*, Generalizing RNA velocity to transient cell states through dynamical modeling. *Nat Biotechnol.* **38**(12):1408-1414 (2020).
25. Qiu X, *et al.*, Reversed graph embedding resolves complex single-cell trajectories. *Nature methods.* **14**(10):979-982 (2017).
26. Lai Y, *et al.*, Multimodal cell atlas of the ageing human skeletal muscle. *Nature.* **629**(8010):154-164 (2024).
27. Hatanaka A, *et al.*, The transcription factor NRF1 (NFE2L1) activates aggrephagy by inducing p62 and GABARAPL1 after proteasome inhibition to maintain proteostasis. *Sci Rep.* **13**(1):14405 (2023).
28. Consortium EP, An integrated encyclopedia of DNA elements in the human genome. *Nature.* **489**(7414):57-74 (2012).

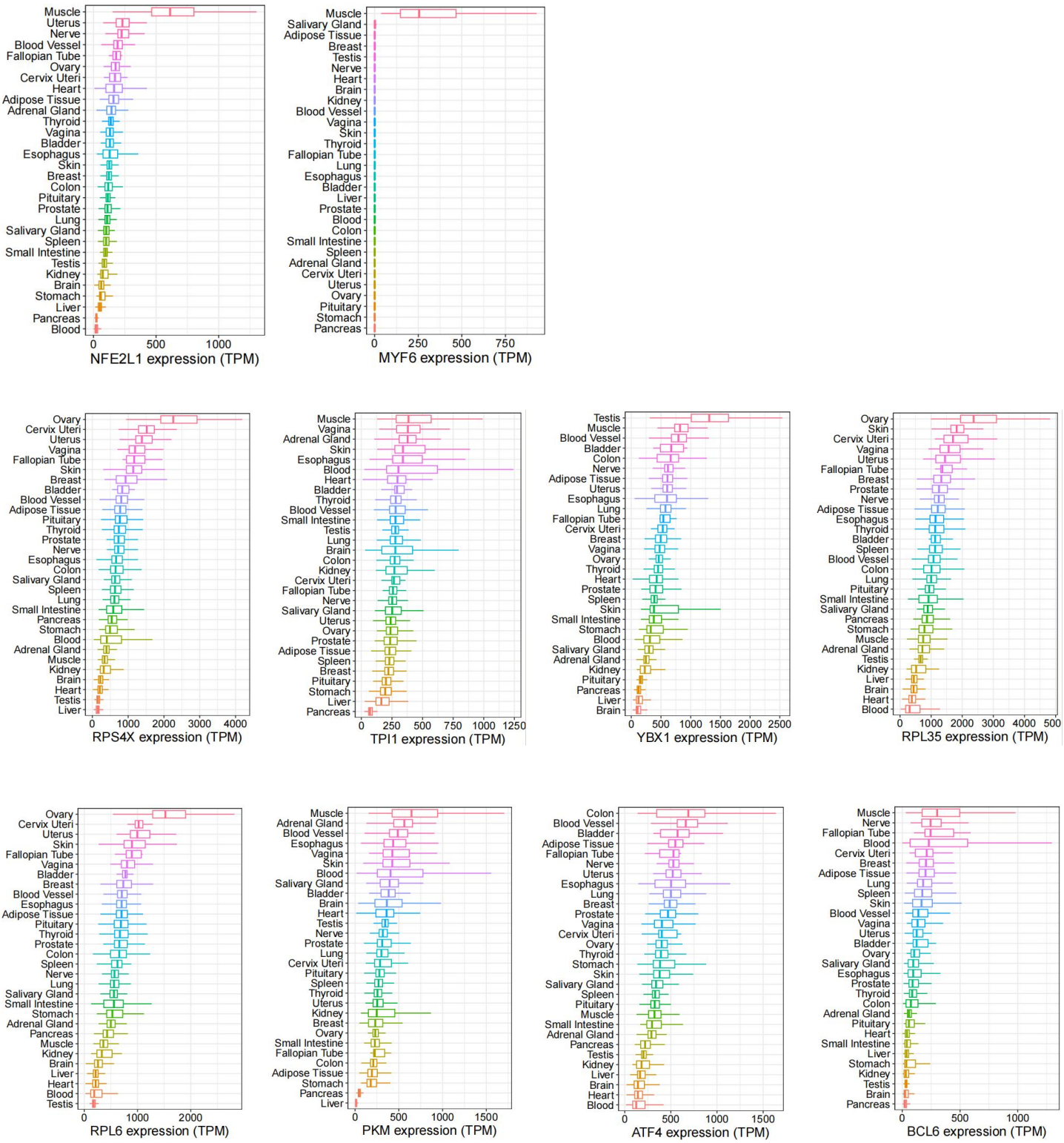

Fig. S1. mRNA expression distribution of the top ten transcription factors in various organs.

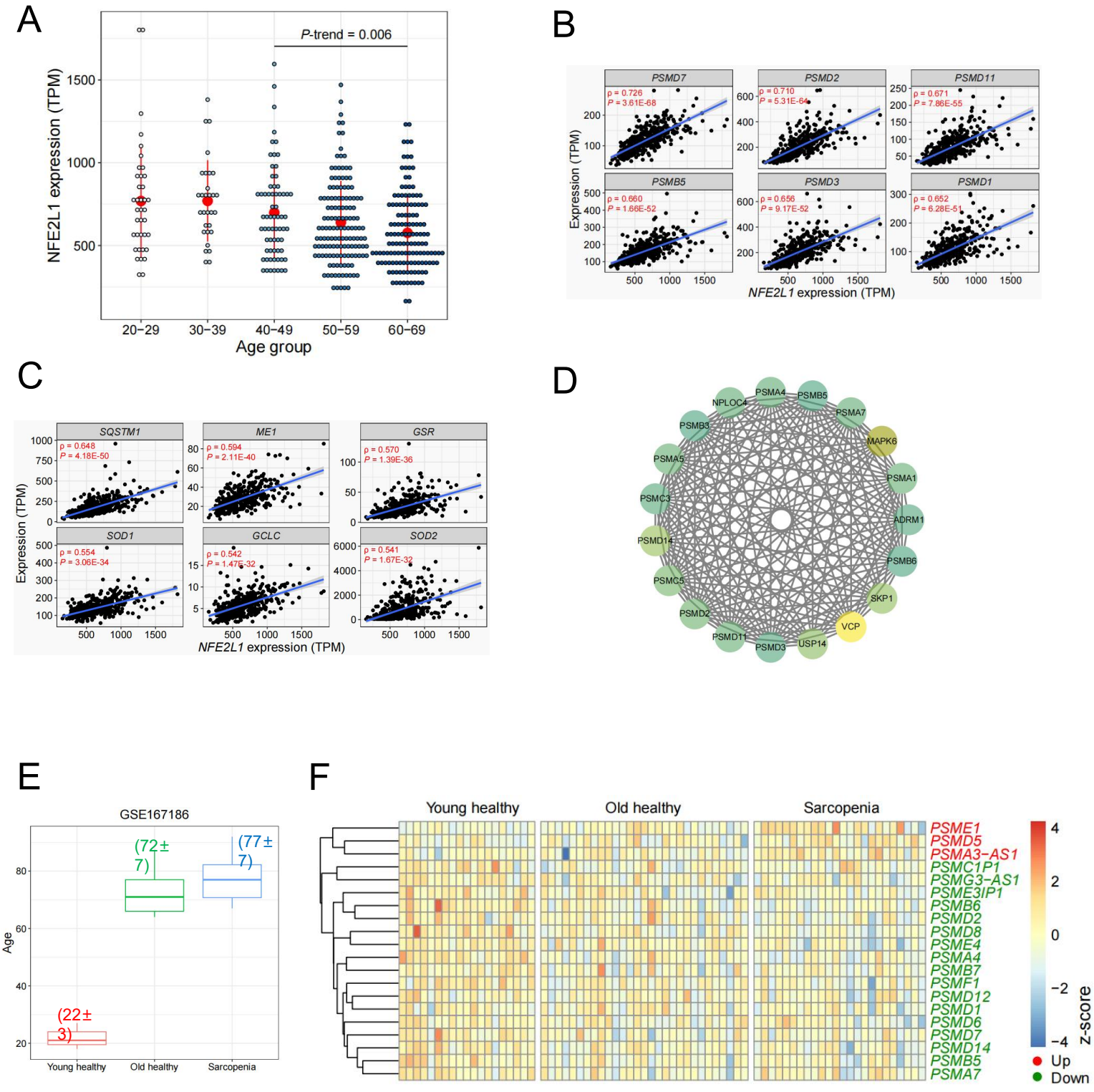

Fig. S2. Analysis of GTEx and GSE167186 datasets. (A) Trend analysis of *NFE2L1* expression across the 40–49, 50–59, and 60–69 age groups (all samples). *P*-trend values were calculated via Jonckheere's trend test. (B–C) Correlation analysis of NFE2L1 with respective proteasome subunit genes and antioxidant genes. (D) Protein–protein interaction analysis of 253 potential NFE2L1 target genes. (E) Box plot showing age distribution (mean ± standard deviation) across the three groups in the GSE167186 dataset. (F) Heatmap of mRNA expression for significantly altered proteasome subunit genes among groups in the GSE167186 dataset.

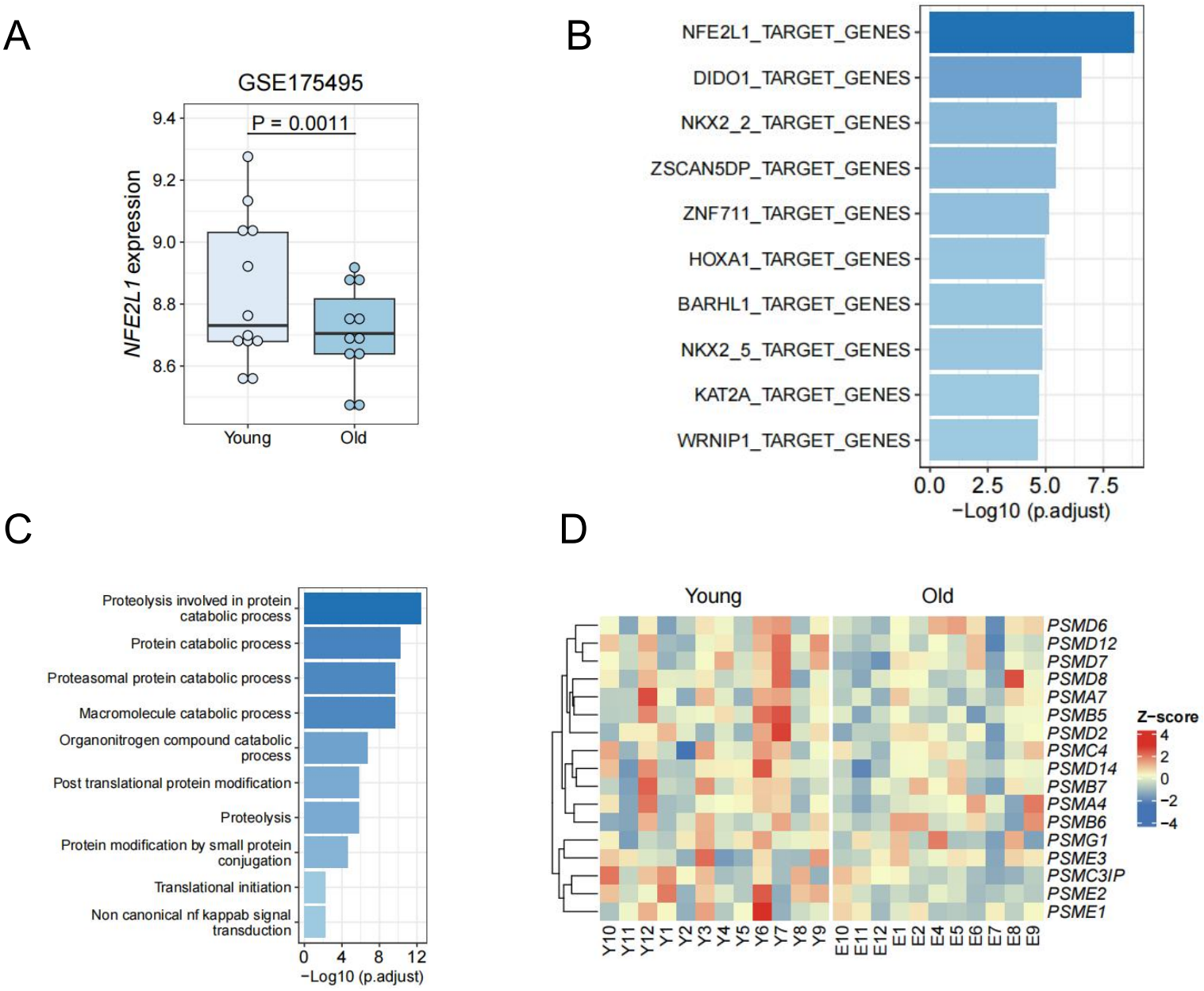

Fig. S3. Analysis of the GSE175495 dataset. (A) Box plot of *NFE2L1* expression in the young and old groups. *P* values were calculated via differential expression analysis (DEA). (B–C) Enrichment analysis of *NFE2L1* co-expressed genes, using the C3 gene set (B) and Gene Ontology (GO) biological process gene set (C), respectively. The most significant terms were NFE2L1_TARGET_GENE (B) and UPS-related terms (C), respectively. (D) Z-score heatmap of proteasome subunit genes with significant decreases in the aged group.

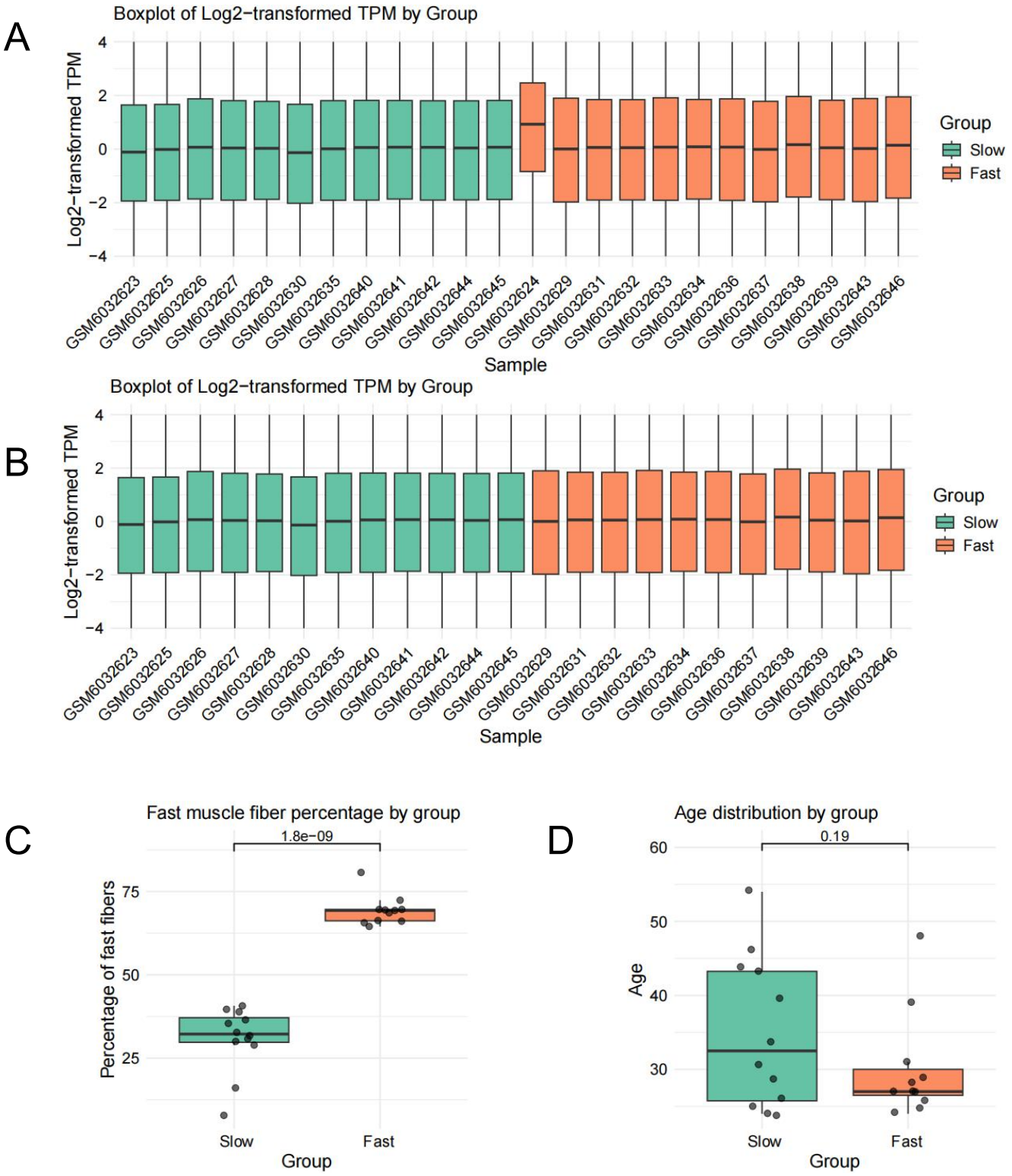

Fig. S4. Analysis of the GSE200398 dataset. (A–B) Box plots of gene expression for sample batch effect inspection and outlier detection, with the abnormal sample GSM6032624 excluded. (C) Samples were divided into two groups based on fast muscle fiber proportion: samples with a proportion above the median were classified as the high fast muscle fiber proportion group (Fast), and those below the median as the low fast muscle fiber proportion group (Slow). (D) No significant age difference was observed between the two groups.

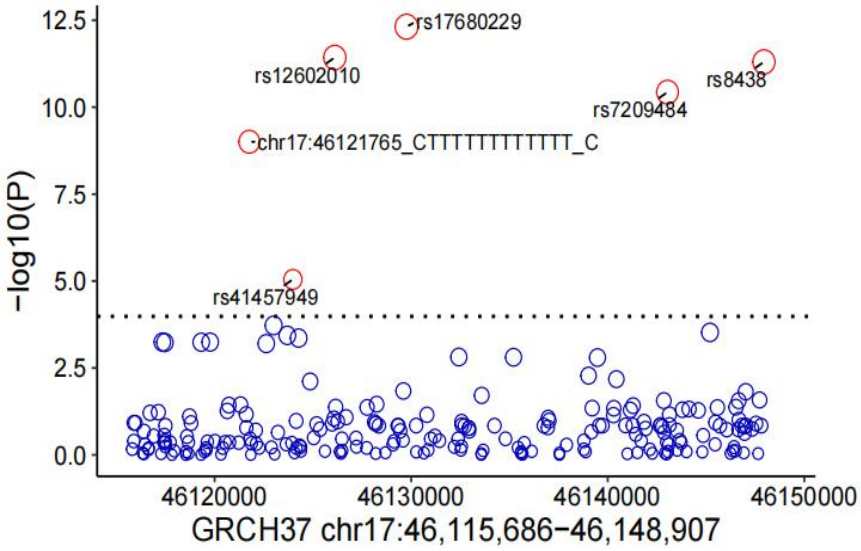

Fig. S5. Associations between *NFE2L1* variants and hand grip strength were analyzed in a candidate gene association study using the UK Biobank (UKB) cohort. For details, see SI Appendix, Tables S5 and S6.

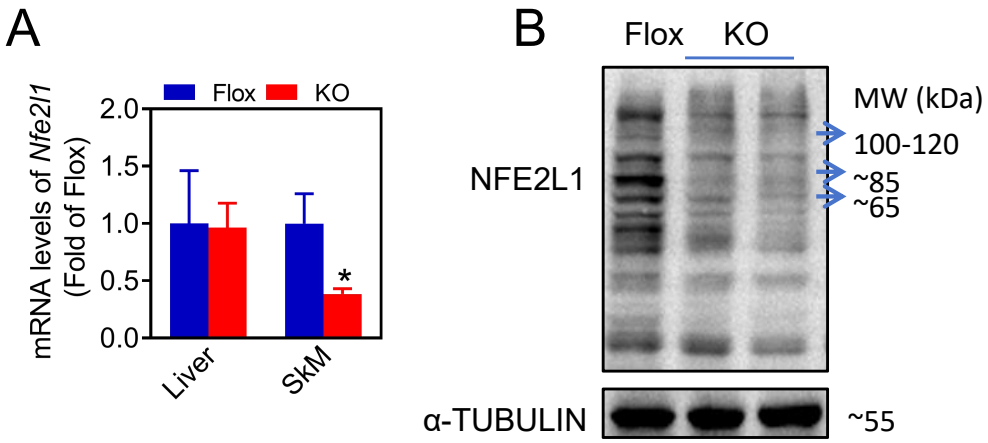

Fig. S6. The mRNA and protein expression levels of NFE2L1 in skeletal muscle tissue. (A) The *Nfe2l1* mRNA levels measured by RT-qPCR in quadriceps muscles. n = 3-4. Animal age = 50 weeks. **P* < 0.05 vs Flox. (B) Protein levels of NFE2L1 in quadriceps muscles.

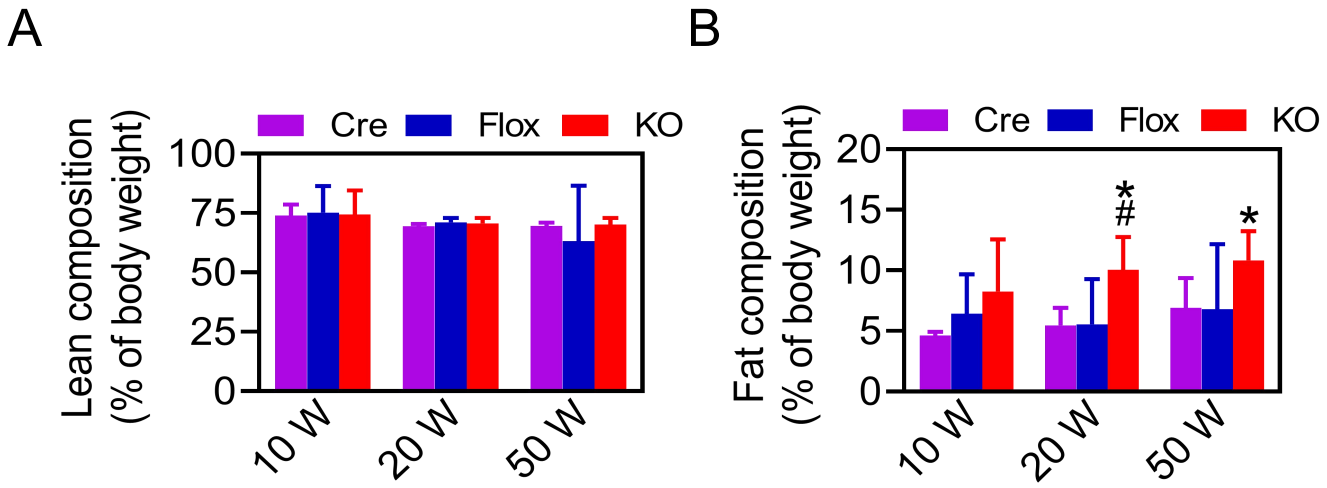

Fig. S7. Body composition of mice. (A) Lean mass in mouse body composition. (B) Fat mass in mice. n = 4–11; *$P < 0.05$ vs. Flox group. All data are presented as mean ± SD in bar plots.

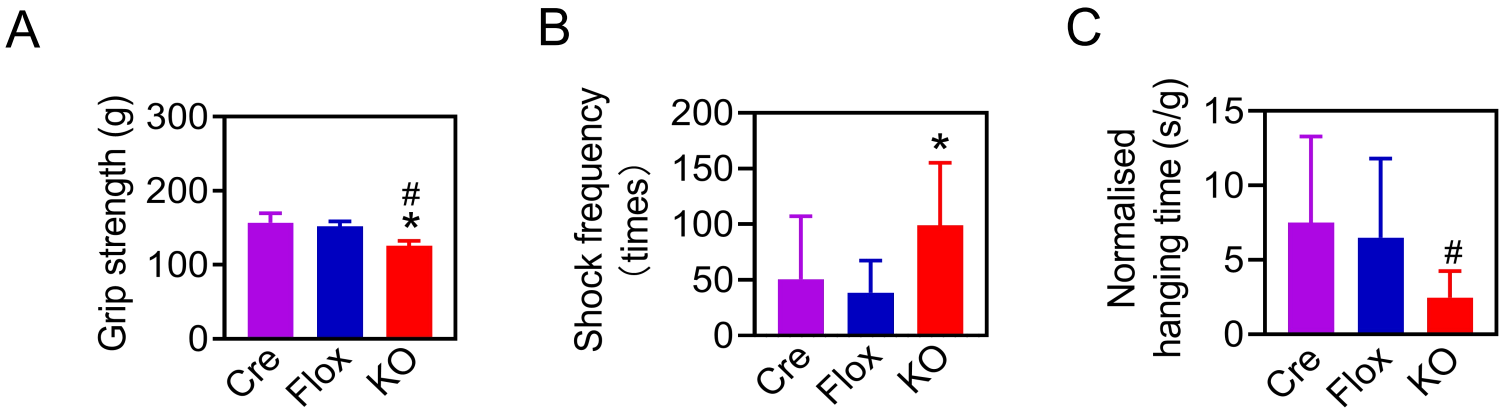

Fig. S8. Motor function of mice. (A) Grip strength of mice; (B) Electric shock frequency when control mice reached the fatigue point during running; (C) Rotarod performance analysis of mice. n = 4–12; animals were 20 weeks old. Statistical significance was assessed via one-way ANOVA. $^{*}P < 0.05$ vs. Flox group; $^{\#}P < 0.05$ vs. Cre group. All data are presented as mean ± SD in bar plots. Flox, *Nfe2l1*$^{fl/fl}$ mice; KO, striated muscle-specific *Nfe2l1* knockout mice ; Cre, *Ckmm*-Cre$^{+/-}$mice.

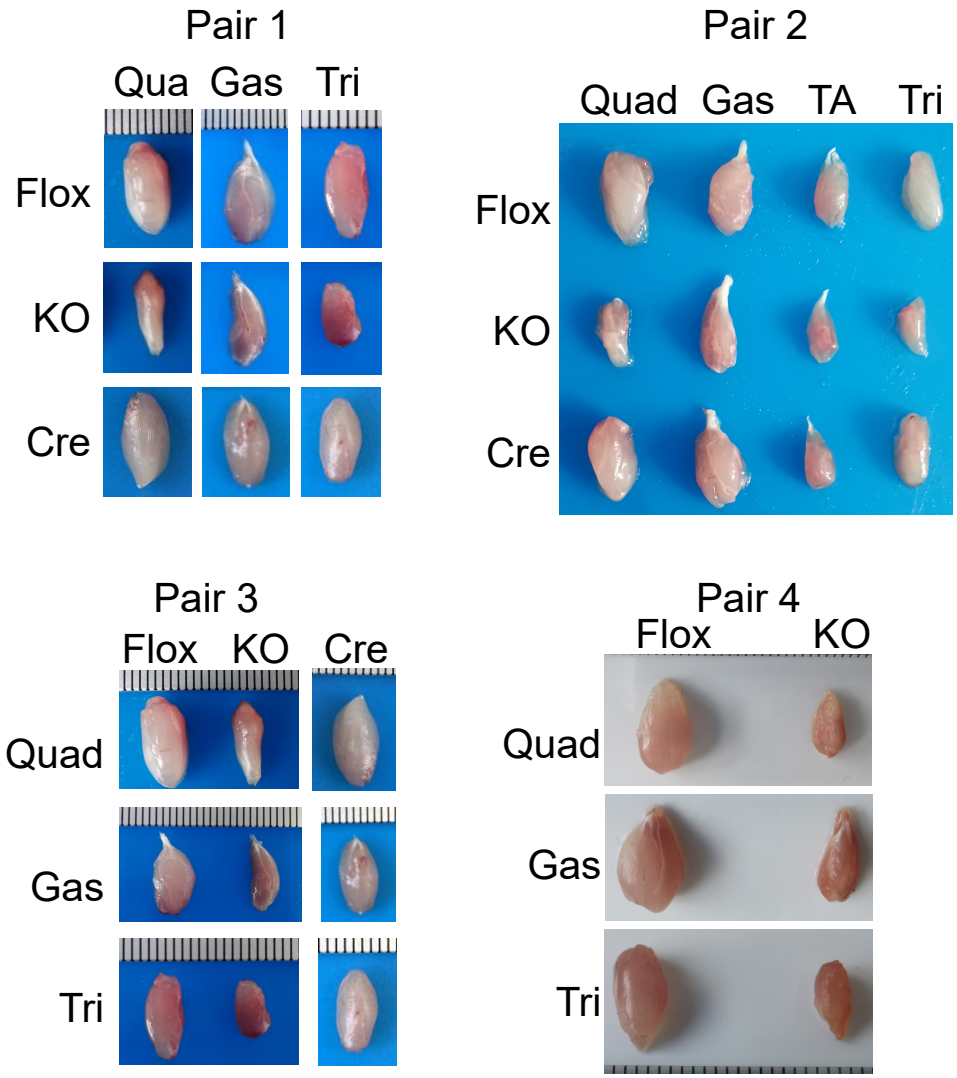

Fig. S9. Representative images of gross morphology of skeletal muscles. n = 5. Animal age = 20 weeks. Quad, quadriceps; Gas, gastrocnemius muscles; Tri, triceps brachii; TA, tibialis anterior. Flox, *Nfe2l1*$^{fl/fl}$ mice; KO, striated muscle-specific *Nfe2l1* knockout mice.

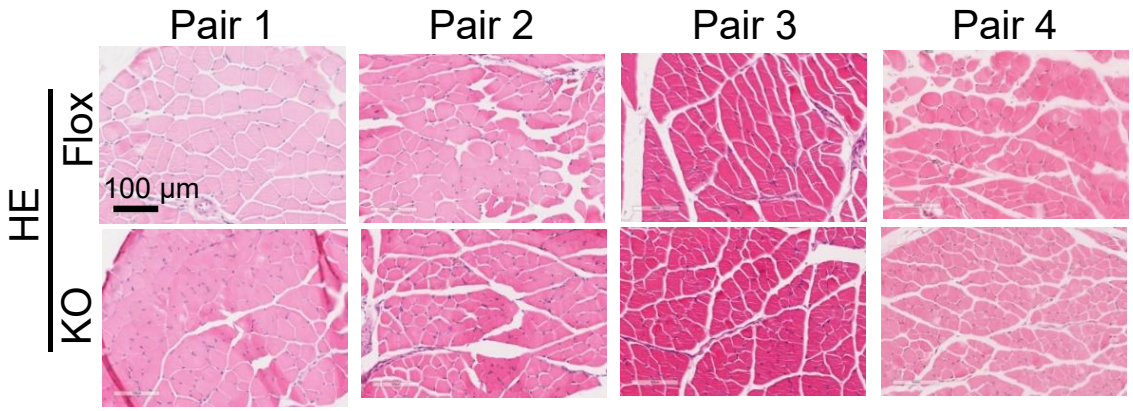

Fig. S10. Representative images of H&E of quadriceps muscles from 4-week- old mice. Scale bar: 100 μm. n = 4.

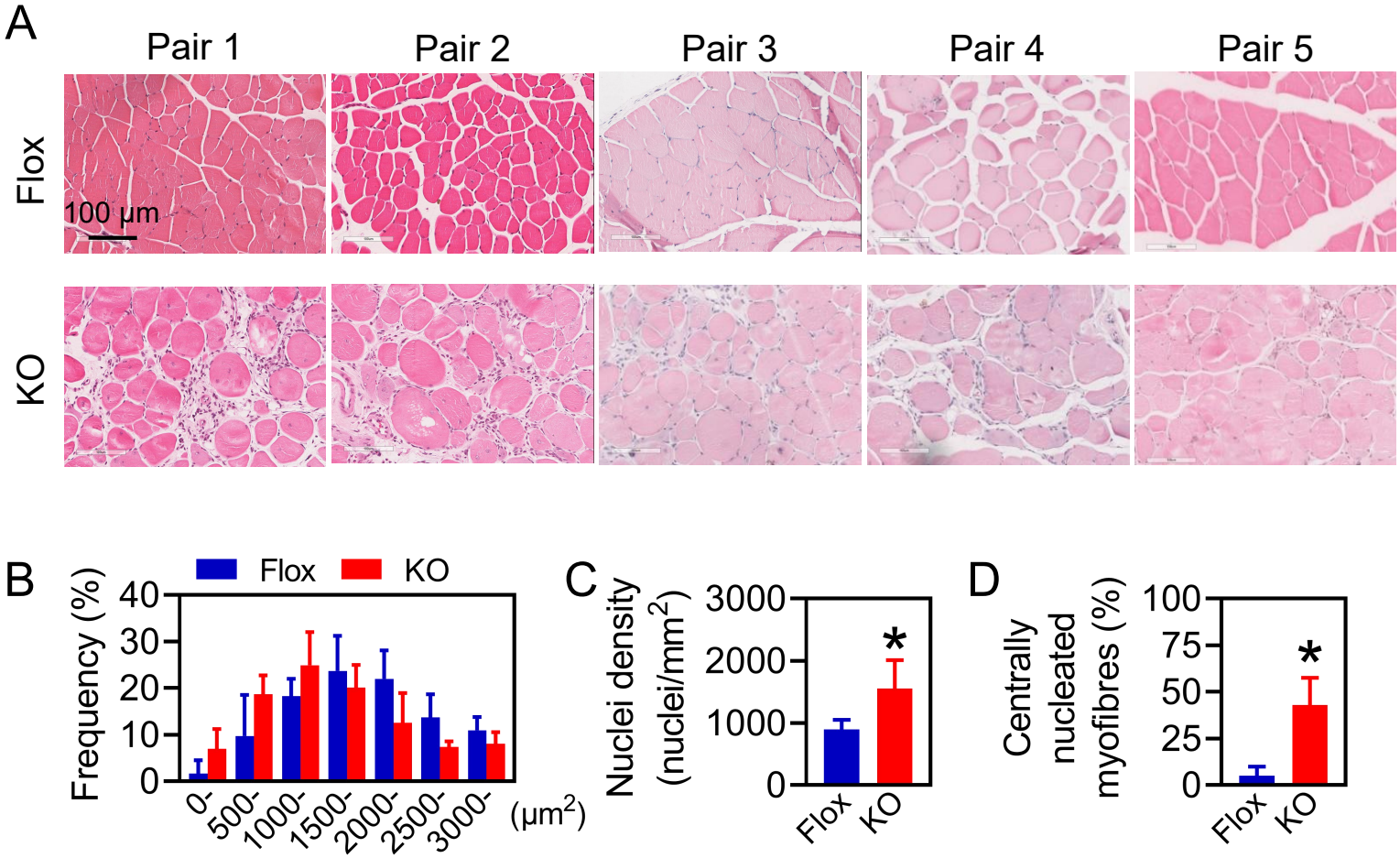

Fig. S11. Pathological staining and quantitative analysis of mouse skeletal muscle tissue. (A) H&E staining of mouse quadriceps muscles. Male mice; n = 5; 20 weeks old. Scale bar: 100 μm. (B–D) Quantitative analysis of muscle fibers in 20-week-old mice from Figure 2 and Figure S10. (B) Fiber size distribution in quadriceps muscles of both genotypes; (C) quantification of nuclear density in quadriceps muscles; (D) quantification of the percentage of centrally nucleated fibers. Male mice; n = 5; 20 weeks old. *$P < 0.05$ vs. Flox group (t-test). All data are presented as mean ± SD in bar plots. Flox, *Nfe2l1*$^{fl/fl}$ mice; KO, striated muscle-specific *Nfe2l1* knockout mice.

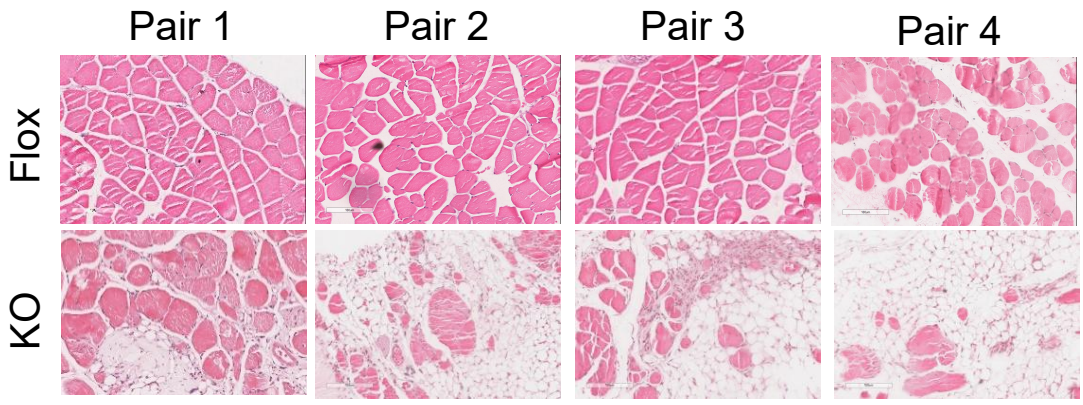

Fig. S12. H&E staining of mouse quadriceps muscles. Male, n = 4, animal age = 50 weeks. Scale bar: 100 µm. Flox, *Nfe2l1*$^{fl/fl}$ mice; KO, striated muscle-specific *Nfe2l1* knockout mice.

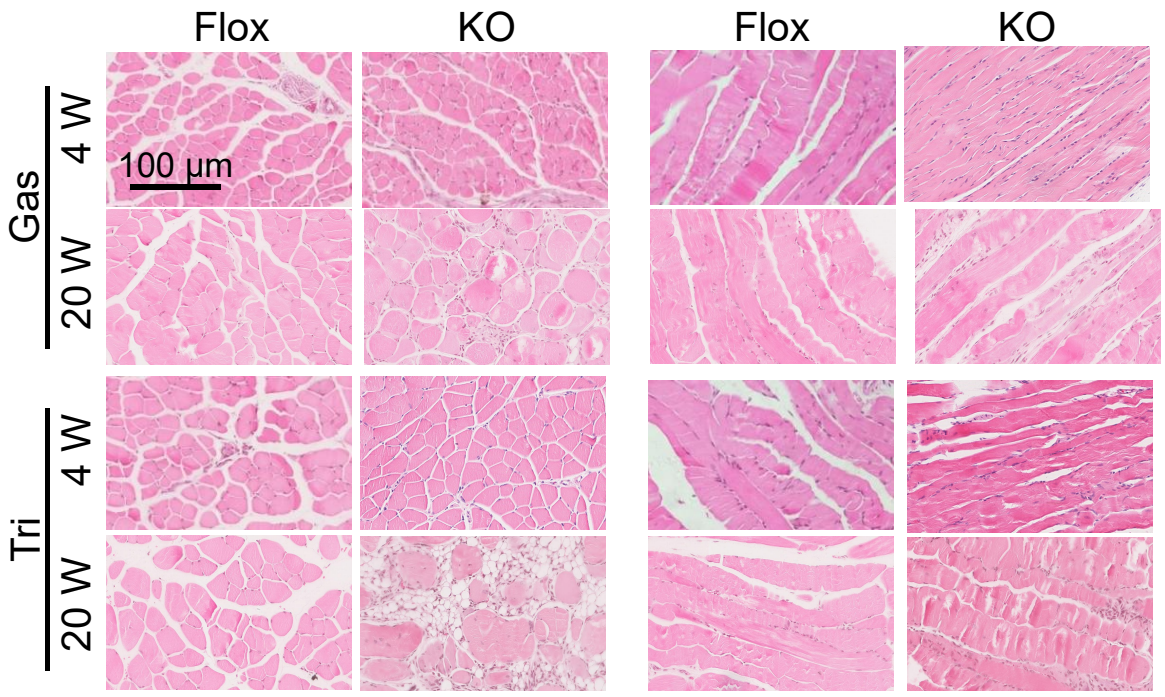

Fig. S13. H&E staining of gastrocnemius muscles and triceps muscles of male mice. The left panels are cross sections; the right panels are longitudinal sections. The animal age = 4 or 20 weeks. Gas, gastrocnemius muscles; Tri, triceps brachii muscles.Flox, *Nfe2l1*$^{fl/fl}$ mice; KO, striated muscle-specific *Nfe2l1* knockout mice.

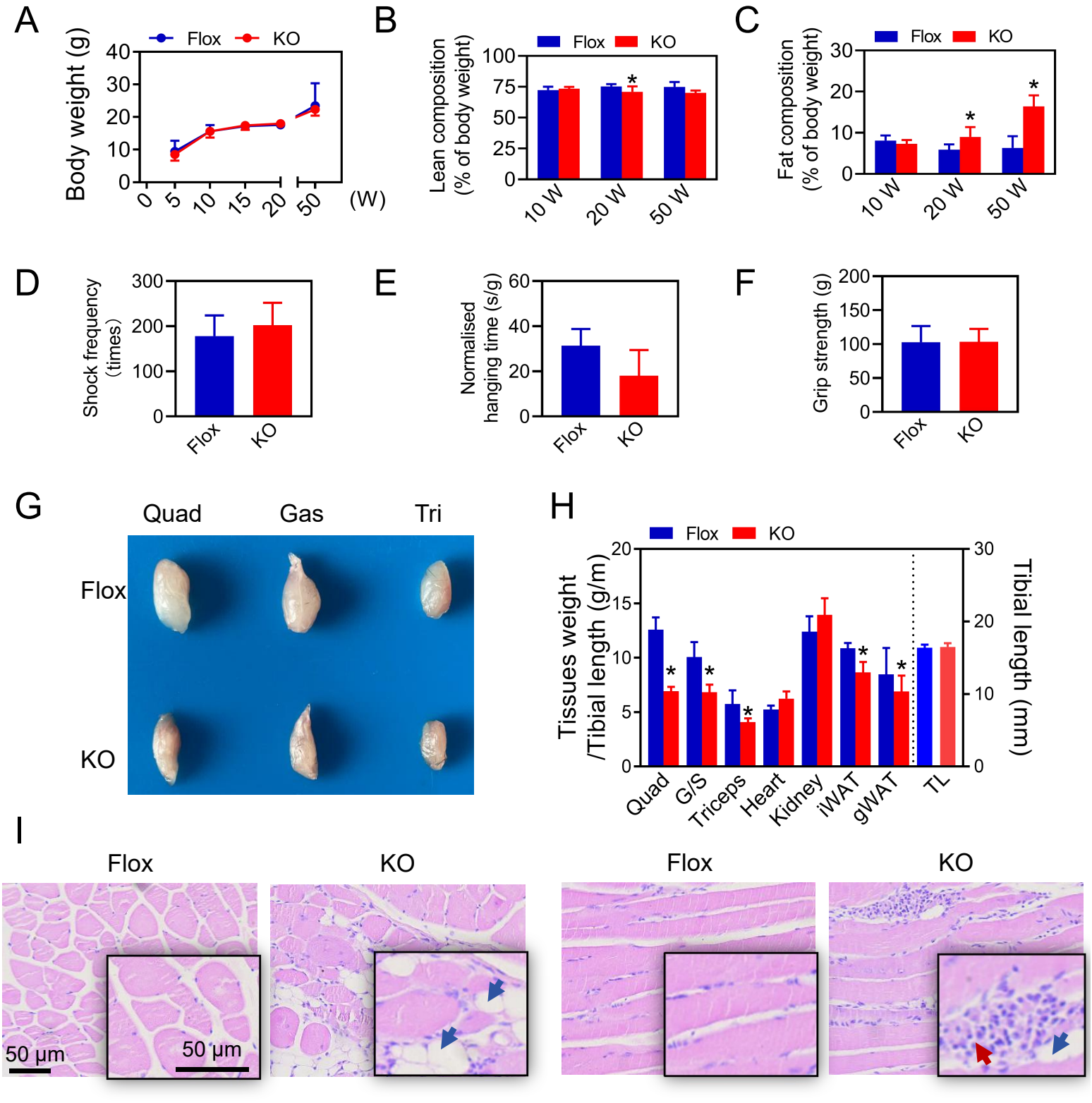

Fig. S14. Impacts of striated muscle-specific deletion of *Nfe2l1* on SkM in female mice. (A) Body weight of mice; (B–C) Analysis of mouse body composition. Female mice; n = 3–8. (D) Electric shock frequency when control mice reached the fatigue point during running; (E) Rotarod performance analysis; (F) Grip strength of mice. Female mice; n = 4–6. **P* < 0.05 vs. Flox group (t-test). All data are presented as mean ± SD in bar plots. (G) Representative images of gross morphology of mouse SkM. n = 3. Quad, Quadriceps muscle; G/S, Gastrocnemius and Soleus muscles; Tri, Triceps brachii muscle; TA, Tibialis anterior muscle. (H) Relative tissue weight of mice. n = 3–7; animals were 20 weeks old. **P* < 0.05 vs. Flox group (t-test). All data are presented as mean ± SD in bar plots. (I) H&E staining of mouse quadriceps muscles. Micrographs show cross-sections (left) and longitudinal sections (right). Aggregation of inflammatory-like cells (red arrows) and adipocyte-like cells in muscle tissue (blue arrows). Scale bar: 50 μm. Flox, *Nfe2l1*$^{fl/fl}$ mice; KO, striated muscle-specific *Nfe2l1* knockout mice.

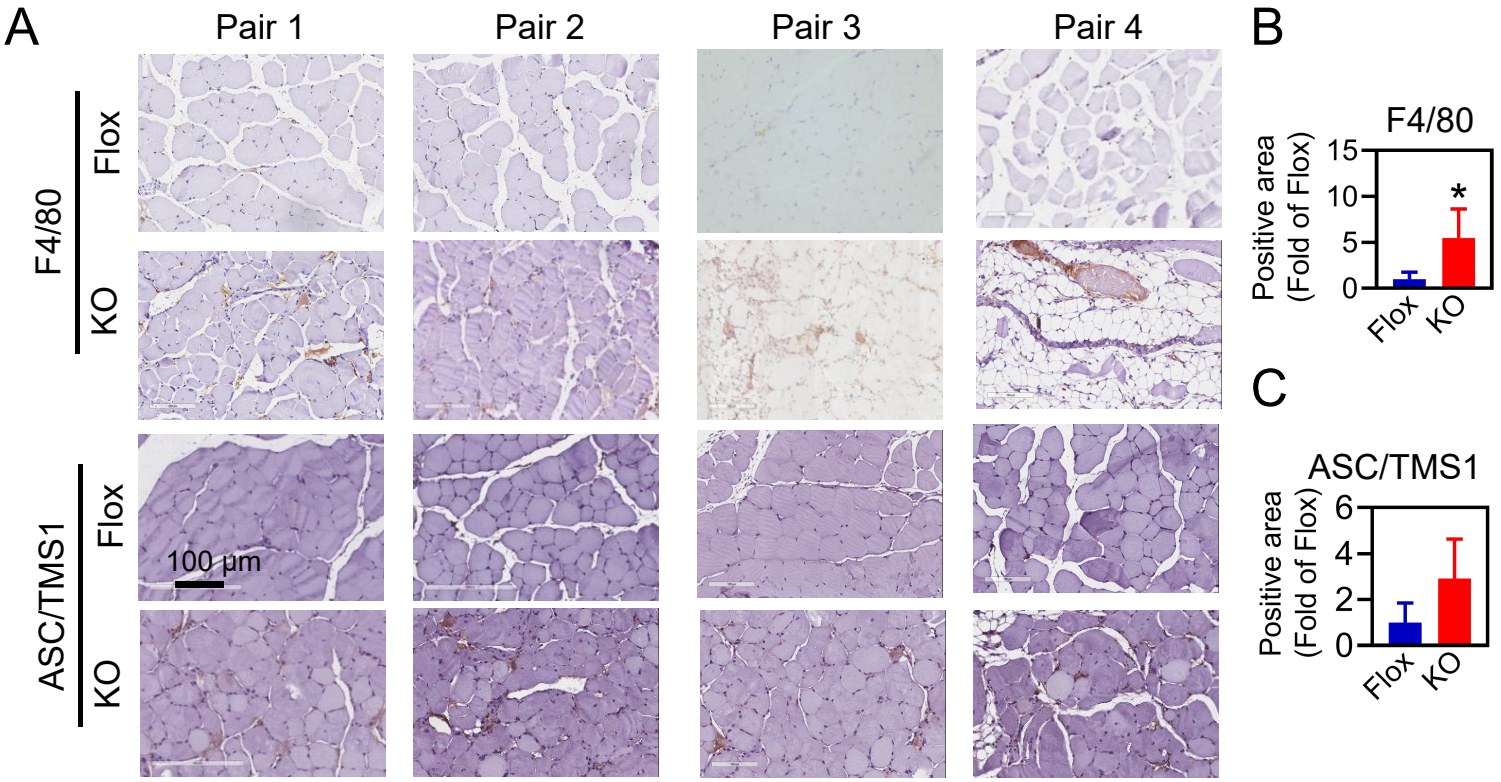

Fig. S15. Representative images of IHC of F4/80 (upper panels) and ASC/TMS1 (lower panels) of quadriceps muscles from 20-week-old male mice. Scale bar: 100 μm. n = 4. Flox, *Nfe2l1*$^{fl/fl}$ mice; KO, striated muscle-specific *Nfe2l1* knockout mice.

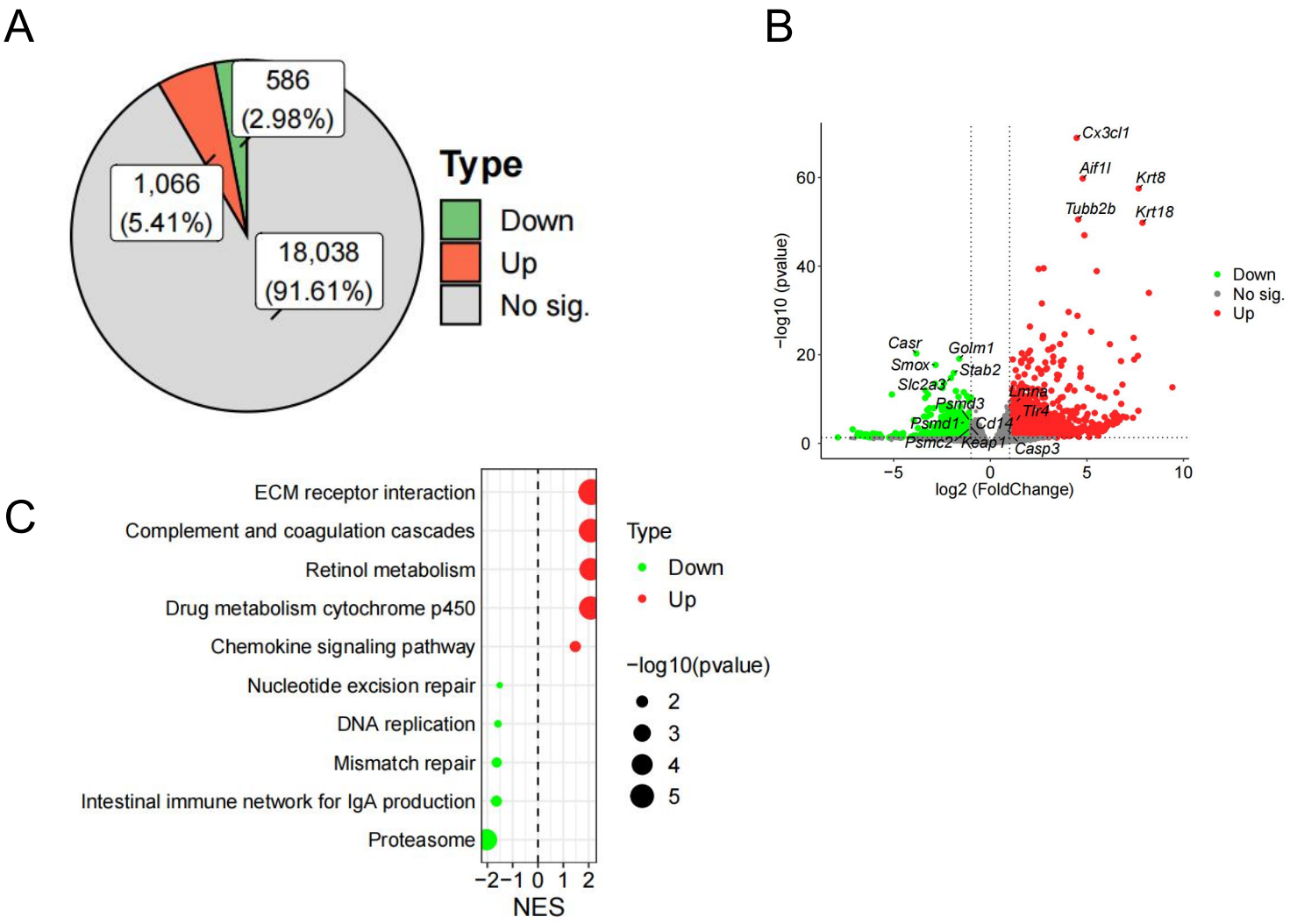

Fig. S16. Analysis results of RNA-seq data. 20-week-old male Flox and KO mice, n = 3. (A) Results of differential expression analysis (DEA) of RNA-seq data. (B) Volcano plot displaying the top five most significantly up-regulated and down-regulated genes, and proteasome subunit genes and apoptosis-related genes. (C) Bubble plot representing gene set enrichment analysis (GSEA) results with the KEGG database.

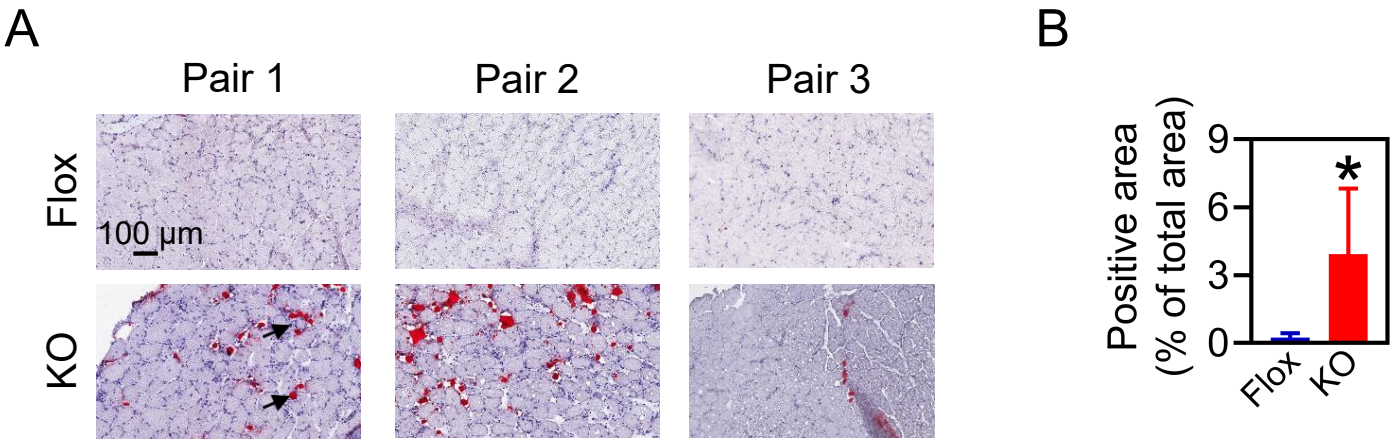

Fig. S17. Oil-red O staining of mouse quadriceps muscles. (A) Representative images of oil-red O staining. (B) Quantitative analysis of positive area in (A). Male, n = 3, animal age = 20 weeks. Scale bar: 100 μm. Flox, *Nfe2l1*$^{fl/fl}$ mice; KO, striated muscle-specific *Nfe2l1* knockout mice.

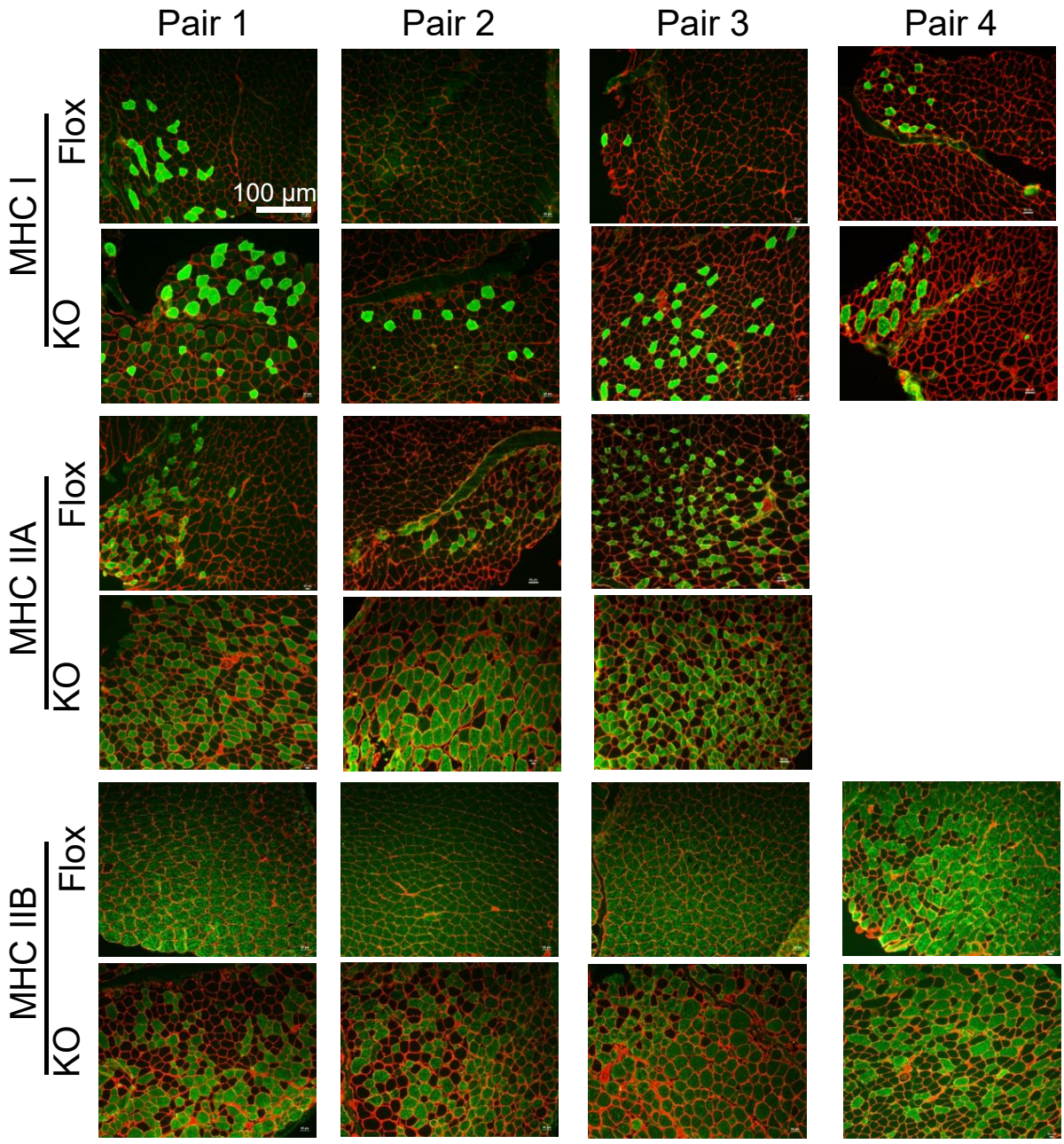

Fig. S18. Representative images of IF staining of gastrocnemius muscles. Animal age = 20 weeks. Male. n = 3-4. Flox: *Nfe2l1*-Floxed; KO: *Nfe2l1*(SM)-KO.

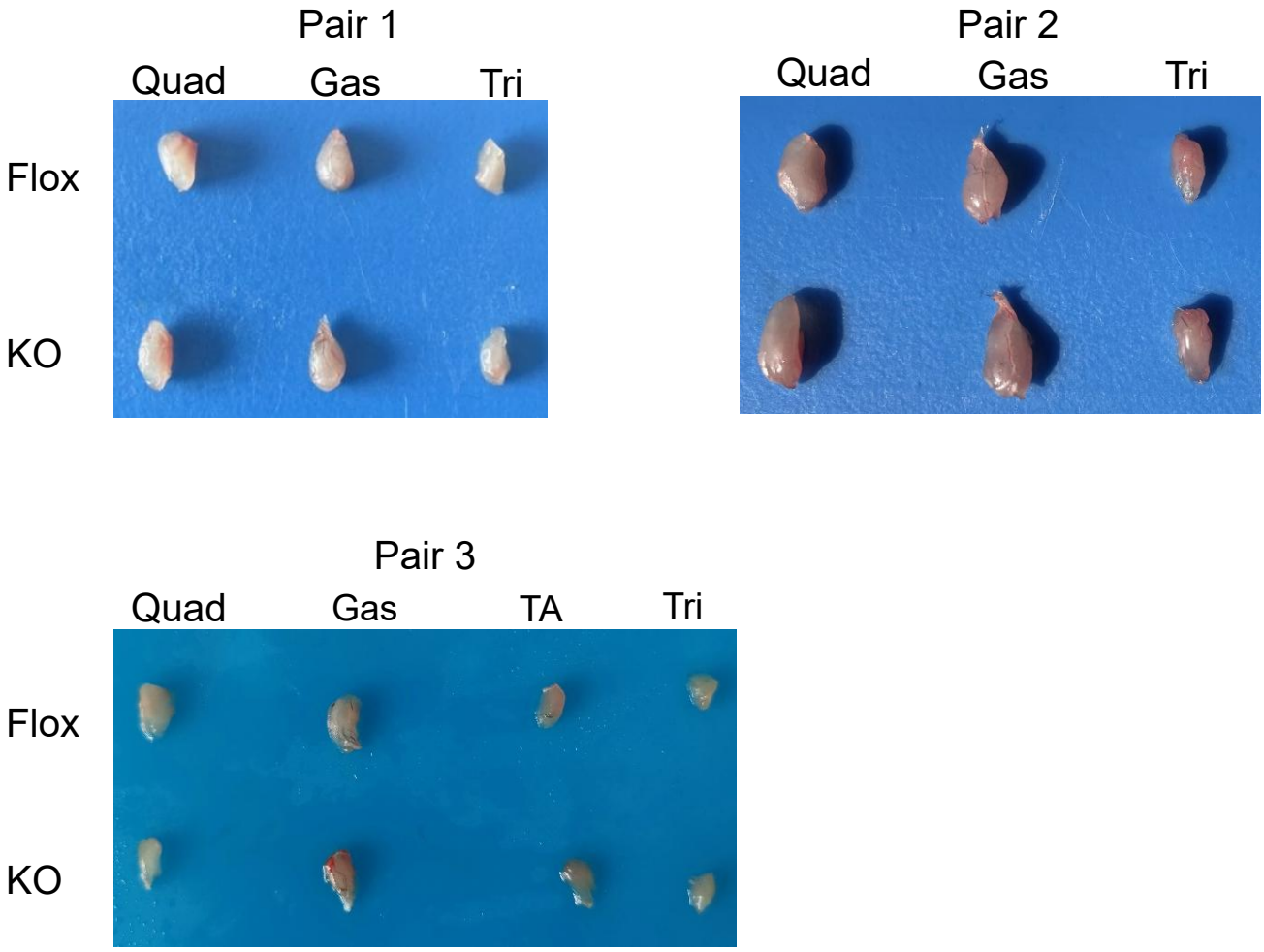

Fig. S19. Gross morphology of skeletal muscles. n = 3 males. Animal age = 4 weeks. Quad, quadriceps; Gas, gastrocnemius muscles; Tri, triceps brachii; TA, tibialis anterior. Flox, *Nfe2l1*$^{fl/fl}$ mice; KO, striated muscle-specific *Nfe2l1* knockout mice.

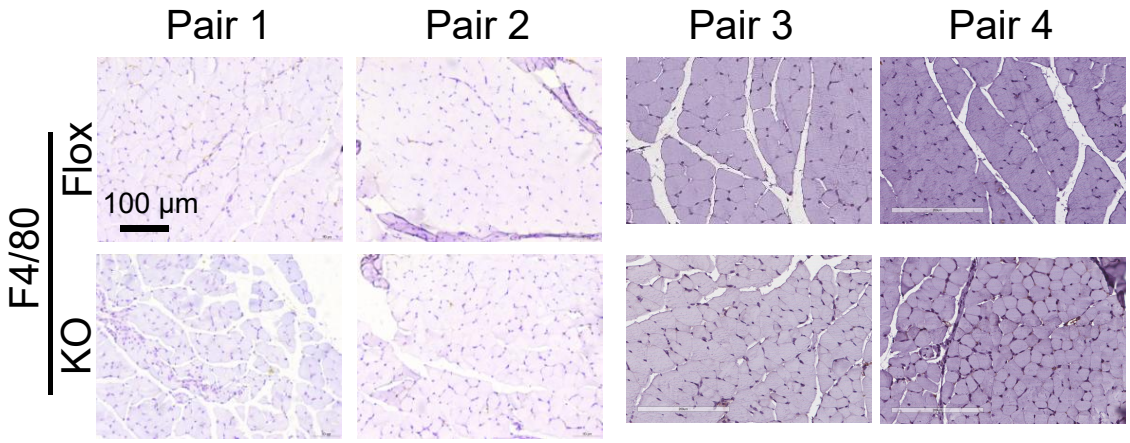

Fig. S20. Representative images of IHC of F4/80 of quadriceps muscles from 4-week-old male mice. Scale bar: 100 μm. n = 4. Flox, *Nfe2l1*$^{fl/fl}$ mice; KO, striated muscle-specific *Nfe2l1* knockout mice.

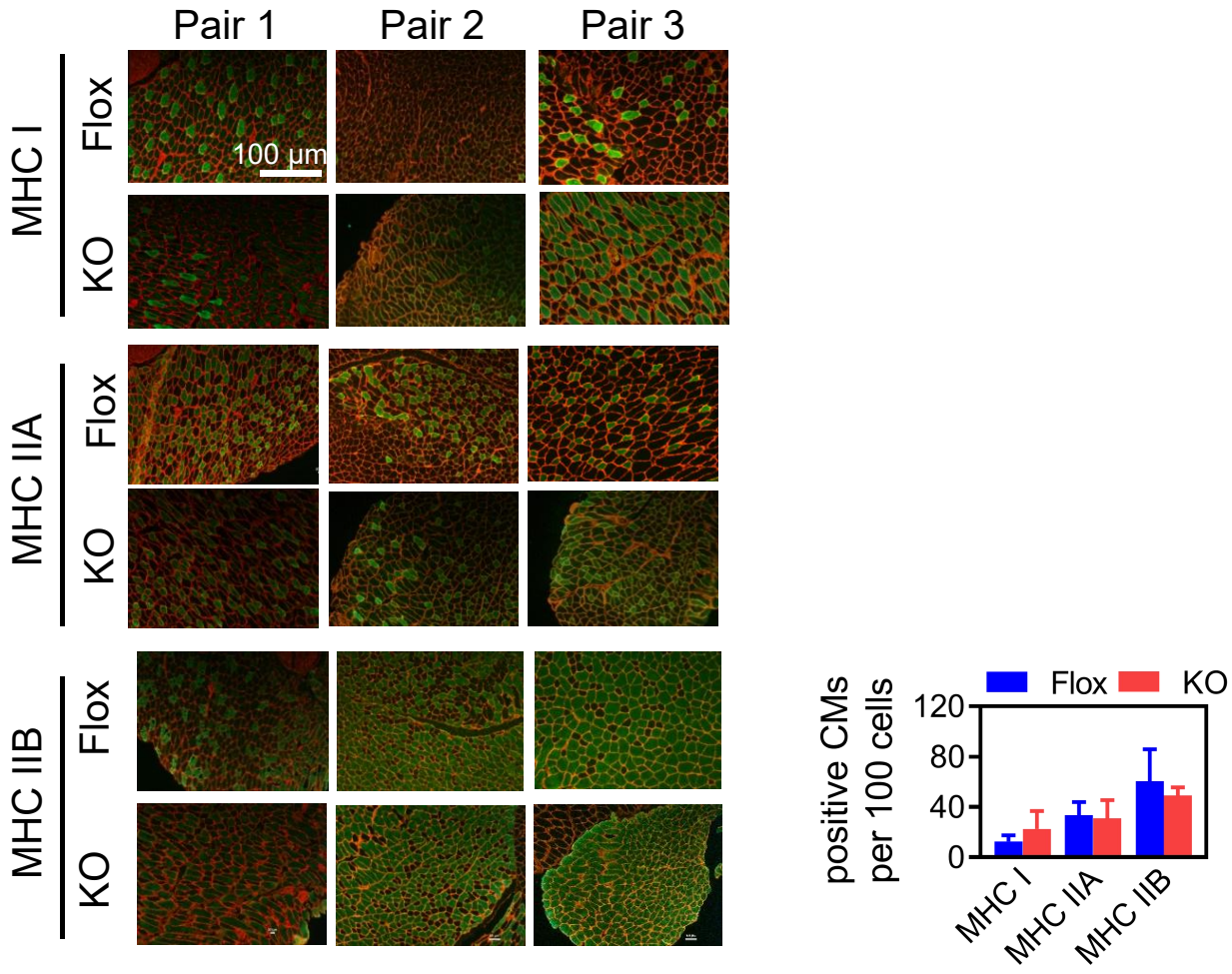

Fig. S21. Representative images (left panels) and quantification (right panel) of immunofluorescence staining of calf muscles. MYH7, Myosin Heavy Chain 7; MYH2, Myosin Heavy Chain 2; MYH4, Myosin Heavy Chain 4. Male animal age = 4 weeks. n = 4.

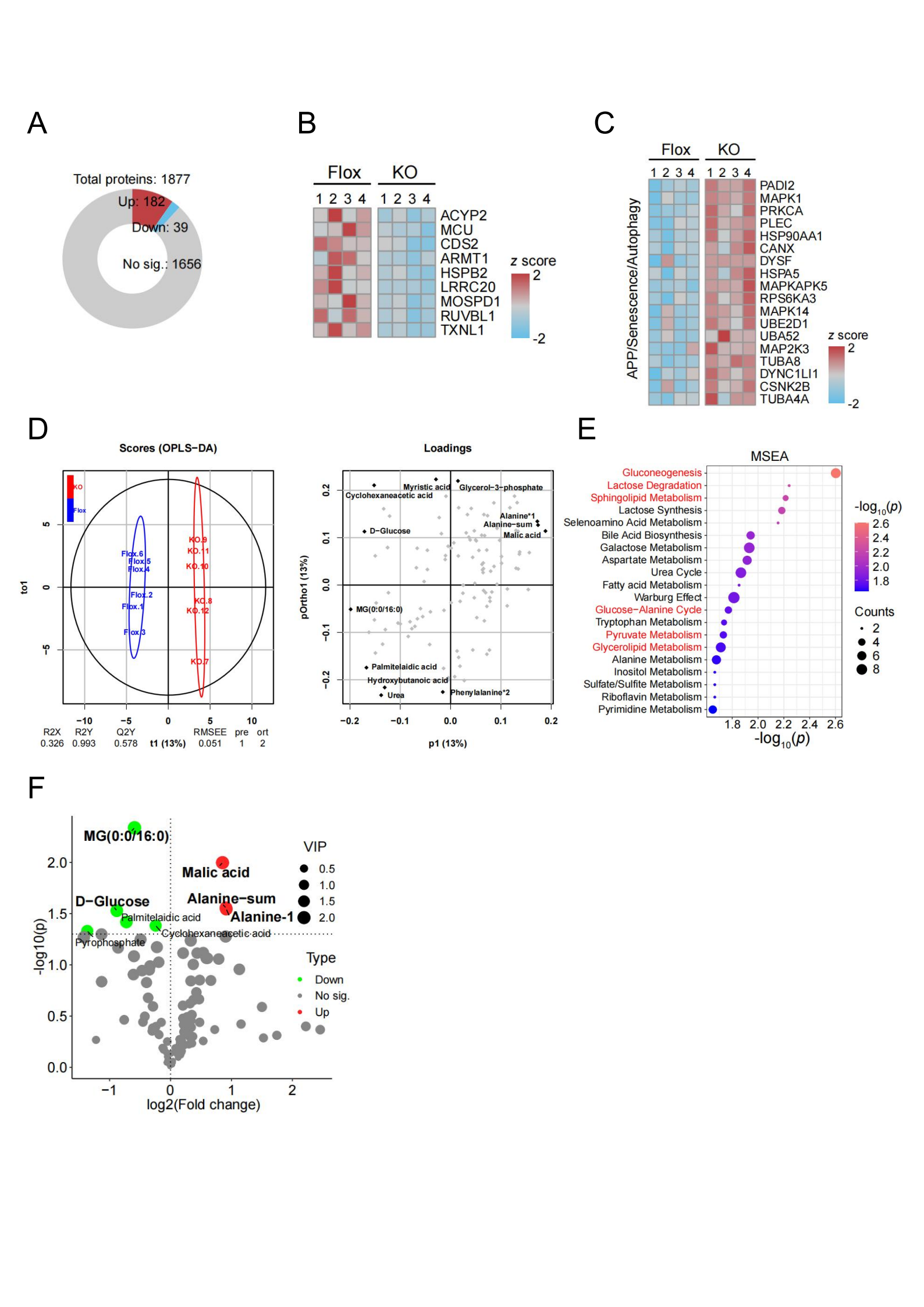
A
Total proteins: 1877
Up: 182
Down: 39
No sig.: 1656
B
Flox
KO
1 2 3 4 1 2 3 4
ACYP2
MCU
CDS2
ARMT1
HSPB2
LRRC20
MOSPD1
RUVBL1
TXNL1
z score
2
-2
C
Flox
KO
1 2 3 4 1 2 3 4
APP/Senescence/Autophagy
PADI2
MAPK1
PRKCA
PLEC
HSP90AA1
CANX
DYSF
HSPA5
MAPKAPK5
RPS6KA3
MAPK14
UBE2D1
UBA52
MAP2K3
TUBA8
DYNC1LI1
CSNK2B
TUBA4A
z score
2
-2
D
Scores (OPLS-DA)
ko
Flox
Flox.6
Flox.5
Flox.4
Flox.2
Flox.1
Flox.3
KO.9
KO.11
KO.10
KO.8
KO.12
KO.7
to1
t1 (13%)
R2X 0.326
R2Y 0.993
Q2Y 0.578
RMSEE 0.051
pre 1
ort 2
Loadings
Myristic acid
Glycerol-3-phosphate
Cyclohexaneacetic acid
Alanine*1
Alanine-sum
Malic acid
D-Glucose
MG(0:0/16:0)
Palmitelaidic acid
Hydroxybutanoic acid
Urea
Phenylalanine*2
pOrtho1 (13%)
p1 (13%)
E
MSEA
Gluconeogenesis
Lactose Degradation
Sphingolipid Metabolism
Lactose Synthesis
Selenoamino Acid Metabolism
Bile Acid Biosynthesis
Galactose Metabolism
Aspartate Metabolism
Urea Cycle
Fatty acid Metabolism
Warburg Effect
Glucose-Alanine Cycle
Tryptophan Metabolism
Pyruvate Metabolism
Glycerolipid Metabolism
Alanine Metabolism
Inositol Metabolism
Sulfate/Sulfite Metabolism
Riboflavin Metabolism
Pyrimidine Metabolism
-log10(p)
Counts
-log10(p)
F
MG(0:0/16:0)
Malic acid
D-Glucose
Alanine-sum
Alanine-1
Palmitelaidic acid
Cyclohexaneacetic acid
Pyrophosphate
VIP
0.5
1.0
1.5
2.0
Type
Down
No sig.
Up
-log10(p)
log2(Fold change)

G

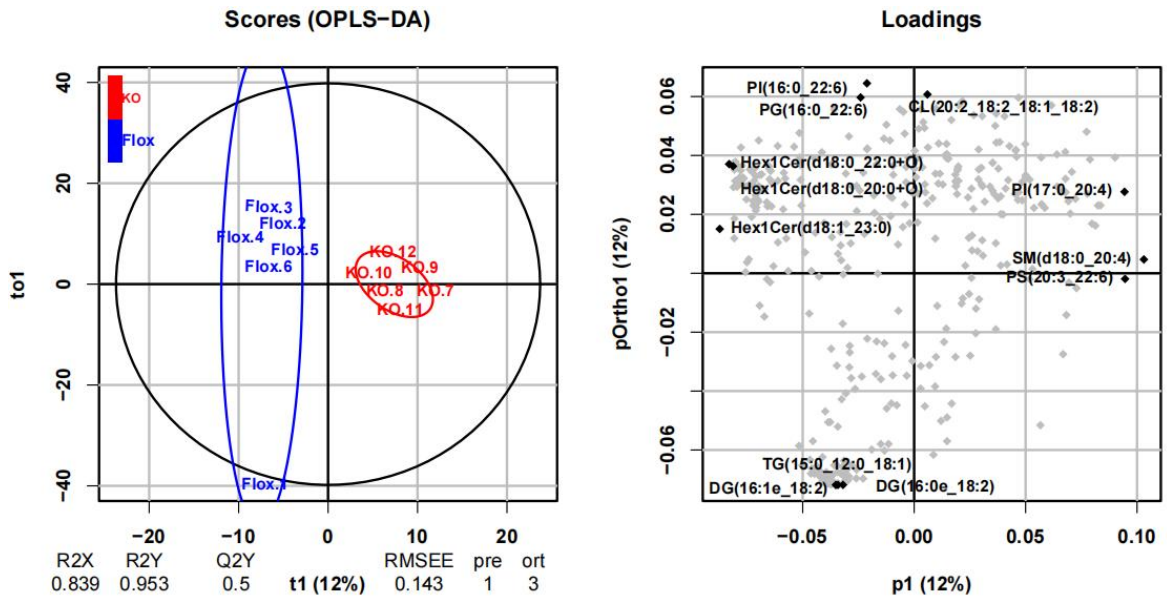
Scores (OPLS−DA)
KO
Flox
Flox.3
Flox.2
Flox.4
Flox.5
Flox.6
Flox.1
KO.12
KO.10
KO.9
KO.8
KO.7
KO.11
to1
R2X R2Y Q2Y RMSEE pre ort
0.839 0.953 0.5 t1 (12%) 0.143 1 3
Loadings
PI(16:0_22:6)
PG(16:0_22:6)
CL(20:2_18:2_18:1_18:2)
Hex1Cer(d18:0_22:0+O)
Hex1Cer(d18:0_20:0+O)
PI(17:0_20:4)
Hex1Cer(d18:1_23:0)
SM(d18:0_20:4)
PS(20:3_22:6)
TG(15:0_12:0_18:1)
DG(16:1e_18:2)
DG(16:0e_18:2)
pOrtho1 (12%)
p1 (12%)

H

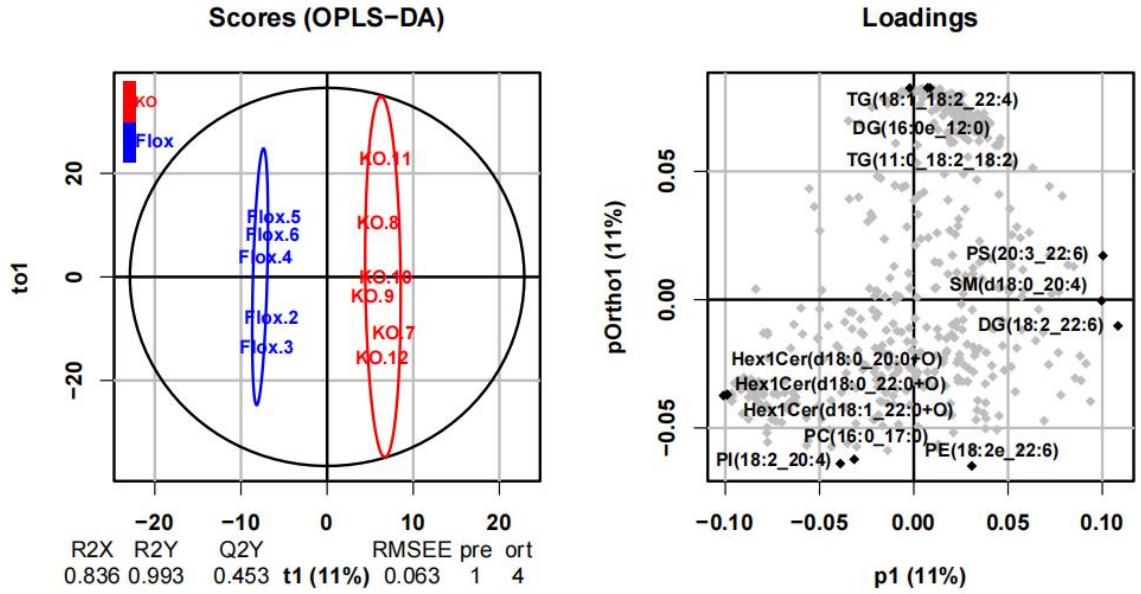
Scores (OPLS−DA)
KO
Flox
KO.11
KO.8
KO.10
KO.9
KO.7
KO.12
Flox.5
Flox.6
Flox.4
Flox.2
Flox.3
to1
R2X R2Y Q2Y RMSEE pre ort
0.836 0.993 0.453 t1 (11%) 0.063 1 4
Loadings
TG(18:1_18:2_22:4)
DG(16:0e_12:0)
TG(11:0_18:2_18:2)
PS(20:3_22:6)
SM(d18:0_20:4)
DG(18:2_22:6)
Hex1Cer(d18:0_20:0+O)
Hex1Cer(d18:0_22:0+O)
Hex1Cer(d18:1_22:0+O)
PC(16:0_17:0)
PI(18:2_20:4)
PE(18:2e_22:6)
pOrtho1 (11%)
p1 (11%)

I

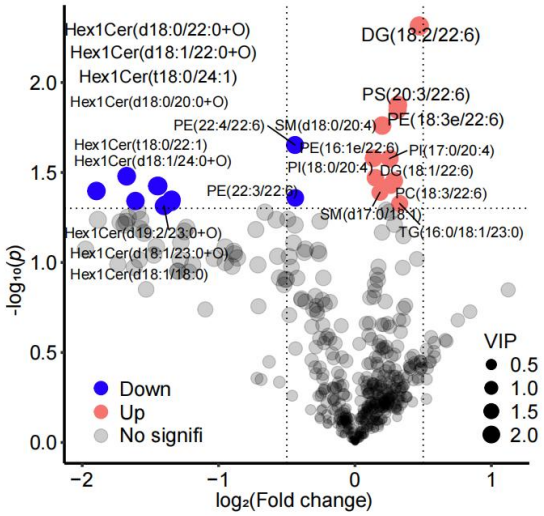
Hex1Cer(d18:0/22:0+O)
Hex1Cer(d18:1/22:0+O)
Hex1Cer(t18:0/24:1)
Hex1Cer(d18:0/20:0+O)
PE(22:4/22:6)
SM(d18:0/20:4)
Hex1Cer(t18:0/22:1)
Hex1Cer(d18:1/24:0+O)
PE(16:1e/22:6)
PI(18:0/20:4)
PE(22:3/22:6)
SM(d17:0/18:1)
Hex1Cer(d19:2/23:0+O)
Hex1Cer(d18:1/23:0+O)
Hex1Cer(d18:1/18:0)
DG(18:2/22:6)
PS(20:3/22:6)
PE(18:3e/22:6)
PI(17:0/20:4)
DG(18:1/22:6)
PC(18:3/22:6)
TG(16:0/18:1/23:0)
-log10(p)
log2(Fold change)
Down
Up
No signifi
VIP
0.5
1.0
1.5
2.0

Fig. S22. Proteomics and metabolomics analysis details. (A) Distribution plot of differentially expressed proteins. (B) Heatmap of selected downregulated proteins (not annotated to the UPS pathway). (C) Heatmap of selected upregulated proteins (annotated to antigen processing and presentation/cellular senescence/autophagy pathways). (D) Results of untargeted metabolomics orthogonal partial least squares discriminant analysis (OPLS-DA). The left panel shows the sample score distribution from OPLS-DA analysis, and the right panel displays the contribution of each metabolite variable in the OPLS-DA model (i.e., their impact on group separation). (E) Bubble plot of MSEA (metabolite set enrichment analysis) results, where bubble color represents statistical significance and bubble size indicates the number of hit metabolites. (F) Volcano plot of differential metabolite analysis results; the color of each dot represents the direction of regulation, and the size indicates the VIP value (obtained from OPLS-DA). (G, H) Lipidomics OPLS-DA results (G shows all samples, H with Flox sample 1 excluded), with details as in (D). (I) Volcano plot of differential analysis results for lipid metabolites. For details of the differential and enrichment analyses, see the Methods section.

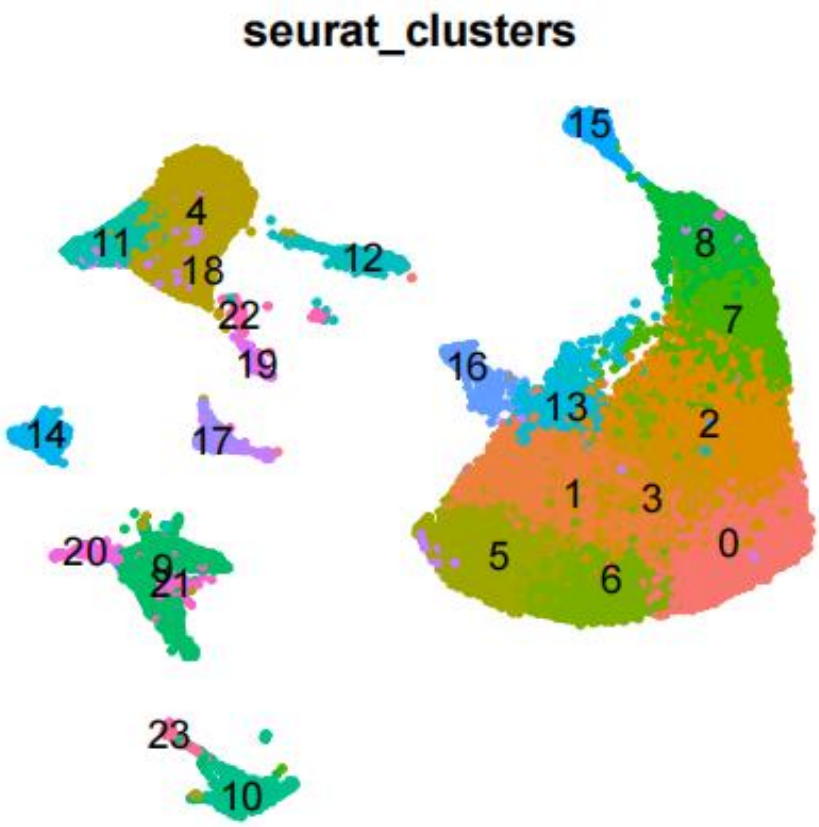

Fig. S23. Identification of 24 clusters, numbered 0 to 23, prior to cell type determination.

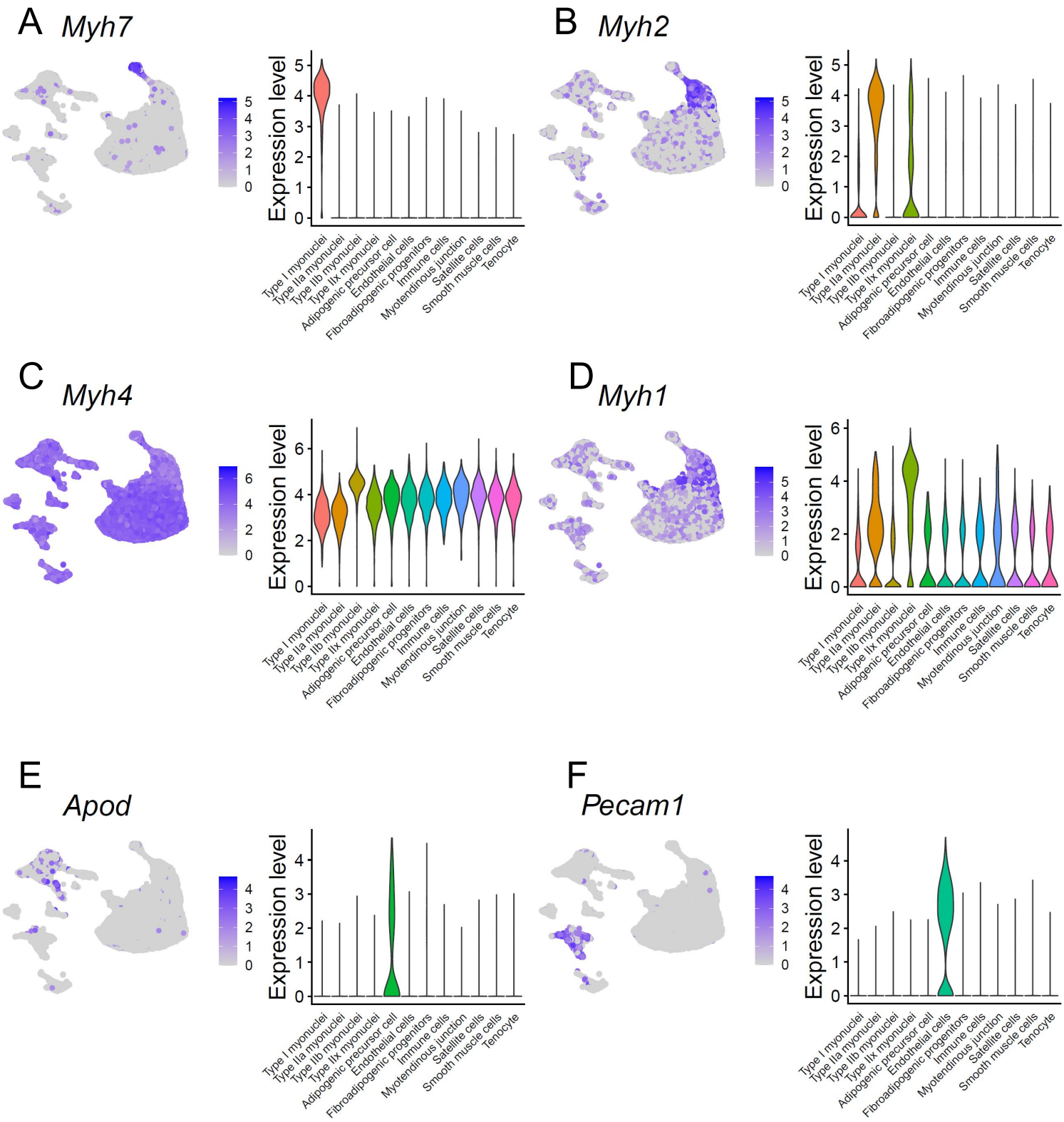
A Myh7
B Myh2
C Myh4
D Myh1
E Apod
F Pecam1
Expression level
Type I myonuclei
Type IIa myonuclei
Type IIb myonuclei
Type IIx myonuclei
Adipogenic precursor cell
Endothelial cells
Fibroadipogenic progenitors
Immune cells
Myotendinous junction
Satellite cells
Smooth muscle cells
Tenocyte

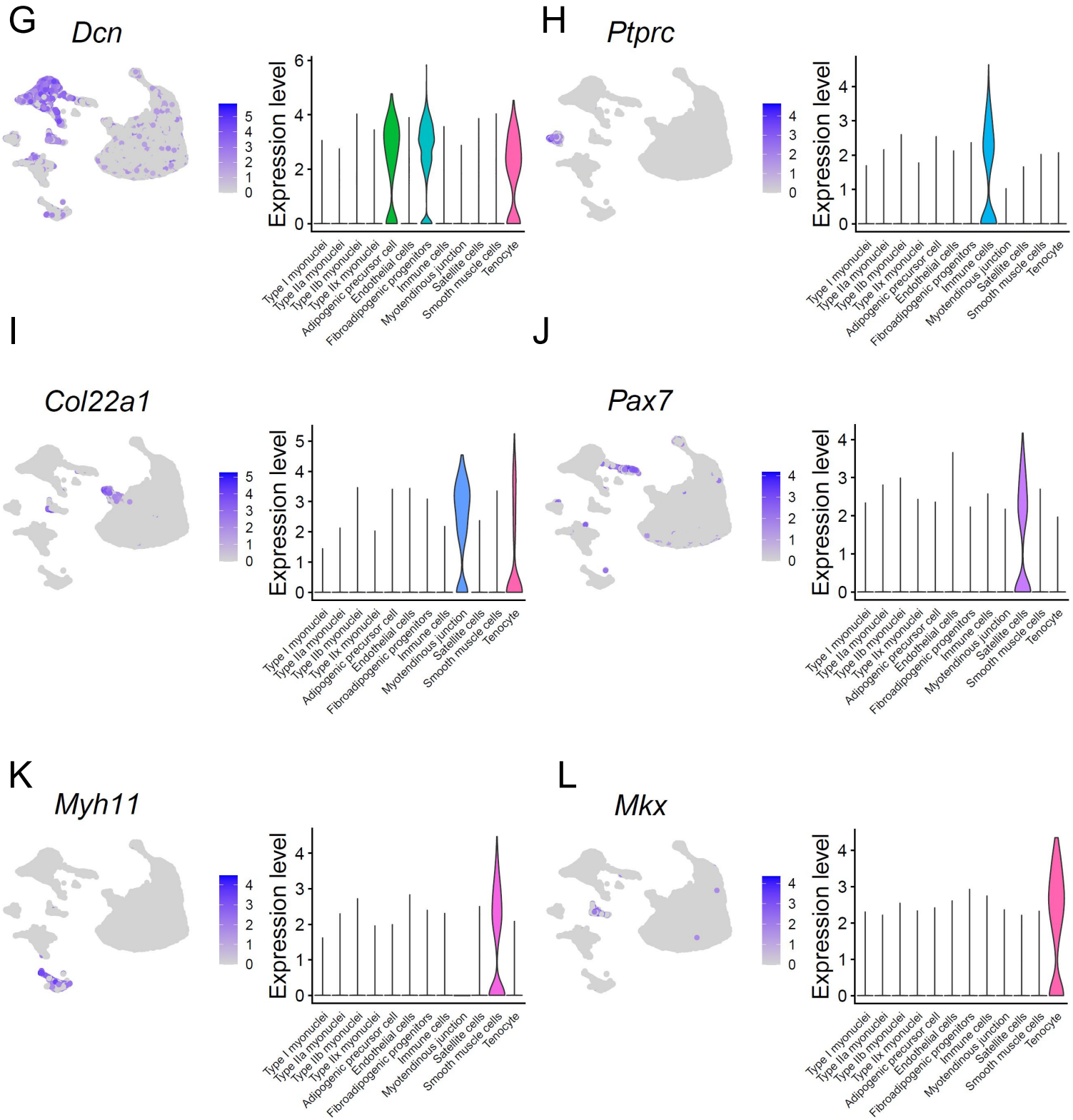
G
Dcn
H
Ptprc
I
Col22a1
J
Pax7
K
Myh11
L
Mkx
Expression level
Type I myonuclei
Type IIa myonuclei
Type IIb myonuclei
Type IIx myonuclei
Adipogenic precursor cell
Endothelial cells
Fibroadipogenic progenitors
Immune cells
Myotendinous junction
Satellite cells
Smooth muscle cells
Tenocyte

M

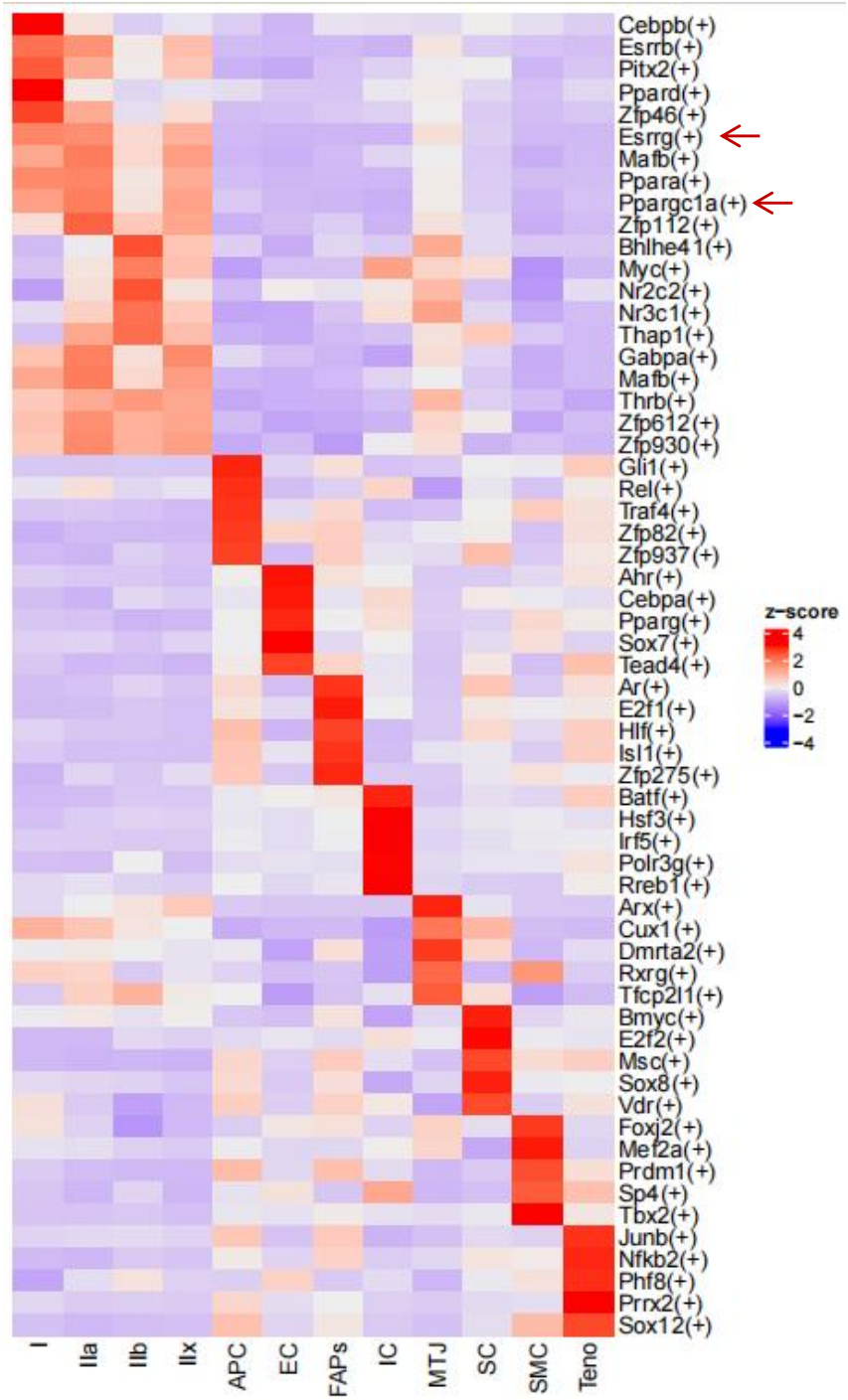

Fig. S24. Cell cluster identification. (A-L) Type I myonuclei (*Myh7*) , type IIa myonuclei (*Myh2*), type IIb myonuclei (*Myh4*) , type IIx myonuclei (*Myh1*), adipogenic precursor cells (*Apod*), endothelial cells (*Pecam1*), fibroadipogenic progenitors (*Dcn*) , immune cells (*Ptprc*), myotendinous junction (*Col22a1*), satellite cells (*Pax7*), smooth muscle cells (*Myh11*) and tenocyte (*Mkx*). (M) Top five specific regulons for each nuclear type.

A

The number of differentially expressed genes between groups (KO/Flox)

Annotation	Down	Up
IIb	200	266
IIx	211	201
IIa	138	188
MTJ	40	30
I	24	24

B

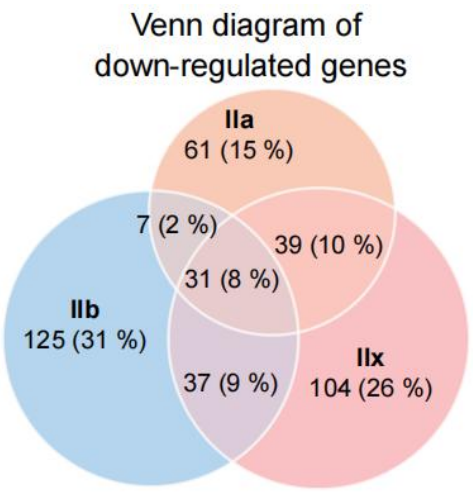

C

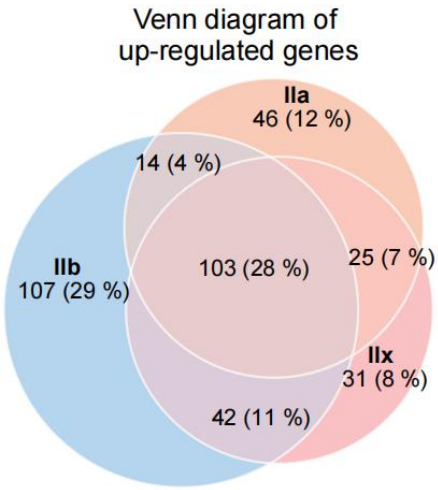

D

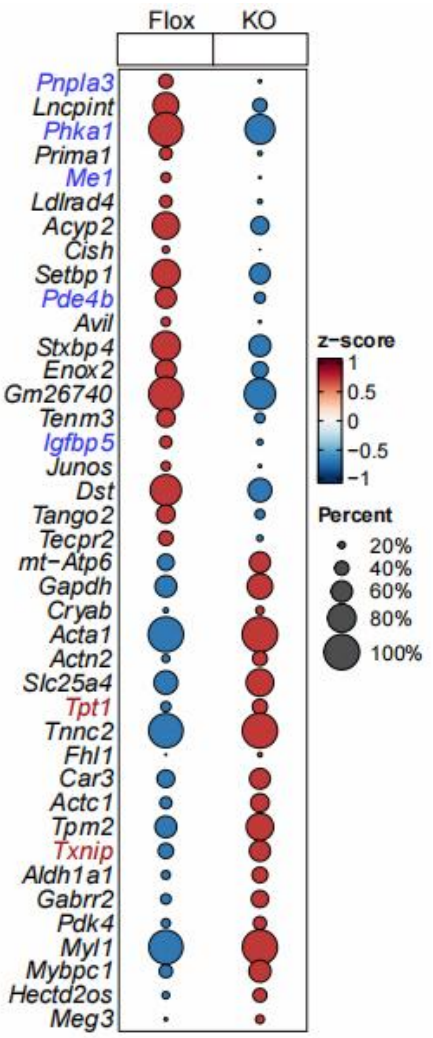

E

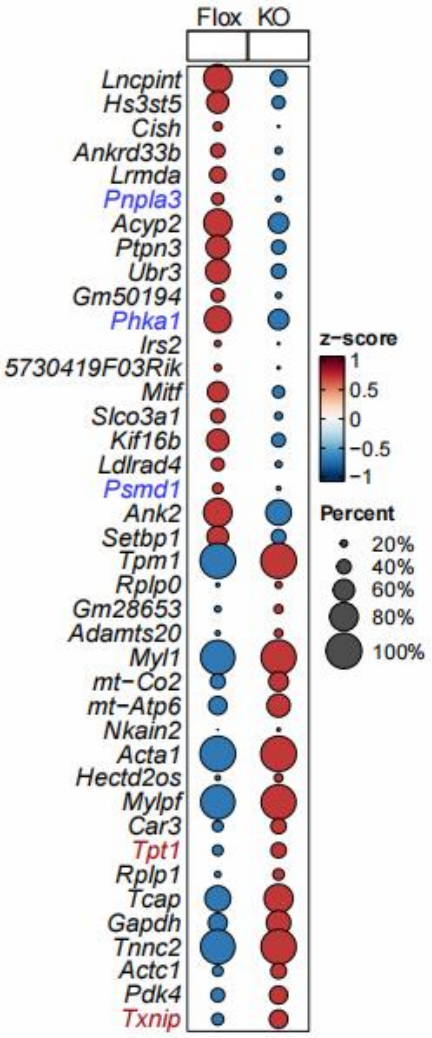

F

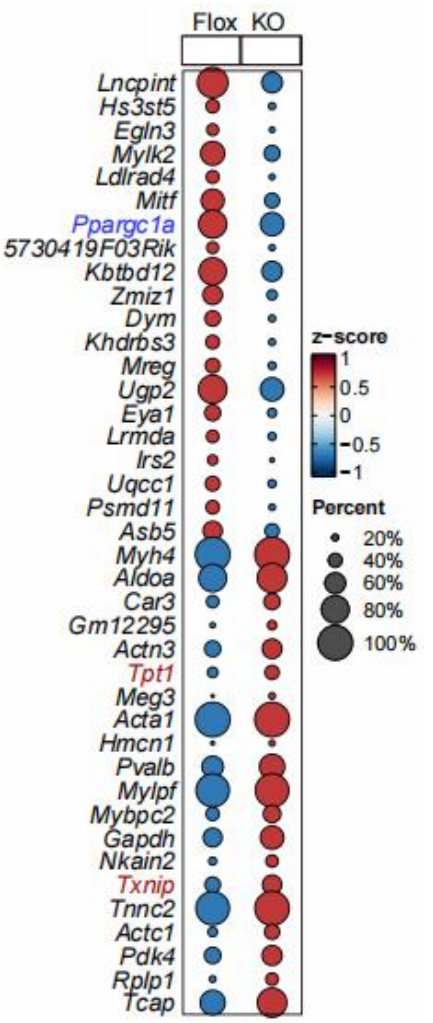

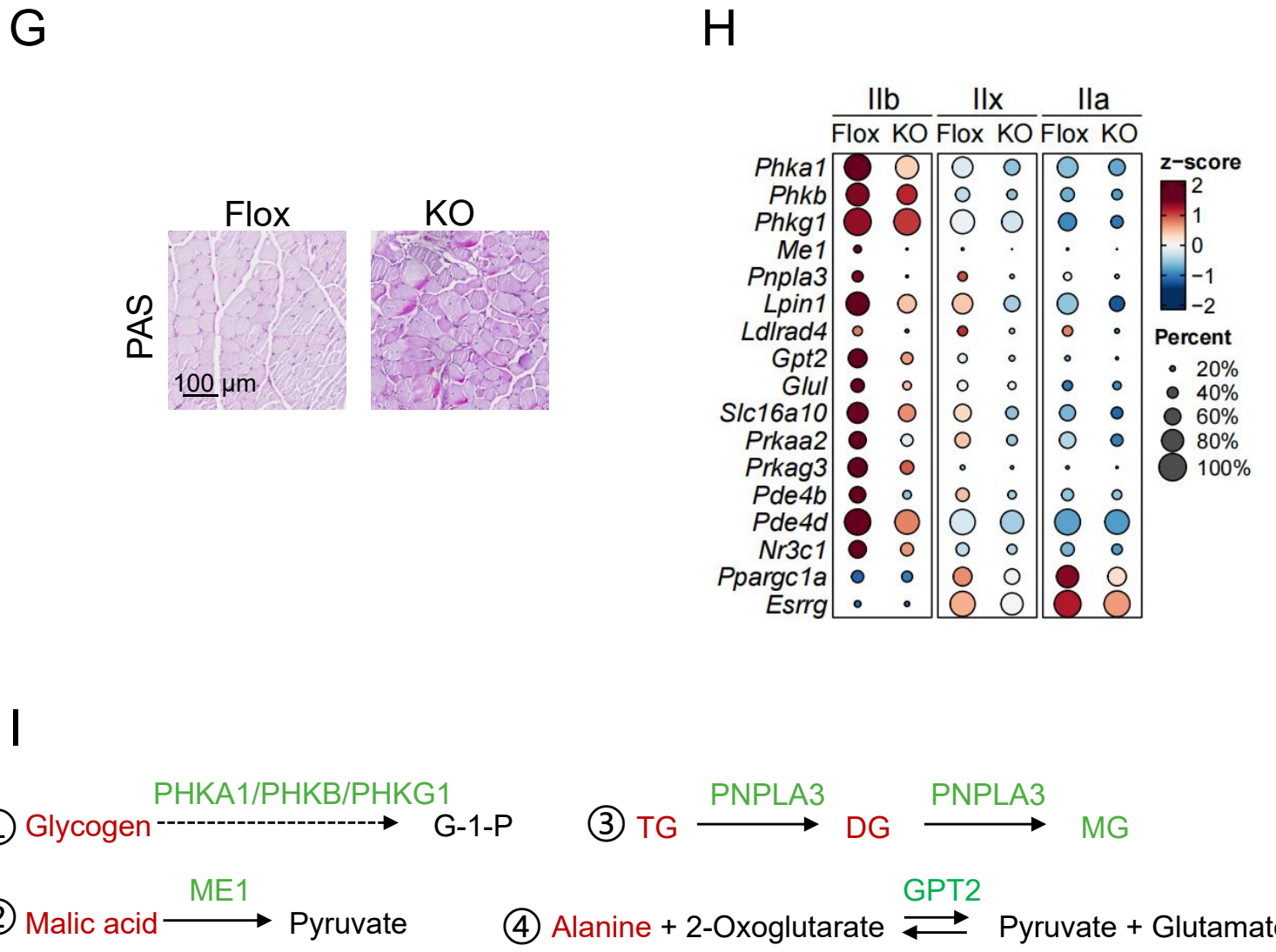

Fig. S25. Details of differential expression analysis between different myonuclear types in KO and Flox groups. (A) Results of differential expression analysis between groups for five types of myonuclei. (B-C) Venn diagrams showing the number of genes that are downregulated (B) and upregulated (C) in type IIb, type IIx, and type IIa myonuclei in the KO group. (D–F) Bubble plots depicting the top 20 down-regulated and up-regulated genes with the greatest fold changes between Flox and KO groups in IIb (D), IIx (E), and IIa (F) myonuclei. The color of each bubble represents the average expression level (z score), and the size represents the percentage of cells expressing the gene. (G) PAS (Periodic acid-Schiff) staining of skeletal muscle glycogen, showing the difference between Flox and KO groups. Scale bar, 100 μm. (H) Bubble plot showing the expression of significantly downregulated metabolism-related genes in three major myonuclear types (IIb, IIx, IIa) in KO mice based on snRNA-seq data. Bubble color represents the mean expression level (z score), and bubble size represents the percentage of expressing cells. (I) Simplified metabolic reaction schematic based on the Reactome database. Dashed lines indicate proteins (such as PHKA1) indirectly involved in catalytic reactions as kinases, while solid lines indicate direct involvement (such as ME1). Red text indicates metabolites significantly increased in the KO group, and green indicates metabolites or gene expression levels significantly decreased in the KO group.

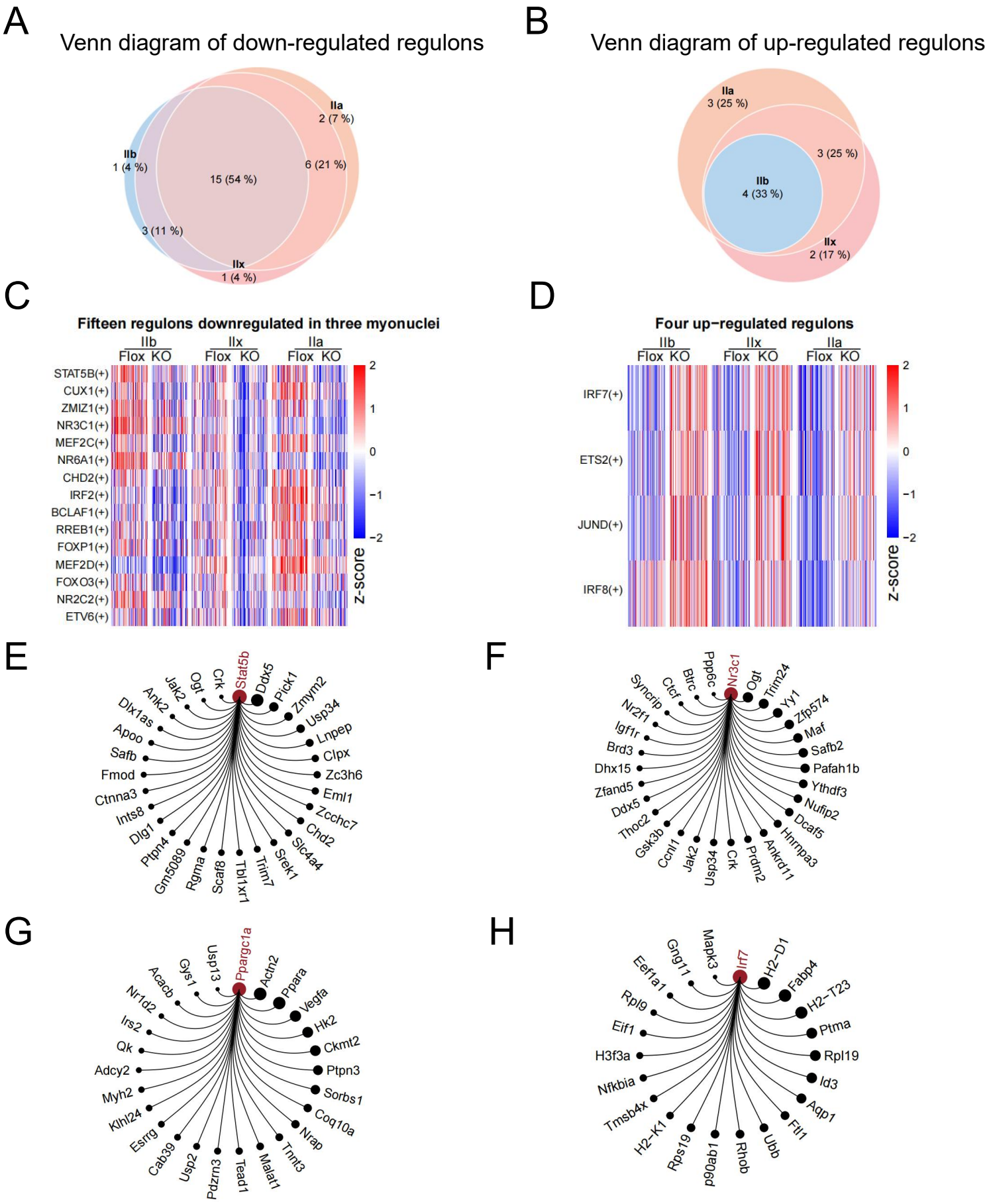

Fig. S26. Details of SCENIC analysis. (A) Venn diagram showing regulons downregulated across three myonuclei. (B) Venn diagram illustrating regulons upregulated across three myonuclei. (C) Heat map displaying the activity of 15 regulons downregulated in all three myonuclei. (D) Heat map showing regulons with upregulated activity across all three myonuclei. (E-H) Regulatory network diagrams of four representative regulons of interest (STAT5B(+), NR3C1(+), PPARGC1A(+), IRF7(+)) obtained from SCENIC analysis.

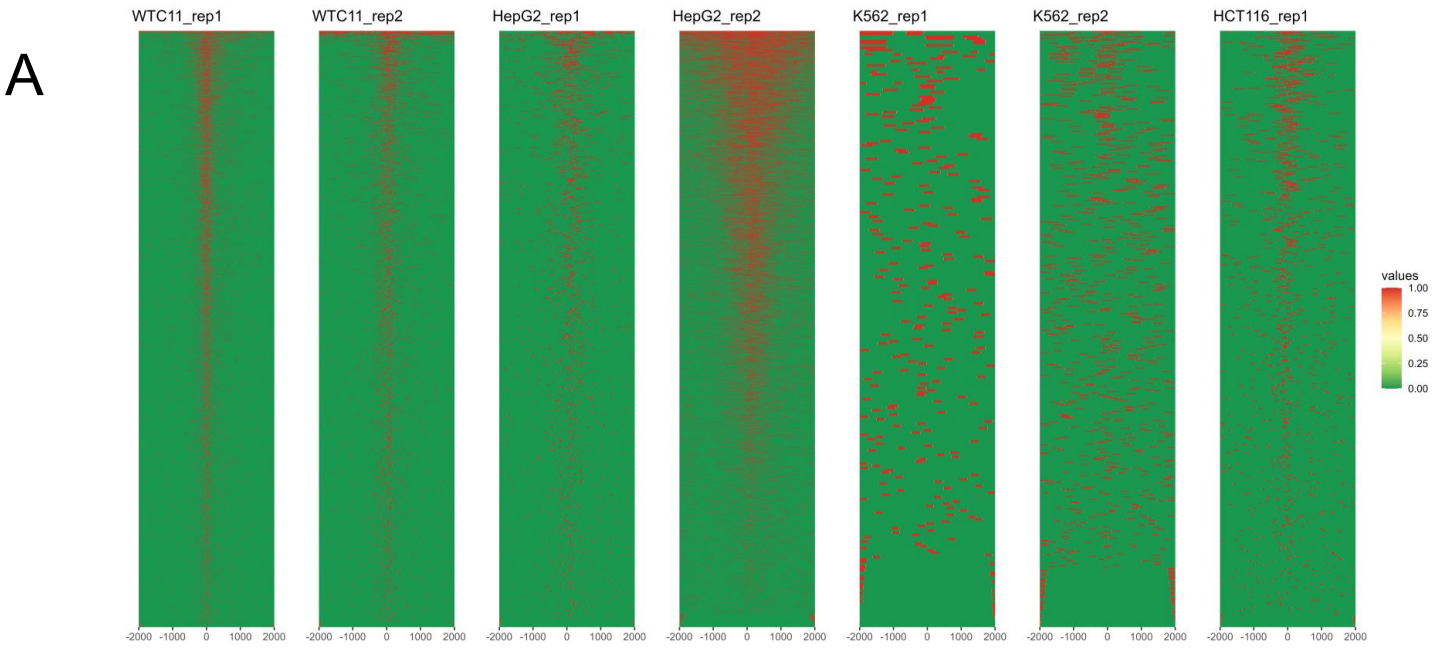
A
WTC11_rep1
WTC11_rep2
HepG2_rep1
HepG2_rep2
K562_rep1
K562_rep2
HCT116_rep1
values
1.00
0.75
0.50
0.25
0.00
-2000 -1000 0 1000 2000

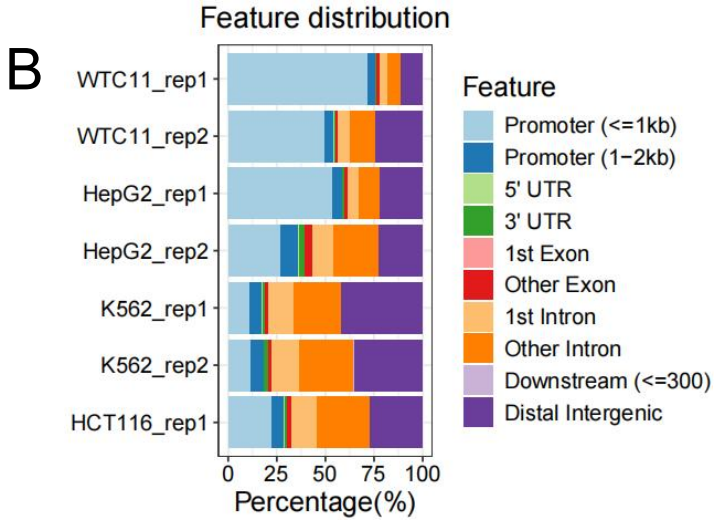
B
Feature distribution
WTC11_rep1
WTC11_rep2
HepG2_rep1
HepG2_rep2
K562_rep1
K562_rep2
HCT116_rep1
0 25 50 75 100
Percentage(%)
Feature
Promoter (<=1kb)
Promoter (1−2kb)
5' UTR
3' UTR
1st Exon
Other Exon
1st Intron
Other Intron
Downstream (<=300)
Distal Intergenic

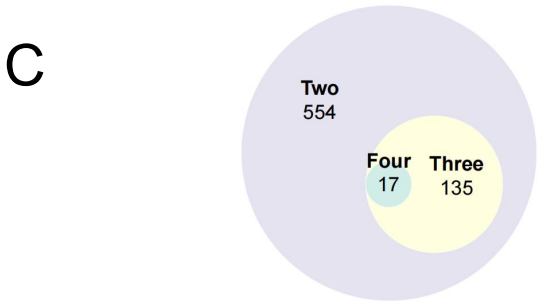
C
Two
554
Four
17
Three
135

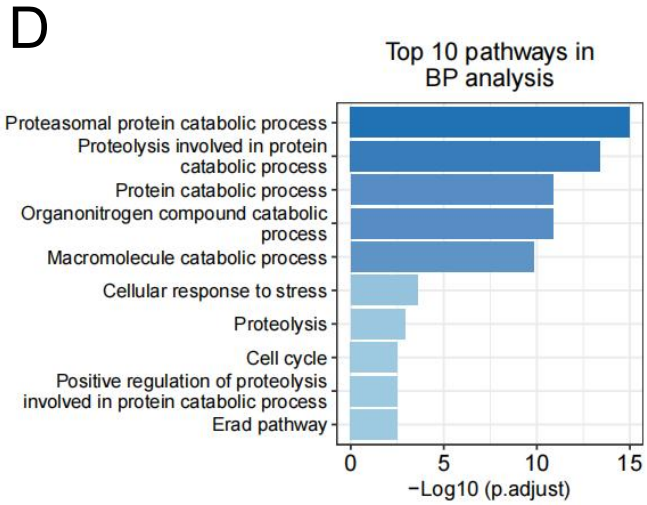
D
Top 10 pathways in
BP analysis
Proteasomal protein catabolic process
Proteolysis involved in protein catabolic process
Protein catabolic process
Organonitrogen compound catabolic process
Macromolecule catabolic process
Cellular response to stress
Proteolysis
Cell cycle
Positive regulation of proteolysis involved in protein catabolic process
Erad pathway
0 5 10 15
−Log10 (p.adjust)

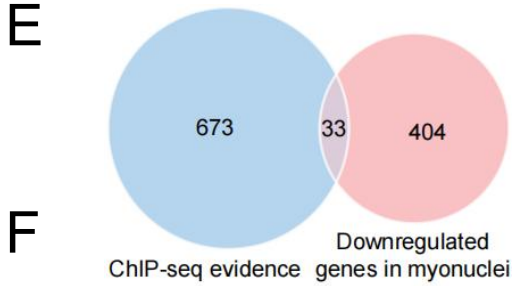
E
673
33
404
ChIP-seq evidence
Downregulated
genes in myonuclei

F

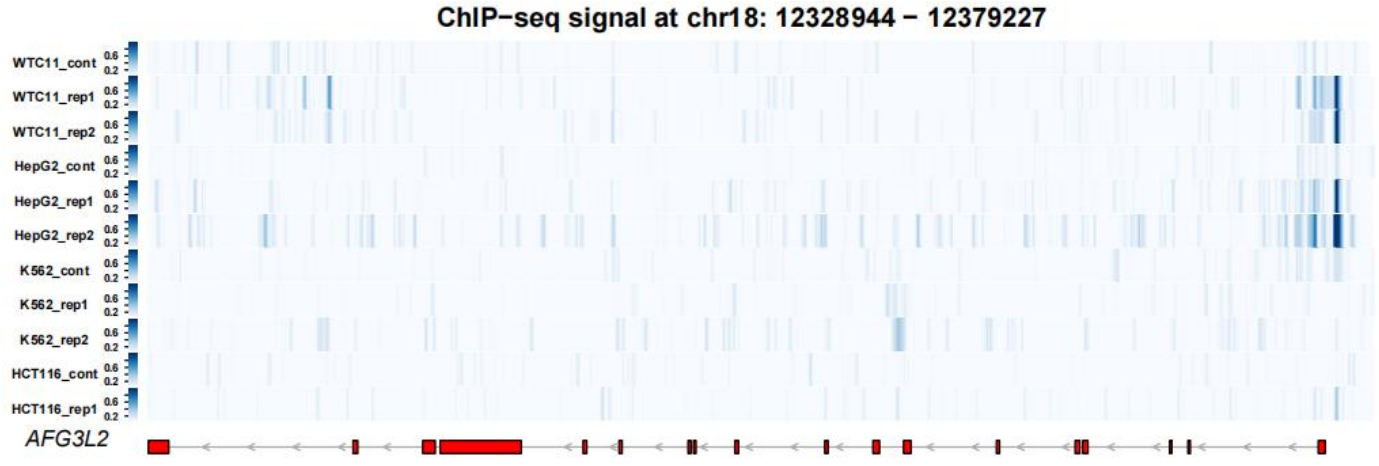
ChIP−seq signal at chr18: 12328944 − 12379227
WTC11_cont
WTC11_rep1
WTC11_rep2
HepG2_cont
HepG2_rep1
HepG2_rep2
K562_cont
K562_rep1
K562_rep2
HCT116_cont
HCT116_rep1
AFG3L2

G

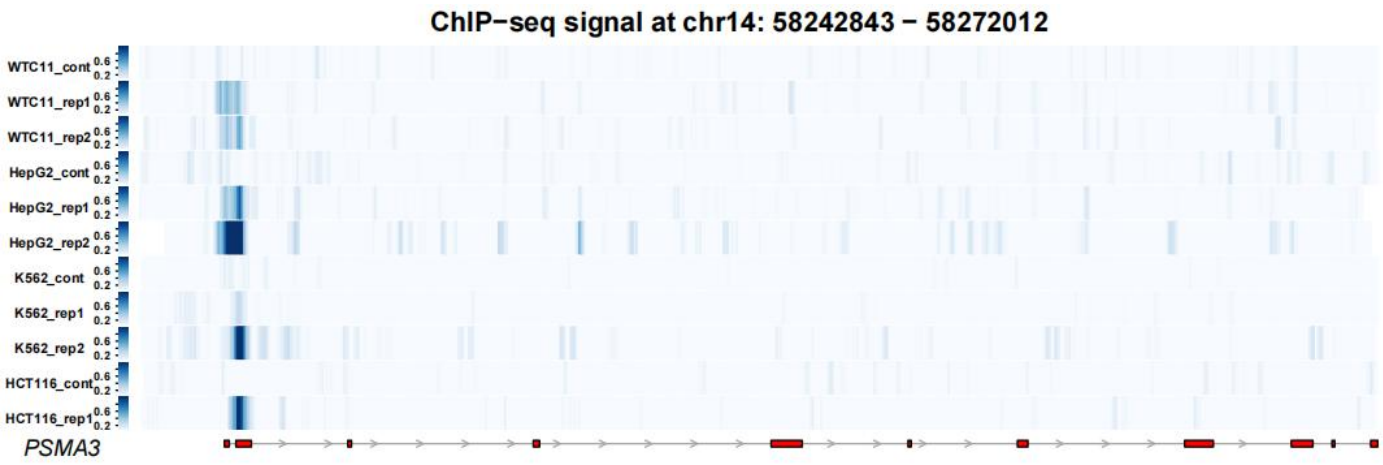
ChIP−seq signal at chr14: 58242843 − 58272012
WTC11_cont
WTC11_rep1
WTC11_rep2
HepG2_cont
HepG2_rep1
HepG2_rep2
K562_cont
K562_rep1
K562_rep2
HCT116_cont
HCT116_rep1
0.6
0.2
PSMA3

H

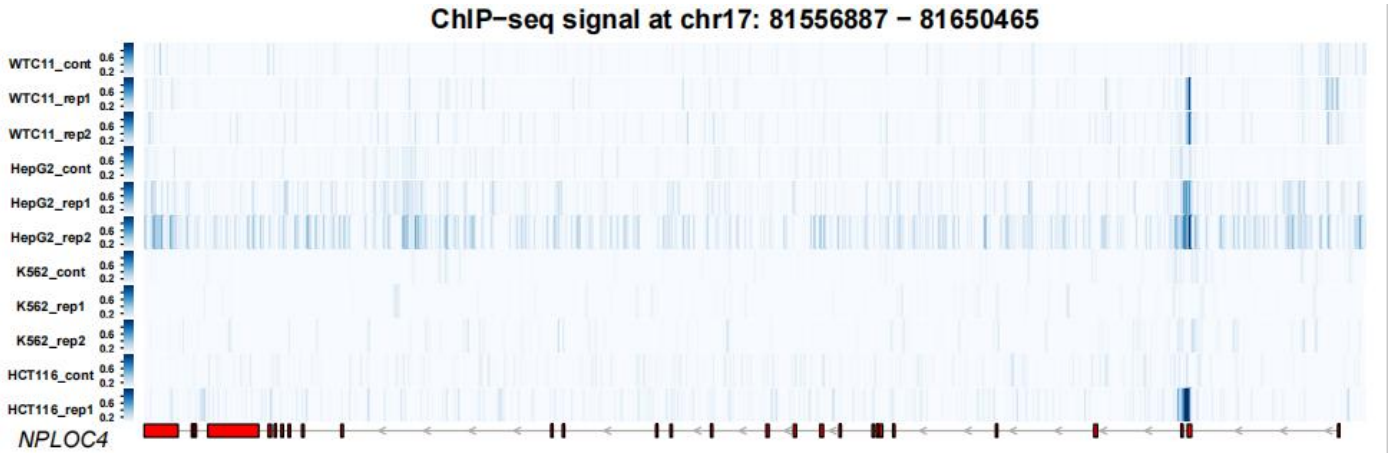
ChIP−seq signal at chr17: 81556887 − 81650465
WTC11_cont
WTC11_rep1
WTC11_rep2
HepG2_cont
HepG2_rep1
HepG2_rep2
K562_cont
K562_rep1
K562_rep2
HCT116_cont
HCT116_rep1
0.6
0.2
NPLOC4

I

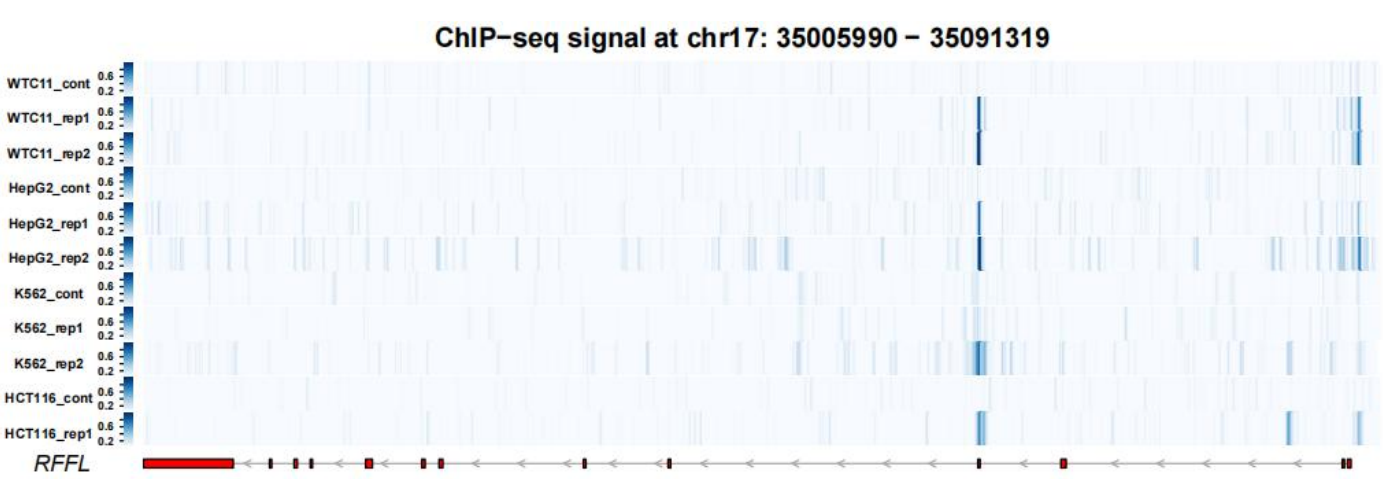
ChIP−seq signal at chr17: 35005990 − 35091319
WTC11_cont
WTC11_rep1
WTC11_rep2
HepG2_cont
HepG2_rep1
HepG2_rep2
K562_cont
K562_rep1
K562_rep2
HCT116_cont
HCT116_rep1
0.6
0.2
RFFL

J

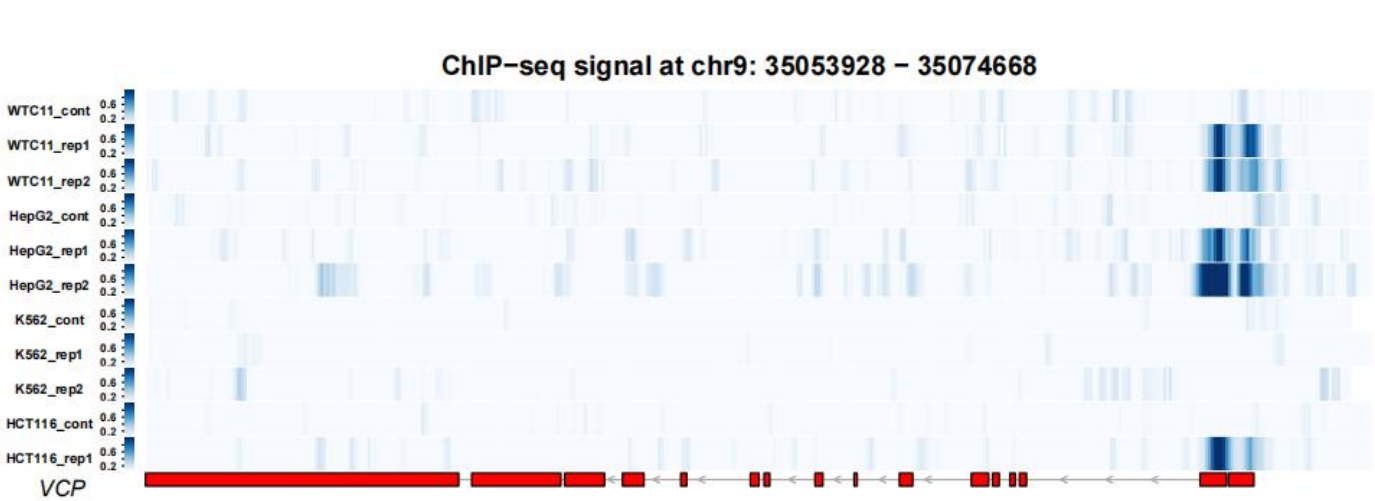
ChIP−seq signal at chr9: 35053928 − 35074668
WTC11_cont
WTC11_rep1
WTC11_rep2
HepG2_cont
HepG2_rep1
HepG2_rep2
K562_cont
K562_rep1
K562_rep2
HCT116_cont
HCT116_rep1
0.6
0.2
VCP

Fig. S27. Details of integrated analysis of four publicly available ChIP-seq datasets targeting NFE2L1. (A) Heatmap showing the distribution of peaks within 2 kb upstream and downstream of genes across seven samples. The samples include four cell lines: WTC11, HepG2, K562, and HCT116; note that HCT116 has only one replicate. (B) Bar chart depicting the distribution of peak annotations. (C) The number of significantly regulated genes present in any two, three, and four cell lines is 706, 152, and 17 genes, respectively. (D) Bar chart showing enrichment analysis results of the 706 genes. (E) Venn diagram showing the overlap between 706 NFE2L1 target genes and 437 down-regulated genes in myonuclei from the KO group, revealing 33 shared genes. Mouse genes were converted to their human orthologs. (F-J) Heatmap displaying the ChIP-seq signal distribution of the representative genes *AFG3L2, PSMA3, NPLOC4, RFFL, VCP*. For each gene, ChIP-seq signals across a region from 2 kb upstream of the transcription start site to the end of the gene are shown. Heatmap colors indicate signal intensity (after normalization). The ChIP-seq signal distributions for all 33 genes in Figure S29E are available upon reasonable request.

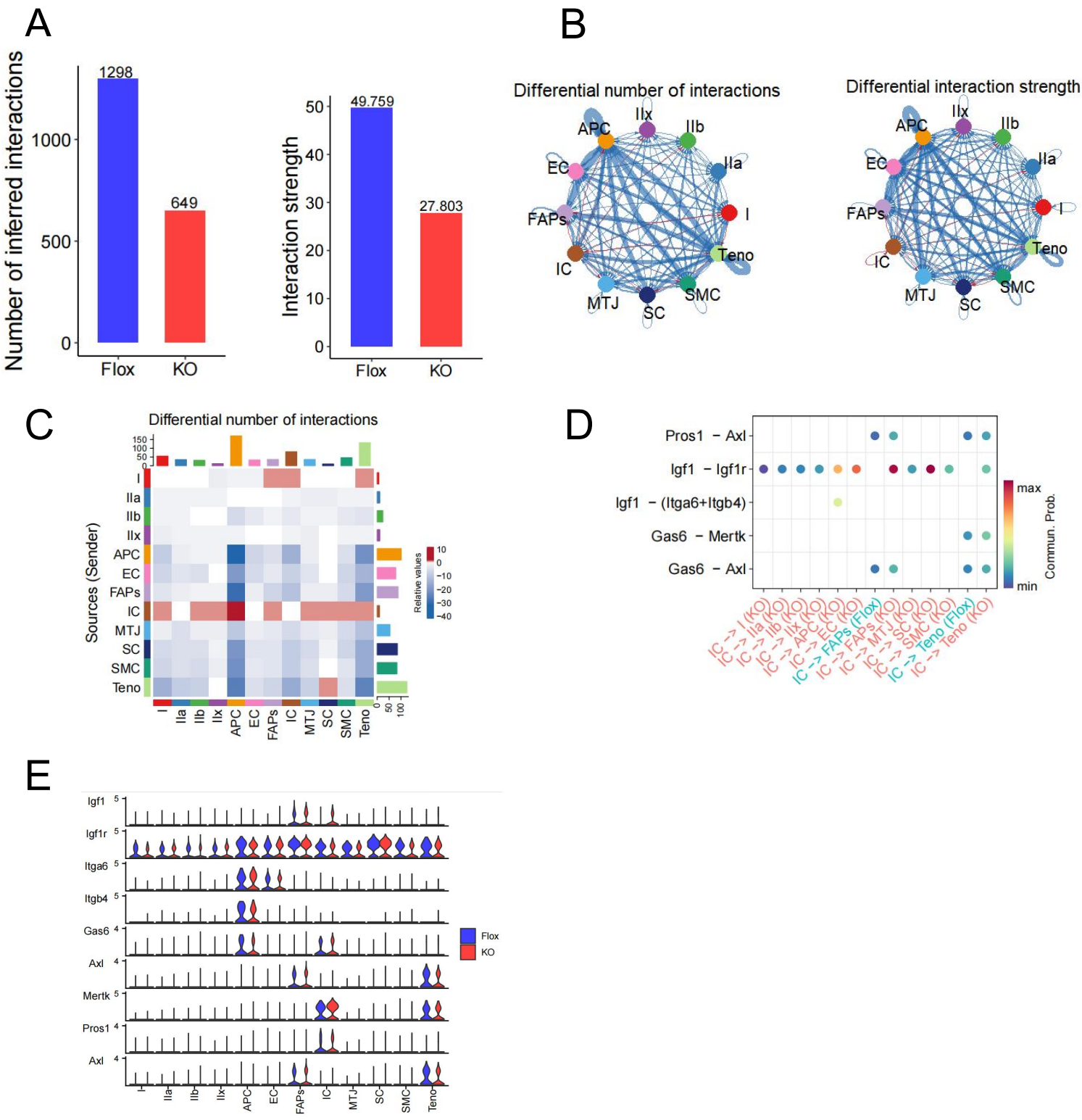

Fig. S28. Details of cell-cell communication analysis using CellChat. (A) Bar plot of the number (left panel) and strength (right panel) of cell-cell communications. (B) Circle plot of the number of cell-cell differential communication (left panel) and the strength of differential communication (right panel) between different cell types. (C) Heat map of the number of cell-cell differential communications between different cell types. (D) Details of cell communication between immune cells and other cell types. (E) Expression levels of ligands and receptors associated with immune cell communication across all cell types.

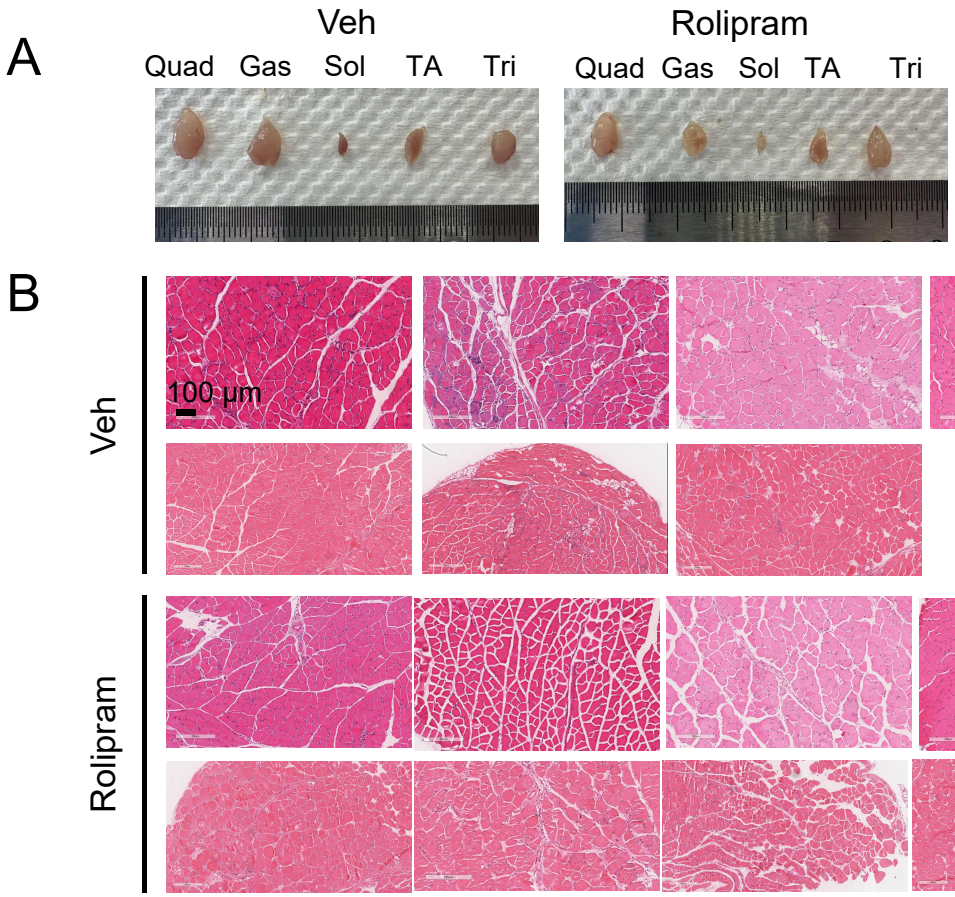
A
Veh
Quad Gas Sol TA Tri
Rolipram
Quad Gas Sol TA Tri
B
Veh
Rolipram
100 μm
C
Quad
Veh
Rolipram
100 μm
Gas
Veh
Rolipram

Fig. S29. Rescue experiment details. (A) Representative gross morphology images of mouse SkM. Quad, Quadriceps muscle; Gas, Gastrocnemius muscle; Sol, Soleus muscle; Tri, Triceps brachii muscle; TA, Tibialis anterior muscle. (B) Representative H&E staining images of quadriceps muscles. Scale bar: 100 μm. (C) Representative immunohistochemistry (IHC) images of F4/80 in mouse quadriceps (top) and gastrocnemius (bottom) muscles. Scale bar: 100 μm.

A

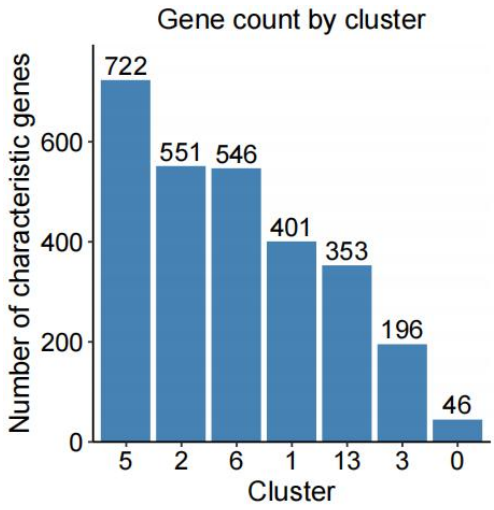

B

subpopulation 5

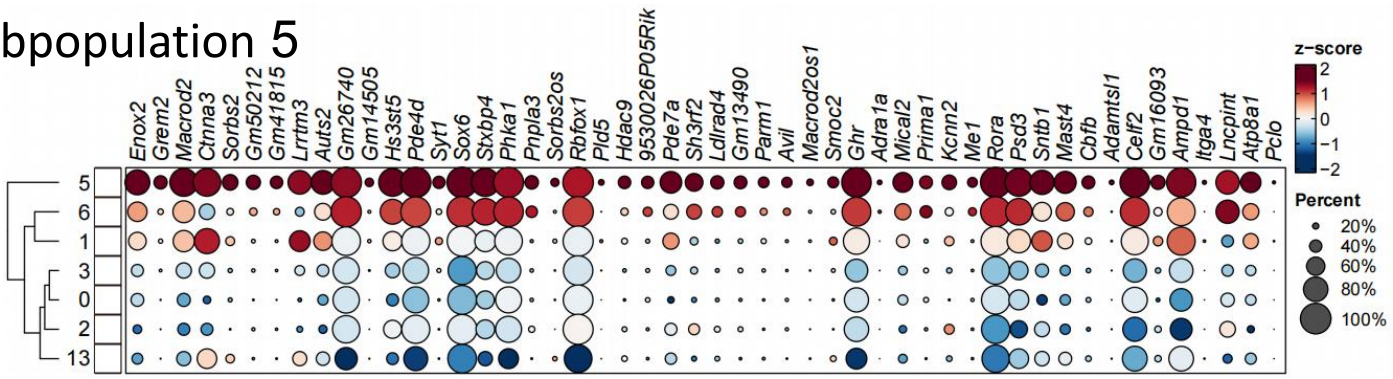

C

subpopulation 6

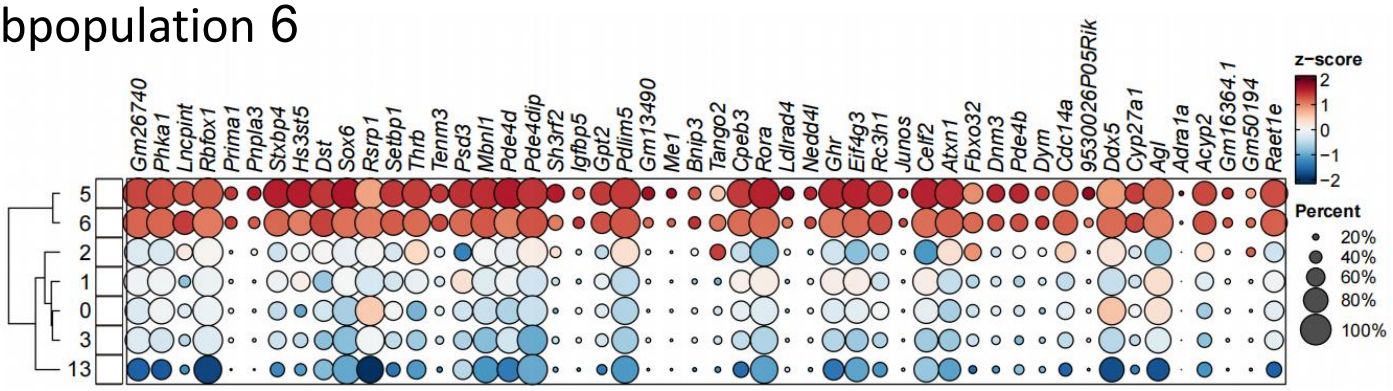

D

subpopulation 13

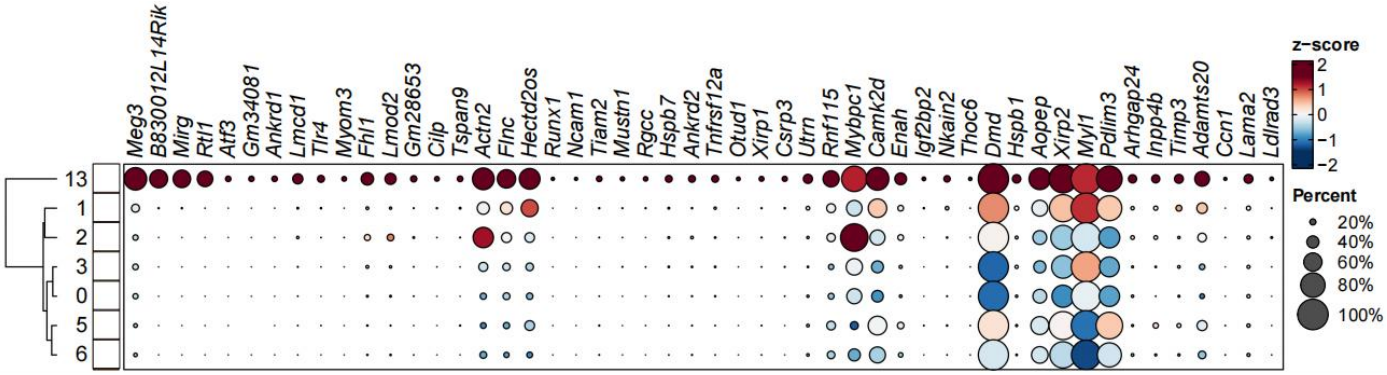

E

subpopulation 0

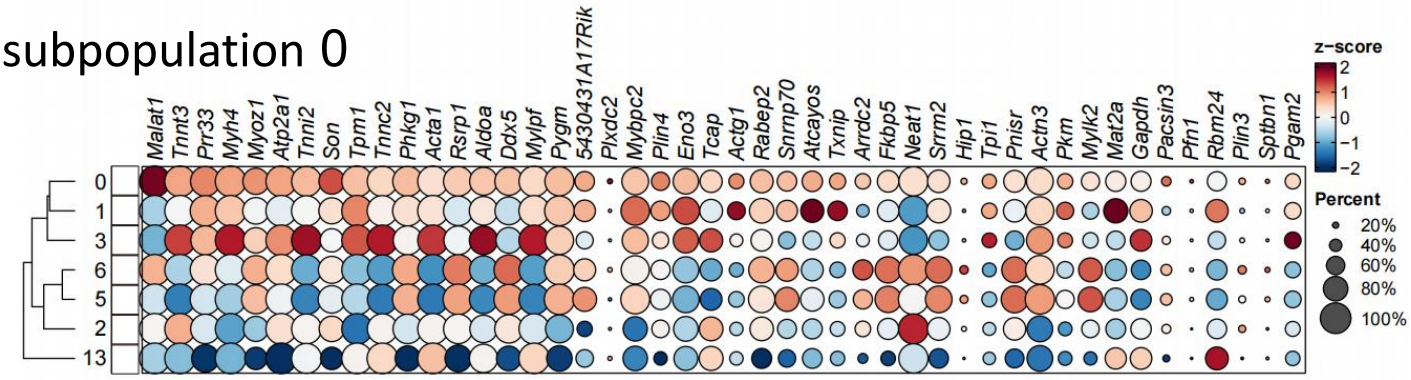

F

subpopulation 1

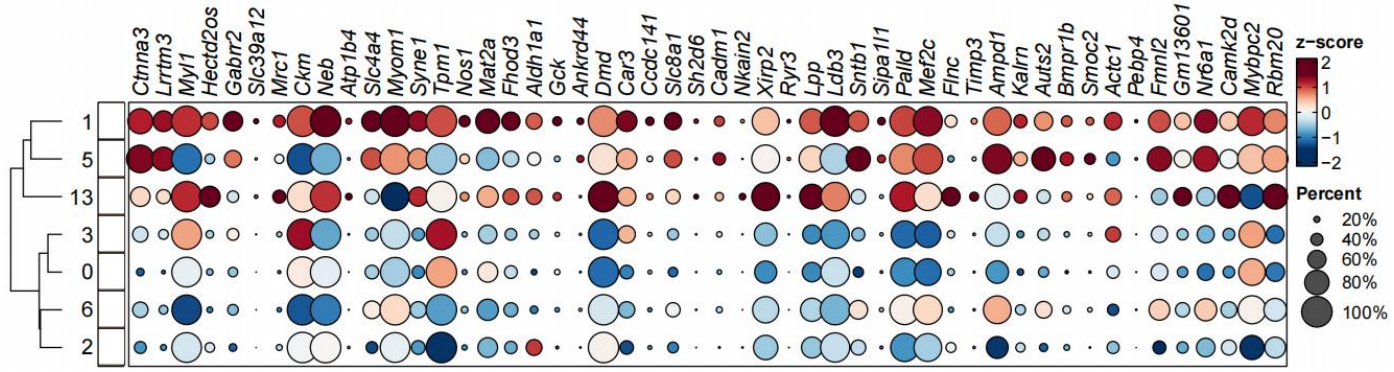

G

subpopulation 2

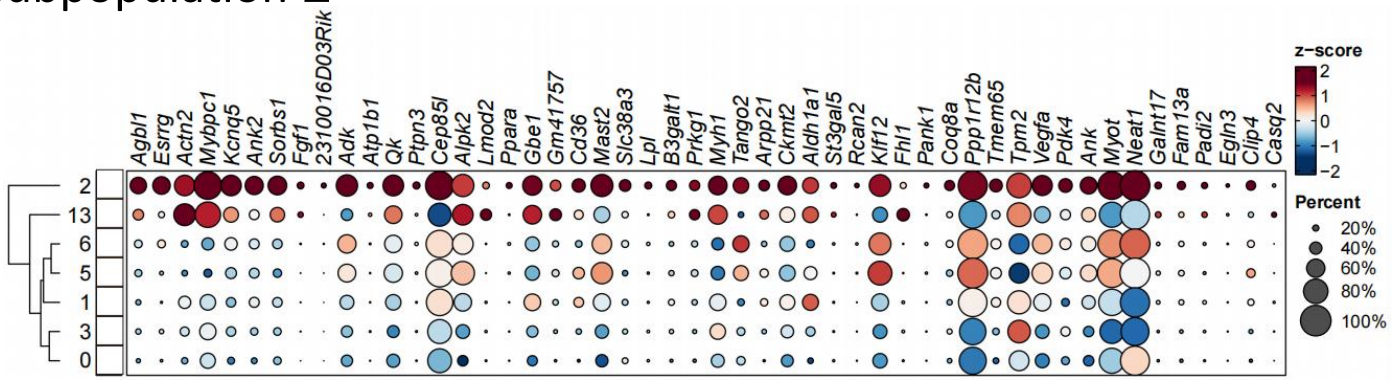

H

subpopulation 3

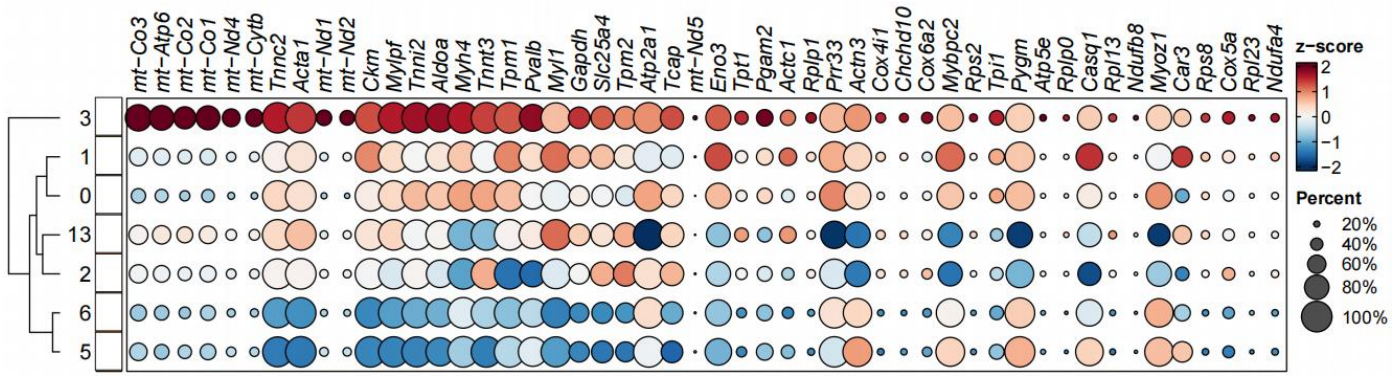

Fig. S30. Characteristic gene analysis of subpopulations of type IIb myonuclei. (A) Bar plot showing the number of characteristic genes in each subpopulation of type IIb myonuclei. (B–H) Bubble plots presenting the top 50 (ranked by significance) characteristic genes for subpopulations 5, 6, 13, 0, 1, 2, and 3, respectively. The color of each bubble represents the average expression level (z score), and the size indicates the percentage of cells expressing the gene. Subpopulations were grouped using K-means clustering.

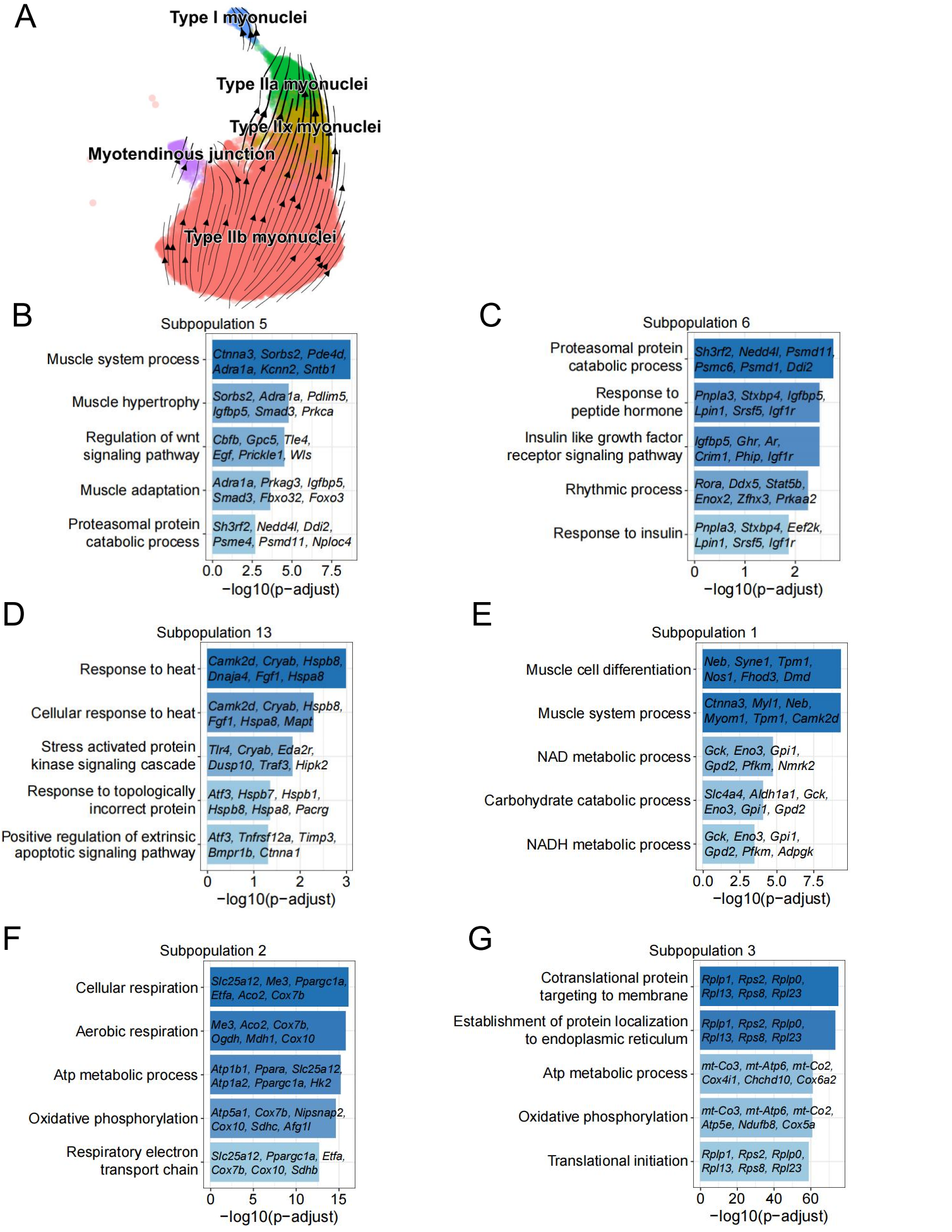

Fig. S31. RNA velocity analysis and enrichment analysis of characteristic genes in subpopulations of type IIb myonuclei. (A) RNA velocity analysis results for all myonuclei. (B–G) GO biological process (BP) enrichment analyses of all characteristic genes in subpopulations 5, 6, 13, 1, 2, and 3, respectively. For each subpopulation, the five most significant or representative pathways and some of their associated genes are shown.

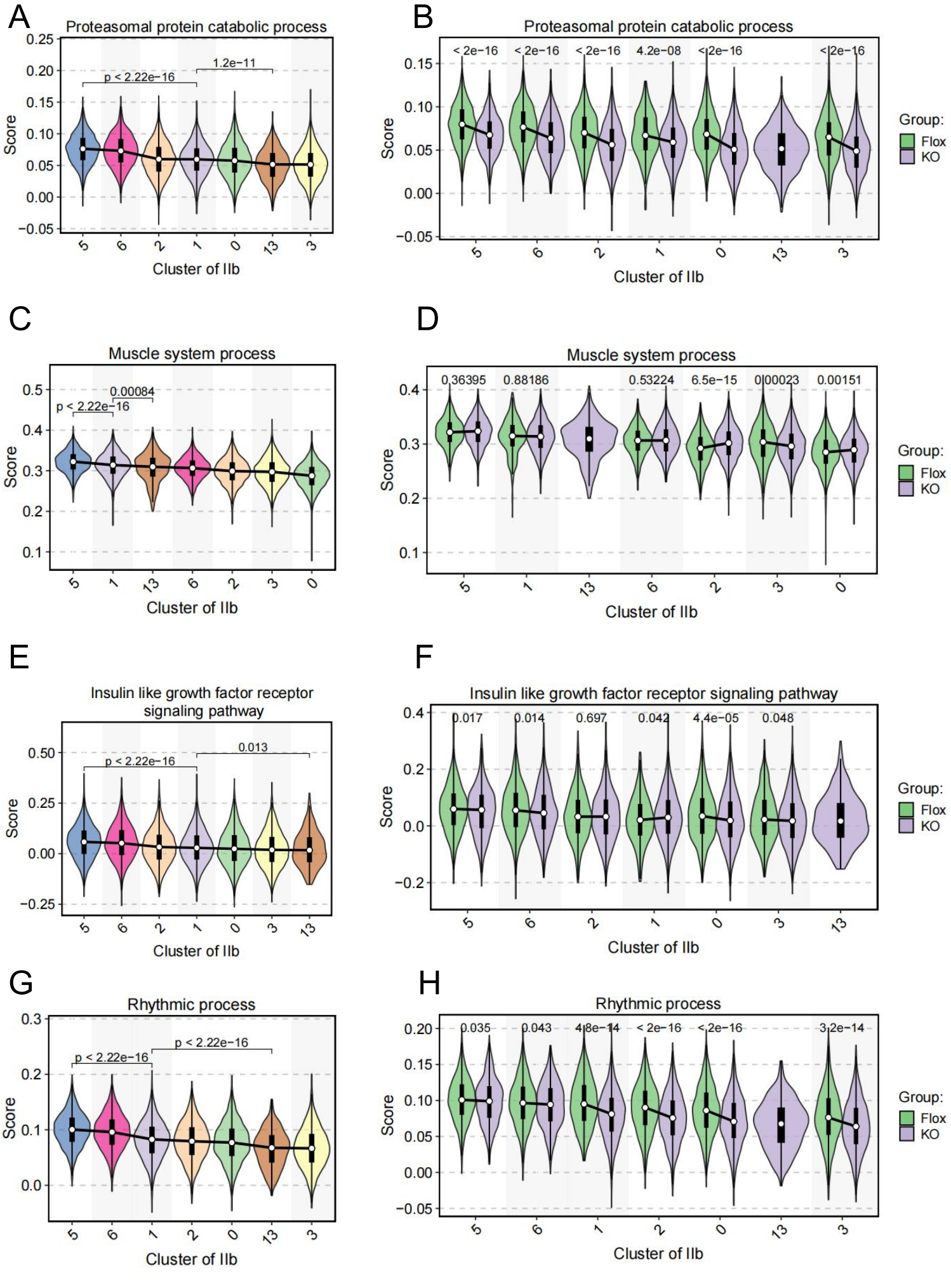
A
Proteasomal protein catabolic process
p < 2.22e−16
1.2e−11
Score
Cluster of IIb
B
Proteasomal protein catabolic process
< 2e−16
< 2e−16
< 2e−16
4.2e−08
< 2e−16
< 2e−16
Group:
Flox
KO
Score
Cluster of IIb
C
Muscle system process
0.00084
p < 2.22e−16
Score
Cluster of IIb
D
Muscle system process
0.36395
0.88186
0.53224
6.5e−15
0.00023
0.00151
Group:
Flox
KO
Score
Cluster of IIb
E
Insulin like growth factor receptor signaling pathway
p < 2.22e−16
0.013
Score
Cluster of IIb
F
Insulin like growth factor receptor signaling pathway
0.017
0.014
0.697
0.042
4.4e−05
0.048
Group:
Flox
KO
Score
Cluster of IIb
G
Rhythmic process
p < 2.22e−16
p < 2.22e−16
Score
Cluster of IIb
H
Rhythmic process
0.035
0.043
4.8e−14
< 2e−16
< 2e−16
3.2e−14
Group:
Flox
KO
Score
Cluster of IIb

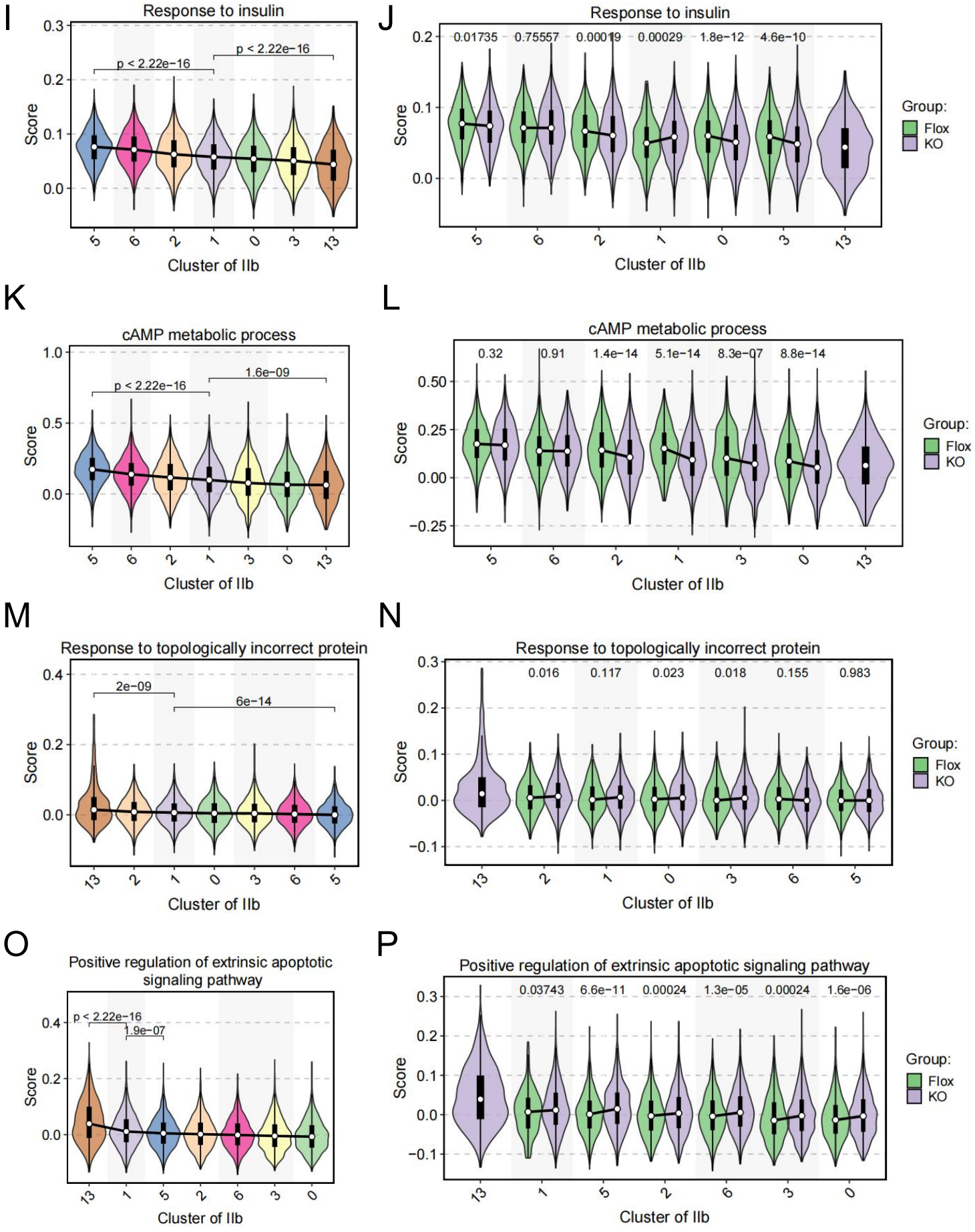

Fig. S32. Comparison of pathway activity scores. (A–P) Violin plots display the distribution of activity scores for eight pathways of interest, including comparisons among subpopulations as well as between Flox and KO groups within the same subpopulation. *P* values were calculated using two-tailed Wilcoxon rank-sum tests.

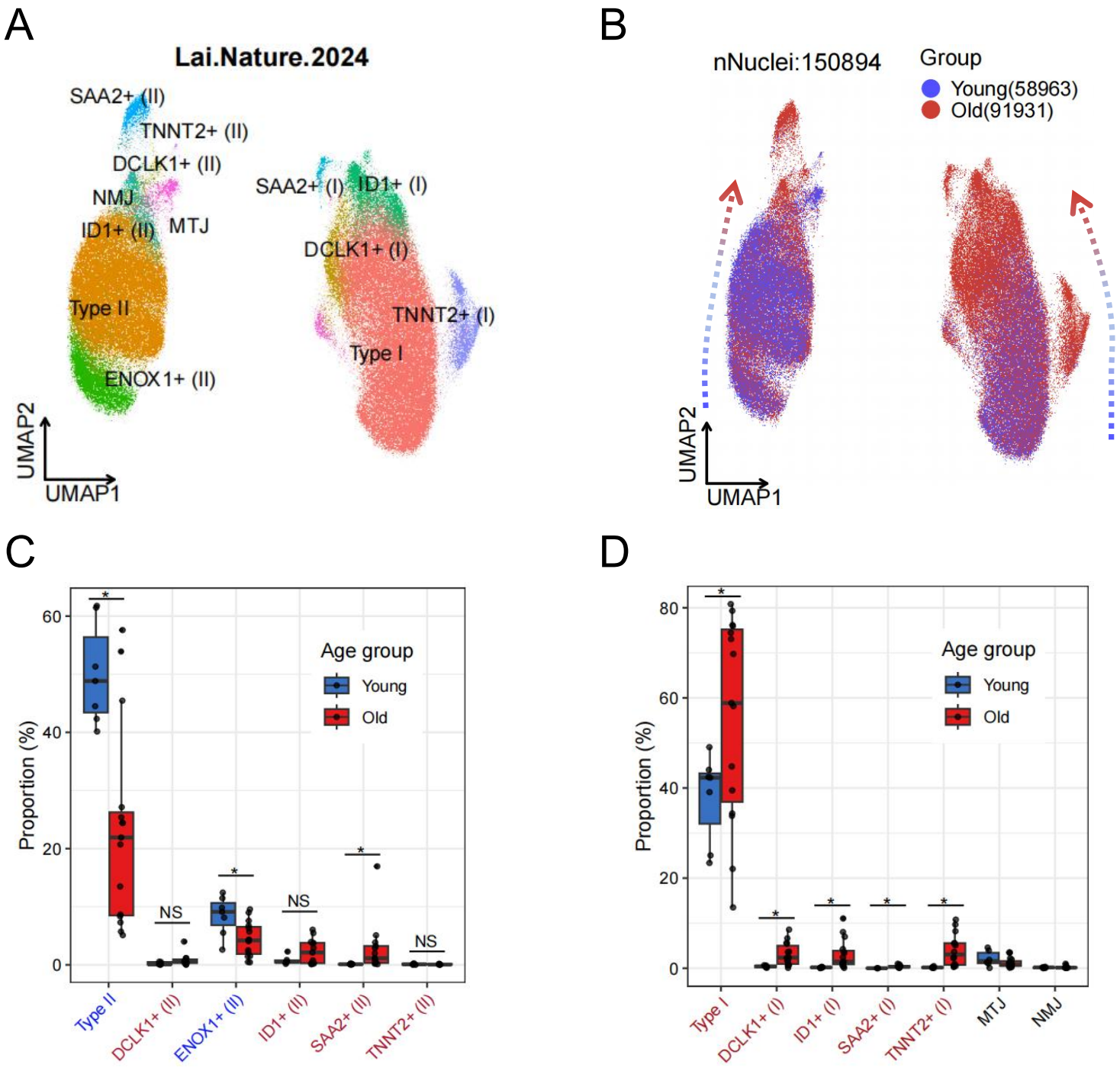
A
Lai.Nature.2024
SAA2+ (II)
TNNT2+ (II)
DCLK1+ (II)
NMJ
ID1+ (II)
MTJ
Type II
ENOX1+ (II)
SAA2+ (I)
ID1+ (I)
DCLK1+ (I)
TNNT2+ (I)
Type I
UMAP2
UMAP1
B
nNuclei:150894
Group
Young(58963)
Old(91931)
UMAP2
UMAP1
C
Proportion (%)
Age group
Young
Old
NS
Type II
DCLK1+ (II)
ENOX1+ (II)
ID1+ (II)
SAA2+ (II)
TNNT2+ (II)
D
Proportion (%)
Age group
Young
Old
Type I
DCLK1+ (I)
ID1+ (I)
SAA2+ (I)
TNNT2+ (I)
MTJ
NMJ

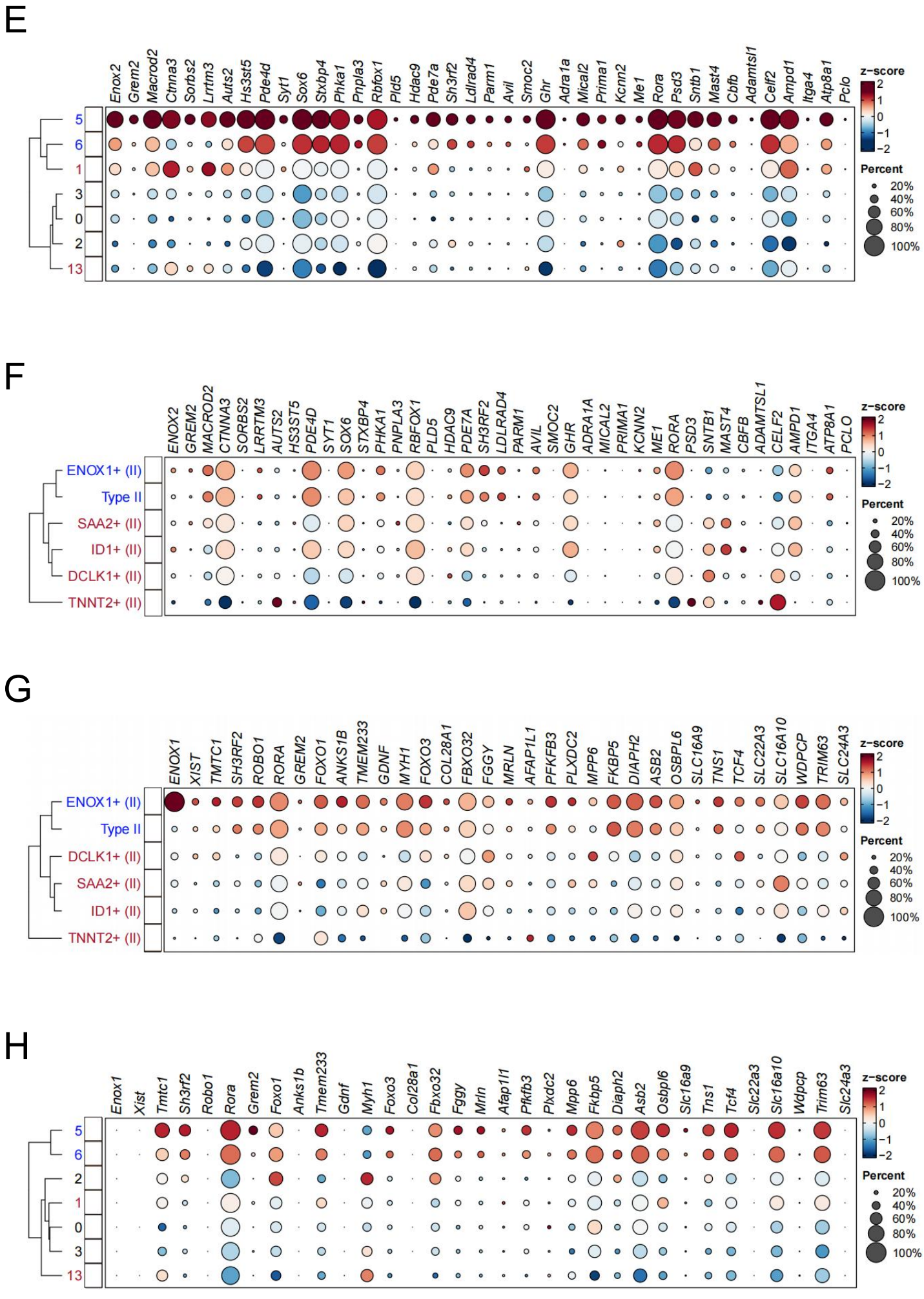
E
Enox2 Grem2 Macrod2 Ctnna3 Sorbs2 Lrrtm3 Auts2 Hs3st5 Pde4d Syt1 Sox6 Stxbp4 Phka1 Pnpla3 Rbfox1 Pld5 Hdac9 Pde7a Sh3rf2 Ldlrad4 Parm1 Avil Smoc2 Ghr Adra1a Mical2 Prima1 Kcnn2 Me1 Rora Psd3 Sntb1 Mast4 Cbfb Adamtsl1 Celf2 Ampd1 Itga4 Atp8a1 Pclo
5 6 1 3 0 2 13
z-score 2 1 0 −1 −2
Percent 20% 40% 60% 80% 100%
F
ENOX2 GREM2 MACROD2 CTNNA3 SORBS2 LRRTM3 AUTS2 HS3ST5 PDE4D SYT1 SOX6 STXBP4 PHKA1 PNPLA3 RBFOX1 PLD5 HDAC9 PDE7A SH3RF2 LDLRAD4 PARM1 AVIL SMOC2 GHR ADRA1A MICAL2 PRIMA1 KCNN2 ME1 RORA PSD3 SNTB1 MAST4 CBFB ADAMTSL1 CELF2 AMPD1 ITGA4 ATP8A1 PCLO
ENOX1+ (II) Type II SAA2+ (II) ID1+ (II) DCLK1+ (II) TNNT2+ (II)
z-score 2 1 0 −1 −2
Percent 20% 40% 60% 80% 100%
G
ENOX1 XIST TMTC1 SH3RF2 ROBO1 RORA GREM2 FOXO1 ANKS1B TMEM233 GDNF MYH1 FOXO3 COL28A1 FBXO32 FGGY MRLN AFAP1L1 PFKFB3 PLXDC2 MPP6 FKBP5 DIAPH2 ASB2 OSBPL6 SLC16A9 TNS1 TCF4 SLC22A3 SLC16A10 WDPCP TRIM63 SLC24A3
ENOX1+ (II) Type II DCLK1+ (II) SAA2+ (II) ID1+ (II) TNNT2+ (II)
z-score 2 1 0 −1 −2
Percent 20% 40% 60% 80% 100%
H
Enox1 Xist Tmtc1 Sh3rf2 Robo1 Rora Grem2 Foxo1 Anks1b Tmem233 Gdnf Myh1 Foxo3 Col28a1 Fbxo32 Fggy Mrln Afap1l1 Pfkfb3 Plxdc2 Mpp6 Fkbp5 Diaph2 Asb2 Osbpl6 Slc16a9 Tns1 Tcf4 Slc22a3 Slc16a10 Wdpcp Trim63 Slc24a3
5 6 2 1 0 3 13
z-score 2 1 0 −1 −2
Percent 20% 40% 60% 80% 100%

I
Meg3
Rtl1
Atf3
Ankrd1
Lmcd1
Tlr4
Myom3
Fhl1
Lmod2
Cilp
Tspan9
Actn2
Flnc
Runx1
Ncam1
Tiam2
Mustn1
Rgcc
Hspb7
Ankrd2
Tnfrsf12a
Otud1
Xirp1
Csrp3
Utrn
Rnf115
Mybpc1
Camk2d
Enah
Igf2bp2
Nkain2
Thoc6
Dmd
Hspb1
Aopep
Xirp2
Myl1
Pdlim3
Arhgap24
Inpp4b
Timp3
Adamts20
Ccn1
Lama2
Ldlrad3
13
1
2
3
0
5
6
z−score
2
1
0
−1
−2
Percent
20%
40%
60%
80%
100%
J
MEG3
RTL1
ATF3
ANKRD1
LMCD1
TLR4
MYOM3
FHL1
LMOD2
CILP
TSPAN9
ACTN2
FLNC
RUNX1
NCAM1
TIAM2
MUSTN1
RGCC
HSPB7
ANKRD2
TNFRSF12A
OTUD1
XIRP1
CSRP3
UTRN
RNF115
MYBPC1
CAMK2D
ENAH
IGF2BP2
NKAIN2
THOC6
DMD
HSPB1
AOPEP
XIRP2
MYL1
PDLIM3
ARHGAP24
INPP4B
TIMP3
ADAMTS20
CCN1
LAMA2
LDLRAD3
ID1+ (II)
SAA2+ (II)
DCLK1+ (II)
Type II
ENOX1+ (II)
TNNT2+ (II)
z−score
2
1
0
−1
−2
Percent
20%
40%
60%
80%
100%
K
SCN5A
MYBPH
EGR1
PRUNE2
CAPN2
SLC16A6
RUNX1
CHGB
ANXA2
ST6GAL1
COLQ
CHRNA1
COL19A1
STK39
ADAMTS17
PCSK6
TMEM63B
FOS
FNIP2
JUNB
DGKD
GADD45A
COL13A1
RRAD
PKIG
EIF4A1
FADS3
PVT1
VMP1
ASB5
ANKRD10
GLRX
PLCE1
CAMK2D
PHC2
TMCC3
BCL2L1
SLC36A1
WWTR1
TSPAN7
KCNQ5
UBC
ID1+ (II)
SAA2+ (II)
DCLK1+ (II)
ENOX1+ (II)
Type II
TNNT2+ (II)
z−score
2
1
0
−1
−2
Percent
20%
40%
60%
80%
100%
L
Scn5a
Mybph
Egr1
Prune2
Capn2
Slc16a6
Runx1
Chgb
Anxa2
St6gal1
Colq
Chrna1
Col19a1
Stk39
Adamts17
Pcsk6
Tmem63b
Fos
Fnip2
Junb
Dgkd
Gadd45a
Col13a1
Rrad
Pkig
Eif4a1
Fads3
Pvt1
Vmp1
Asb5
Ankrd10
Glrx
Plce1
Camk2d
Phc2
Tmcc3
Bcl2l1
Slc36a1
Wwtr1
Tspan7
Kcnq5
Ubc
13
5
6
2
1
3
0
z−score
2
1
0
−1
−2
Percent
20%
40%
60%
80%
100%

M

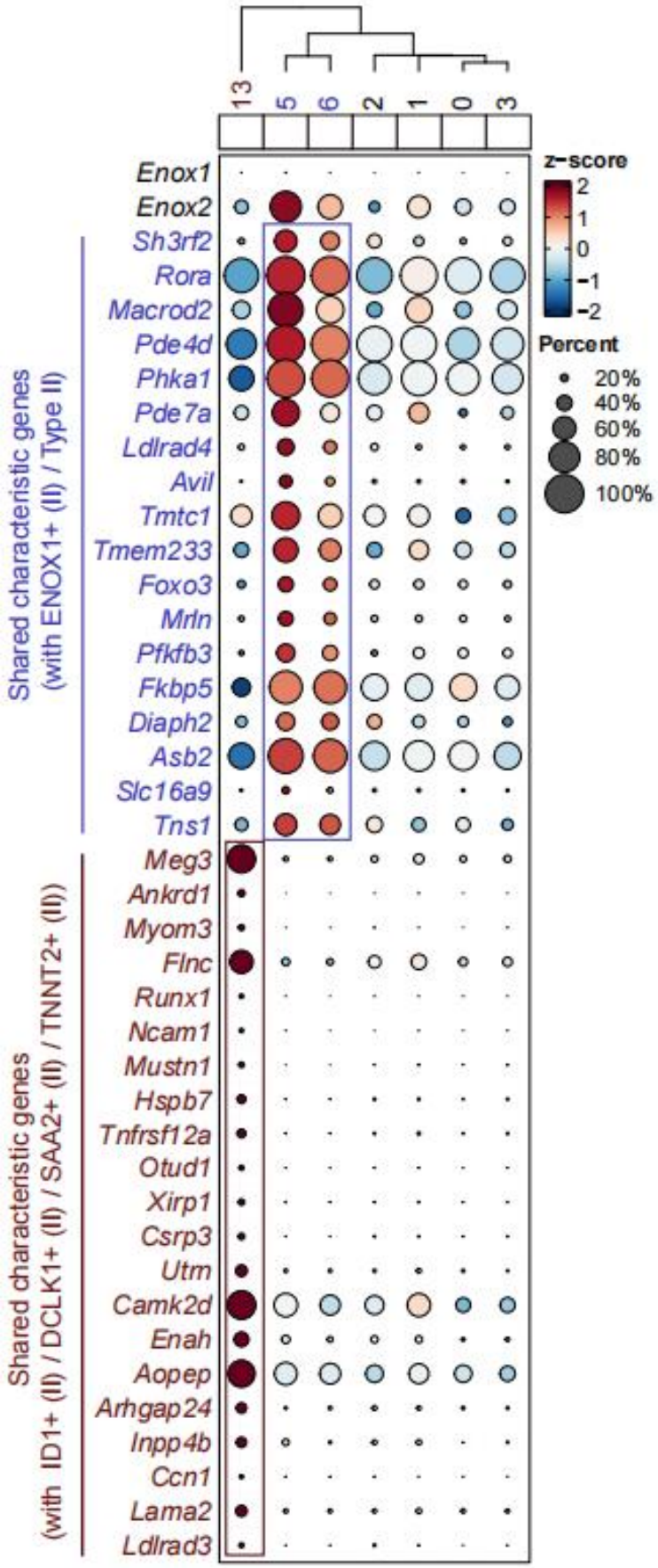
13
5
6
2
1
0
3
z-score
2
1
0
−1
−2
Percent
20%
40%
60%
80%
100%
Enox1
Enox2
Sh3rf2
Rora
Macrod2
Pde4d
Phka1
Pde7a
Ldlrad4
Avil
Tmtc1
Tmem233
Foxo3
Mrln
Pfkfb3
Fkbp5
Diaph2
Asb2
Slc16a9
Tns1
Meg3
Ankrd1
Myom3
Flnc
Runx1
Ncam1
Mustn1
Hspb7
Tnfrsf12a
Otud1
Xirp1
Csrp3
Utm
Camk2d
Enah
Aopep
Arhgap24
Inpp4b
Ccn1
Lama2
Ldlrad3
Shared characteristic genes
(with ENOX1+ (II) / Type II)
Shared characteristic genes
(with ID1+ (II) / DCLK1+ (II) / SAA2+ (II) / TNNT2+ (II))

Fig. S33. Integrative analysis of type IIb subpopulations and the Lai's dataset (Nature, 2024). (A) UMAP plot of myonuclei from the publicly available dataset published by Lai et al. (Nature, 2024) (hereafter referred to as Lai's dataset), using original annotations. (B) Same UMAP plot as in panel A, but colored by age groups. Pseudotime trajectory lines were manually added based on the analysis results from Lai et al. (Nature, 2024). (C-D) Box plots showing the proportions of different age groups in Type II muscle fibers (C) and Type I muscle fibers (D) from the Lai dataset. Cell type labels of declining myonuclear populations are shown in blue (i.e., Type II and *ENOX1*$^+$ (II)), while labels of increasing myonuclear populations are shown in red (all other myonuclear types except Type II and *ENOX1*$^+$ (II); MTJ and NMJ were not considered). *$P < 0.05$, NS, not significant. (E-F) Bubble plots showing gene expression of the top characteristic genes from subpopulation 5 across type IIb subpopulations in our study (E) and different Type II fibers in the Lai dataset (F). The top 50 most significant characteristic genes were identified, of which 40 homologous genes present in both mouse and human datasets were used for the bubble plots. Subpopulation clustering (row clustering) was performed using the k-means algorithm. Blue cell labels indicate subpopulations significantly decreased in mouse KO groups (i.e., 5 and 6) or in human aging groups (Type II and *ENOX1*$^+$ (II)), while red cell labels indicate increased populations. (G-H) Bubble plots showing gene expression of the top characteristic genes from *ENOX1*$^+$ (II) myonuclei across different Type II fibers in the Lai dataset (G) and type IIb subpopulations in our study (H). The top 50 most significant characteristic genes were identified, of which 33 homologous genes present in both mouse and human datasets were used for the bubble plots. Color details are the same as in panels E-F. (I-J) Bubble plots showing gene expression of the top characteristic genes from subpopulation 13 across type IIb subpopulations in our study (I) and different Type II fibers in the Lai dataset (J). The top 50 most significant characteristic genes were identified, of which 45 homologous genes present in both mouse and human datasets were used for the bubble plots. Row clustering and color details are similar to those previously described. Cell type labels in red indicate populations that increased in KO mice (i.e., 13 and 1) or in aging humans (e.g., *ID1*$^+$ (II)). (K-L) Bubble plots showing gene expression of the top characteristic genes from *ID1*$^+$ (II) myonuclei across different Type II fibers in the Lai dataset (K) and type IIb subpopulations in our study (L). The top 50 most significant characteristic genes were identified, of which 42 homologous genes present in both mouse and human datasets were used for the bubble plots. Details are as described above. (M) The bubble plot shows the expression levels of genes across different IIb myonuclear subpopulations in the mouse dataset from this study. The genes include *Enox1* and *Enox2*; shared characteristic genes between human *ENOX1*$^+$ (II) myonuclei and mouse subpopulation 5 (blue text); and characteristic genes shared between mouse subpopulation 13 and any one or more of the human *DCLK1*$^+$ (II), *ID1*$^+$ (II), *SAA2*$^+$ (II), and *TNNT2*$^+$ (II) myonuclear types (red text). Columns are organized using k-means clustering. Bubble color represents the mean expression level (z score), and bubble size indicates the percentage of expressing cells.

Table S1. Descriptive statistics of *NFE2L1* by age in the GTEx SkM dataset

Age （years）	Male		Female	
	N	*NFE2L1* (TPM)	N	*NFE2L1* (TPM)
20-29	24	733 ± 249	14	830 ± 462
30-39	23	767 ± 266	7	778 ± 182
40-49	37	686 ± 237	30	715 ± 327
50-59	92	666 ± 264	47	588 ± 215
60-69	87	592 ± 232	48	549 ± 222

Note: TPM, transcripts per million

Table S2. 253 potential target genes of NFE2L1

Gene	*R*	*P*	Gene	*R*	*P*	Gene	*R*	*P*
ACOX1	0.50	7.54E-28	CANX	0.62	1.16E-44	DYNC1LI1	0.71	5.23E-64
ADRM1	0.61	1.63E-43	CAPRIN1	0.52	3.19E-29	EDC3	0.56	1.04E-35
AFG3L2	0.52	8.78E-30	CCDC127	0.65	7.08E-50	EFTUD2	0.60	3.97E-41
AIDA	0.56	1.08E-34	CCDC25	0.66	2.39E-53	EIF2A	0.51	7.06E-29
AIFM2	0.56	2.00E-34	CCPG1	0.56	3.16E-35	EIF3J	0.59	2.65E-40
AKT1S1	0.57	5.03E-36	CCT5	0.52	1.50E-29	EIF4A2	0.51	4.62E-28
ALS2	0.61	1.49E-43	CDK5RAP2	0.55	7.94E-34	EMC3	0.68	8.36E-57
ANKRD28	0.51	5.76E-29	CDK7	0.56	7.86E-35	ERC1	0.57	2.58E-37
AP1G1	0.52	1.20E-29	CHMP3	0.69	1.16E-58	ERLEC1	0.54	3.49E-32
AP4E1	0.50	1.82E-27	CLCN3	0.62	2.14E-45	FAM204A	0.67	1.34E-53
ARHGEF37	0.62	1.66E-44	CLIP1	0.68	9.66E-56	FAM219A	0.66	1.14E-52
ARID1B	0.63	1.20E-46	CLPTM1	0.62	9.84E-45	FAN1	0.60	4.93E-41
ARID4B	0.52	6.75E-30	COASY	0.52	3.00E-30	FARS2	0.55	1.12E-33
ARIH1	0.52	5.18E-30	CPSF2	0.54	4.14E-32	GCC2	0.56	9.20E-36
ASCC2	0.50	2.67E-27	CUX1	0.54	5.47E-32	GDPD5	0.54	1.61E-32
ATG13	0.62	1.30E-45	DCAF12	0.59	3.45E-39	GGPS1	0.59	3.52E-39
ATP6V0A1	0.52	7.98E-30	DCAF6	0.52	4.50E-30	GLYR1	0.62	4.46E-44
BAG6	0.59	2.80E-39	DCAF8	0.70	1.89E-60	GNPDA1	0.54	3.28E-32
BECN1	0.66	8.43E-52	DCTN4	0.58	2.01E-37	GOLGA2	0.64	3.55E-49
BICD2	0.60	1.23E-40	DDX23	0.53	6.40E-31	GOLGA5	0.65	2.56E-51
BLMH	0.56	7.39E-36	DHX29	0.66	1.99E-53	GPATCH4	0.54	7.68E-33
BRF2	0.55	2.46E-33	DHX8	0.55	7.66E-34	GTF2A1	0.66	1.30E-52
BROX	0.64	2.02E-48	DNAJB12	0.62	1.32E-45	GTF3C4	0.52	2.90E-29
C2orf68	0.63	8.46E-46	DPP3	0.59	5.81E-40	HAGH	0.51	7.27E-29

Gene	*R*	*P*
HDGF	0.58	3.91E-38
HECTD3	0.61	5.61E-43
HEXIM2	0.62	1.63E-44
HS2ST1	0.54	6.41E-32
HSPA4	0.55	2.57E-34
HTATIP2	0.67	5.18E-55
ILF3	0.52	2.77E-30
INO80	0.60	2.52E-41
INTS13	0.58	2.95E-38
ITGB5	0.60	4.04E-42
KANSL2	0.57	3.98E-36
KANSL3	0.75	1.28E-73
KBTBD2	0.66	1.82E-52
KBTBD4	0.56	1.25E-35
KDM5C	0.59	1.69E-40
KIAA0930	0.54	3.27E-32
KIDINS220	0.56	1.45E-34
KPNA4	0.66	8.04E-52
KRIT1	0.54	5.17E-33
LRRC28	0.55	4.49E-33
LSM1	0.51	3.91E-28
MAFG	0.58	2.13E-37
MAP3K3	0.50	7.93E-28
MAP4	0.75	1.71E-76

Gene	*R*	*P*
MAPK6	0.64	1.49E-48
ME1	0.59	2.11E-40
MFSD11	0.51	7.50E-29
MMADHC	0.58	1.22E-38
MORF4L1	0.54	6.61E-33
NADK2	0.50	2.86E-27
NEK4	0.57	8.71E-37
NKIRAS1	0.57	1.20E-36
NKIRAS2	0.71	4.10E-63
NMT1	0.62	3.28E-45
NOA1	0.56	9.48E-36
NORAD	0.63	6.12E-47
NPLOC4	0.67	4.54E-55
NRDC	0.69	1.94E-59
PAFAH1B1	0.71	1.71E-64
PAIP2	0.68	7.52E-58
PARN	0.62	2.10E-45
PCBP1	0.57	2.27E-36
PCGF5	0.57	4.73E-36
PDAP1	0.56	1.66E-34
PDCD6IP	0.55	2.34E-34
PDXDC1	0.60	8.97E-42
PEX13	0.62	7.99E-45
PFDN4	0.52	2.42E-29

Gene	*R*	*P*
PHF5A	0.53	1.44E-30
PI4KB	0.51	1.59E-28
PIGT	0.57	4.01E-36
PIR	0.58	5.20E-38
POLR2B	0.54	7.49E-33
PPME1	0.54	2.01E-32
PPP2R2A	0.56	1.50E-34
PPP6R1	0.63	5.06E-46
PRKCI	0.52	3.42E-30
PSMA1	0.60	3.22E-41
PSMA4	0.57	6.62E-37
PSMA5	0.59	4.67E-39
PSMA7	0.56	2.60E-35
PSMB3	0.50	1.57E-27
PSMB5	0.66	1.66E-52
PSMB6	0.62	2.49E-44
PSMC3	0.60	1.60E-41
PSMC5	0.55	1.09E-33
PSMD11	0.67	7.85E-55
PSMD14	0.56	8.09E-35
PSMD2	0.71	5.31E-64
PSMD3	0.66	9.17E-52
PTGES3	0.51	4.92E-29
PTP4A2	0.55	2.21E-34

Gene	*R*	*P*
PUM1	0.55	1.40E-33
PURB	0.60	1.30E-41
RAB3GAP1	0.62	4.20E-44
RAD23A	0.69	1.15E-59
RAD23B	0.66	7.51E-52
RBBP5	0.53	1.17E-30
RBFA	0.58	2.93E-38
RFFL	0.60	4.10E-41
RHEB	0.57	2.17E-36
RNF167	0.59	3.85E-39
RPAP3	0.56	3.17E-35
RPRD2	0.55	2.17E-33
RPTOR	0.53	2.04E-31
RSRC1	0.57	3.18E-37
RXRB	0.54	6.56E-32
SAMD4B	0.54	9.68E-32
SBNO1	0.55	1.87E-33
SCAPER	0.55	3.43E-33
SEC24C	0.60	1.19E-41
SEC31A	0.52	3.38E-29
SERBP1	0.58	1.81E-37
SETD1A	0.51	7.50E-29
SETD7	0.57	1.31E-36
SH3GLB1	0.66	1.07E-51
SHOC2	0.52	2.51E-29
SKP1	0.53	2.04E-30
SLC35E1	0.59	2.37E-39
SLC48A1	0.62	6.14E-45
SLTM	0.56	2.00E-35
SMC3	0.55	7.49E-34
SMCR8	0.51	1.75E-28
SNX13	0.59	2.87E-39
SNX9	0.57	2.53E-37
SQSTM1	0.65	4.18E-50
SRP68	0.58	7.94E-38
SSNA1	0.58	1.08E-37
ST13	0.58	4.54E-38
STAG2	0.54	8.13E-33
STAM	0.57	1.79E-36
STAM2	0.50	1.58E-27
STK40	0.72	8.06E-66
STRIP1	0.57	2.56E-37
SVIL	0.69	1.58E-59
SYS1	0.57	4.67E-36
SZRD1	0.57	3.08E-37
TACC2	0.58	3.85E-38
TAF6	0.59	1.60E-40
TAF8	0.55	3.72E-33
TAX1BP1	0.55	6.79E-34
TBC1D14	0.55	5.13E-34
TBC1D17	0.62	3.97E-44
TBK1	0.61	1.45E-42
TBL1X	0.53	2.30E-31
TCEANC2	0.64	4.68E-49
TGOLN2	0.61	2.96E-42
THAP1	0.50	2.91E-27
THRAP3	0.55	2.18E-33
TM9SF1	0.53	1.77E-30
TMEM59	0.50	1.19E-27
TNIP1	0.71	8.93E-64
TNPO3	0.65	1.91E-50
TOM1	0.63	4.44E-47
TOPORS	0.50	1.12E-27
TOR1B	0.57	3.06E-37
TOX4	0.57	3.07E-36
TRAPPC8	0.61	2.65E-42
TRIM23	0.50	9.83E-28
TRIM41	0.75	1.08E-75
TRIP12	0.52	2.49E-30
TRMT12	0.52	4.25E-30
TXNRD1	0.61	2.86E-42
UACA	0.67	2.15E-55

Gene	*R*	*P*
UBE2R2	0.68	2.90E-56
UBE2Z	0.51	2.87E-28
UBE4B	0.73	1.21E-68
UBIAD1	0.51	1.55E-28
UBN1	0.62	2.86E-44
UFC1	0.58	1.42E-37
UGGT1	0.58	7.11E-39
UNKL	0.50	1.30E-27
UPF2	0.66	8.91E-53
USP10	0.57	8.21E-37
USP14	0.59	2.28E-39
USP33	0.53	2.12E-30
USP34	0.52	2.86E-30
USP39	0.59	1.98E-40
USP5	0.66	2.37E-52
UTP11	0.52	4.64E-30
VCP	0.67	3.32E-55
VEZT	0.63	3.02E-47
VIPAS39	0.55	8.67E-34
VPS29	0.55	2.43E-33
VPS50	0.50	2.85E-27
VTI1B	0.58	4.28E-38
WDR74	0.52	5.24E-30
WTAP	0.50	1.89E-27
XRCC5	0.54	4.75E-32
XRN1	0.54	3.14E-32
YKT6	0.60	1.22E-40
YWHAE	0.53	2.49E-31
YWHAG	0.66	2.17E-52
ZDHHC16	0.62	8.75E-45
ZEB1	0.63	6.81E-46
ZFAND3	0.66	1.17E-52
ZNF148	0.51	4.75E-28
ZNF197	0.59	6.32E-39
ZNF213	0.62	2.32E-44
ZNF592	0.73	3.21E-69
ZNF770	0.61	1.44E-42

Note: *R*, Pearson correlation coefficient; *P*, two-sided *P* value

Table S3. *NFE2L1* and significantly altered proteasome subunit genes between the sarcopenia group and the young healthy group

Gene	baseMean	Log2 FoldChange	lfcSE	stat	pvalue	Padj	Sig
NFE2L1	571.78	-0.1698	0.0591	-2.8717	4.08E-03	4.16E-02	Down
PSMB6	204.70	-0.2984	0.0545	-5.4795	4.27E-08	4.80E-06	Down
PSMA4	174.77	-0.3167	0.0587	-5.3937	6.90E-08	6.90E-06	Down
PSMD8	174.97	-0.3822	0.0770	-4.9623	6.97E-07	4.66E-05	Down
PSMF1	90.16	-0.3137	0.0764	-4.1047	4.05E-05	1.33E-03	Down
PSME4	135.80	-0.3086	0.0791	-3.9029	9.50E-05	2.68E-03	Down
PSMB5	174.27	-0.3196	0.0824	-3.8780	1.05E-04	2.90E-03	Down
PSMD14	75.88	-0.2515	0.0671	-3.7471	1.79E-04	4.34E-03	Down
PSMD7	291.24	-0.1874	0.0545	-3.4399	5.82E-04	1.06E-02	Down
PSMB7	96.17	-0.1777	0.0579	-3.0696	2.14E-03	2.69E-02	Down
PSMD2	239.72	-0.1691	0.0564	-2.9966	2.73E-03	3.18E-02	Down
PSMD6	68.43	-0.2001	0.0678	-2.9532	3.15E-03	3.49E-02	Down
PSMD12	157.65	-0.1659	0.0596	-2.7849	5.35E-03	5.12E-02	Down
PSMA7	486.90	-0.1208	0.0435	-2.7785	5.46E-03	5.15E-02	Down
PSME3IP1	77.79	-0.1667	0.0622	-2.6801	7.36E-03	6.36E-02	Down
PSMD1	468.91	-0.1140	0.0485	-2.3479	1.89E-02	1.22E-01	Down
PSMC1P1	31.49	-0.2819	0.1236	-2.2800	2.26E-02	1.37E-01	Down
PSMG3-AS1	3.61	-0.5782	0.2632	-2.1968	2.80E-02	1.57E-01	Down

Continued

Gene	baseMean	log2 FoldChange	lfcSE	stat	pvalue	Padj	Sig
PSME1	81.52	0.2672	0.0813	3.2866	1.01E-03	1.58E-02	Up
PSMD5	5.50	0.5084	0.2389	2.1281	3.33E-02	1.74E-01	Up
PSMA3-AS1	26.93	0.2155	0.1094	1.9693	4.89E-02	2.22E-01	Up

lfcSE, log fold change standard error; pvalue, probability value; padj, adjusted p-value; Sig, statistical significance.

Table S4. *NFE2L1* and significantly altered proteasome subunit genes between the sarcopenia group and the aged healthy group

Gene	baseMean	Log2 FoldChange	lfcSE	stat	pvalue	Padj	Sig
NFE2L1	563.28	-0.0930	0.0495	-1.8793	6.02E-02	5.06E-01	No sig.
PSME4	134.19	-0.2179	0.0760	-2.8678	4.13E-03	1.78E-01	Down
PSMD1	469.76	-0.0902	0.0411	-2.1918	2.84E-02	4.02E-01	Down
PSMD2	237.66	-0.1081	0.0520	-2.0814	3.74E-02	4.45E-01	Down
PSME1	82.50	0.1841	0.0728	2.5286	1.15E-02	2.97E-01	Up

lfcSE, log fold change standard error; pvalue, probability value; padj, adjusted p-value; Sig, statistical significance

Table S5. The association analysis between the *NFE2L1* gene SNPs and lean mass

			Male			Female			Meta		
rs	POS	EA/OA	BETA	SE	P	BETA	SE	P	BETA	SE	P
rs41457949	46123983	G/A	0.0640	0.0148	1.40E-05	0.0330	0.0073	4.43E-06	0.0390	0.0065	1.60E-09
rs7209484	46143042	T/C	0.0330	0.0082	5.13E-05	0.0150	0.004	3.01E-04	0.0180	0.0036	4.89E-07
rs12602010	46126116	G/A	0.0280	0.0081	5.98E-04	0.0140	0.004	5.71E-04	0.0170	0.0036	4.09E-06
rs8438	46147945	G/A	0.0270	0.0081	8.15E-04	0.0150	0.004	2.38E-04	0.0170	0.0036	1.79E-06
rs72823594	46124276	C/T	-0.0210	0.0087	2.00E-02	-0.0170	0.0043	5.78E-05	-0.0180	0.0039	3.07E-06
rs72823599	46132424	C/G	-0.0190	0.0085	3.00E-02	-0.0170	0.0042	3.87E-05	-0.0180	0.0037	3.02E-06
rs72825504	46139479	C/T	-0.0190	0.0085	3.00E-02	-0.0170	0.0042	3.96E-05	-0.0180	0.0037	3.16E-06
rs72823601	46135208	C/T	-0.0190	0.0085	3.00E-02	-0.0170	0.0042	4.03E-05	-0.0170	0.0037	3.29E-06
rs72823591	46122628	C/T	-0.0170	0.0084	4.00E-02	-0.0170	0.0041	2.21E-05	-0.0170	0.0037	2.37E-06
rs7216504	46117341	G/A	-0.0170	0.0084	4.00E-02	-0.0170	0.0041	2.48E-05	-0.0170	0.0037	2.73E-06
rs72823534	46119320	T/A	-0.0170	0.0083	4.00E-02	-0.0170	0.0041	2.32E-05	-0.0170	0.0037	2.62E-06
rs113187178	46117471	G/A	-0.0170	0.0084	4.00E-02	-0.0180	0.0041	2.07E-05	-0.0180	0.0037	2.42E-06
rs8067005	46119775	C/T	-0.0170	0.0083	4.00E-02	-0.0180	0.0041	2.07E-05	-0.0170	0.0037	2.45E-06

rs, reference SNP ID; POS, position; EA, effect allele; OA, other allele; SE, standard error; P, probability statistics.

Table S6. The association analysis between the *NFE2L1* gene SNPs and grip strength

			Male			Female			Meta		
rs	POS	EA/OA	BETA	SE	P	BETA	SE	P	BETA	SE	P
rs17680229	46129762	G/A	0.4680	0.0709	3.96E-11	0.2000	0.0463	1.55E-05	0.2800	0.0388	4.84E-13
rs12602010	46126116	G/A	0.3600	0.0594	1.44E-09	0.1690	0.0388	1.38E-05	0.2260	0.0325	3.73E-12
rs8438	46147945	G/A	0.3620	0.0591	9.31E-10	0.1640	0.0386	2.12E-05	0.2230	0.0323	5.00E-12
rs7209484	46143042	T/C	0.3650	0.0600	1.17E-09	0.1540	0.0391	8.46E-05	0.2170	0.0328	3.69E-11
chr17:46121765	46121765	CTTTTTTTTTTT/C	0.3610	0.0642	1.87E-08	0.1520	0.0418	2.83E-04	0.2140	0.0350	9.86E-10
rs41457949	46123983	G/A	0.4350	0.1086	6.14E-05	0.1900	0.0706	7.10E-03	0.2630	0.0592	8.96E-06

rs, reference SNP ID; POS, position; EA, effect allele; OA, other allele; SE, standard error; P, probability statistics.

Table S7. The sequences of primers for genotyping

Gene	Sequences (5'-3')	Product size (bp)
Nfe2l1-Flox		
Forward	TGACGGGACAGAATCACCA	
WT-reverse	CATGTCAGCCCATGCTTTGC	262
KI-reverse	GAGAGCCATTTGACTCTTTCCACAA	360
Ckm-Cre		
WT-forward	CTAGGCCACAGAATTGAAAGATCT	
WT- reverse	GTAGGTGGAAATTCTAGCATCATCC	324
TG- forward	TAAGTCTGAACCCGGTCTGC	
TG- reverse	GTGAAACAGCATTGCTGTCACTT	455

Table S8. Primer sequences for RT-qPCR

Genes	Accession no.	Forward (3'-5')	Reverse (5'-3')
Acta1	NM_001272041.1	ACGCCAGCCTCTGAAACTAGA	GAGCCGTTGTCACACACAAG
Adgre1	NM_010130.4	TCAGCCATGTGGGTACAGTCA	CACAGCAGGAAGGTGGCTATG
Casp1	NM_009807.2	CCAAGCTTGAAAGACAAGCCC	ACACCACTCCTTGTTTCTCTCC
Cd68	NM_001291058.1	ACTGGTGTAGCCTAGCTGGT	CCTTGGGCTATAAGCGGTCC
Desmin	NM_010043.2	AACTTCCGAGAAACCAGCCC	TCTCCATCCCGGGTCTCAAT
Il6	NM_031168.2	CTGCAAGAGACTTCCATCCAGTT	AGGGAAGGCCGTGGTTGT
Mlkl	NM_029005.3	ATCAAAGTATTCAACAACCCC	GCAAATCCCAAATATACGCAA
Myh6	NM_008657.3	AGTGGCCAAGTGTTTCGGAT	ATCCACGTTTGCTCCTCCTTC
MyoG	NM_031189.2	GTCCCAACCCAGGAGATCAT	GCTGTCCACGATGGACGTAA
Ndufs4	NM_010887.2	TTGGGGCGAAGGGCAATG	GTCAGCGGTTGATGCCCAA
Nfe2l1	NM_001361682	GGCAGTGTCCTCCTCATTCC	TCCGGTCCTTTGGCTTTCT
Nlrp3	NM_145827.3	TGGCTGTGTGGATCTTTGCT	ACGTGTCATTCCACTCTGGC
Pycard	NM_023258.4	GTACAGCCAGAACAGGACACTT	ACTGCCATGCAAAGCATCCA
Ripk1	NM_009068.3	AGAAGAAGGGAACTATTCGC	TTCTATGGCCTCCACGAT
Ripk3	NM_019955.2	CGGGCACACCACAGAACAT	GTAGCACATCCCCAGCACCAC
Tnf	NM_013693.3	GAGCCGATGGGTTGTACCTT	GGCAGCCTTGTCCCTTGA

Table S9. Cluster numbers, marker genes and proportions corresponding to nuclear type

Nuclear type	Marker gene	Cluster number	Proportion (%)	Flox_proportion (%)	KO_proportion (%)
Type I myonuclei	*Myh7*	15	1.25	1.39	1.17
Type IIa myonuclei	*Myh2*	8	4.39	5.37	3.83
Type IIx myonuclei	*Myh1*	7	6.53	6.35	6.63
Type IIb myonuclei	*Myh4*	0, 1, 2, 3, 5, 6, 13	61.73	61.71	61.75
Myotendinous junction	*Col22a1*	16	1.14	1.21	1.10
Tenocyte	*Mkx*	17	0.92	0.60	1.10
Fibroadipogenic progenitors	*Dcn*	4, 11, 18	11.77	9.41	13.11
Smooth muscle cells	*Myh11*	10, 23	2.88	3.70	2.41
Endothelial cells	*Pecam1*	9, 20, 21	4.68	6.27	3.77
Immune cells	*Ptprc*	14	1.46	1.08	1.67
Adipogenic precursor cells	*Apod*	19, 22	1.13	0.94	1.25
Satellite cells	*Pax7*	12	2.12	1.96	2.22

Table S10. Subclusters of type IIb myonuclei and their proportions

Cluster number	Flox Freq (%, Subcluster/IIb)	KO Freq (%, Subcluster/IIb)	Flox (%, Subcluster/total)	KO (%, Subcluster/total)
1	324 (4.51)	3359 (26.56)	2.78	16.40
2	9165 (12.76)	2391 (18.91)	7.87	11.68
3	632 (8.80)	2494 (19.72)	5.43	12.18
13	24 (0.33)	532 (4.21)	0.21	2.60
0	1400 (19.50)	2295 (18.15)	12.03	11.21
5	1940 (27.02)	847 (6.70)	16.68	4.14
6	1943 (27.07)	727 (5.75)	16.70	3.55

Table S11. Internal standard for sample analysis

Name	Concentration (μg/mL)
PC 38:0	1.0
PE 30:0	0.8
SM 12:0	0.7
LPC 19:0	0.8
FA C16:0-d3	0.5
FA C18:0-d3	0.2
TG 45:0	0.6
Cer 17:0	0.8